Conjugate Forced Convection Heat Transfer in Eccentric Annuli

by

Saiyed Aijaz Haidar

A Thesis Presented to the

FACULTY OF THE COLLEGE OF GRADUATE STUDIES

KING FAHD UNIVERSITY OF PETROLEUM & MINERALS

DHAHRAN, SAUDI ARABIA

In Partial Fulfillment of the
Requirements for the Degree of

MASTER OF SCIENCE

In

MECHANICAL ENGINEERING

May, 1999

INFORMATION TO USERS

This manuscript has been reproduced from the microfilm master. UMI films the text directly from the original or copy submitted. Thus, some thesis and dissertation copies are in typewriter face, while others may be from any type of computer printer.

The quality of this reproduction is dependent upon the quality of the copy submitted. Broken or indistinct print, colored or poor quality illustrations and photographs, print bleedthrough, substandard margins, and improper alignment can adversely affect reproduction.

In the unlikely event that the author did not send UMI a complete manuscript and there are missing pages, these will be noted. Also, if unauthorized copyright material had to be removed, a note will indicate the deletion.

Oversize materials (e.g., maps, drawings, charts) are reproduced by sectioning the original, beginning at the upper left-hand corner and continuing from left to right in equal sections with small overlaps. Each original is also photographed in one exposure and is included in reduced form at the back of the book.

Photographs included in the original manuscript have been reproduced xerographically in this copy. Higher quality 6" x 9" black and white photographic prints are available for any photographs or illustrations appearing in this copy for an additional charge. Contact UMI directly to order.

UMI®

Bell & Howell Information and Learning
300 North Zeeb Road, Ann Arbor, MI 48106-1346 USA
800-521-0600

Conjugate Forced Convection Heat Transfer in Eccentric Annuli

BY

Saiyed Aijaz Haider

A Thesis Presented to the

DEANSHIP OF GRADUATE STUDIES

KING FAHD UNIVERSITY OF PETROLEUM & MINERALS

DHAHRAN, SAUDI ARABIA

In Partial Fulfillment of the
Requirements for the Degree of

MASTER OF SCIENCE

In

MECHANICAL ENGINEERING

May 1999

KING FAHD UNIVERSITY OF PETROLEUM AND MINERALS

DHAHRAN 31261, SAUDI ARABIA

DEANSHIP OF GRADUATE STUDIES

This thesis, written by

SAIYED AIJAZ HAIDER

under the direction of his Thesis Advisor and approved by his Thesis Committee, has been presented to and accepted by the Dean of Graduate Studies, in partial fulfillment of the requirements for the degree of

MASTER OF SCIENCE IN MECHANICAL ENGINEERING

Thesis Committee

Dr. M.A.I. El – Shaarawi (Chairman)

Dr. H.I. Abualhamayel (Member)

Dr. S.M. Zubair (Member)

Dr. M.A. Antar (Member)

15/6/1999

Dr.AbdulGhani A. Al – Farayedhi
Department Chairman

Dr.Abdullah M. Al – Shehri
Dean of Graduate Studies

Date 15/6/99

To my parents,

brother and sister

Acknowledgements

I am extremely grateful to Allah who alone made this accomplishment possible. Research is basically unveiling the mysteries of the Universe by trying to understand the laws of nature as set by the Creator.

Acknowledgements are due to King Fahd University of Petroleum & Minerals for the support in carrying out this research.

Special thanks are due to my thesis advisor Dr. Maged A.I. El-Shaarawi for his constant help during the course of this work. His emphasis on the practical aspects of the work and untiring effort to ensure good presentation and high quality made the work more interesting and challenging. Thanks are due to members of my thesis committee, Dr. S.M. Zubair, Dr. H.I. Abualhamayel and Dr. M.A. Antar for their cooperation and support and to Dr. E.M.A. Mokheimer for helping in the early stages of the work.

I also appreciate the assistance and encouragement received from the Chairman, faculty members, staff and graduate students of the department. Special thanks to Mr. Owais Iqbal, Mr. Jameel-ur-Rehman Khan, Mr. Irfan Hussaini,

Mr. Mohammed Yaqub and Dr. S.Z. Shuja for both moral and technical support and to Mr. Shafeeq Ahmed Khan for assisting in departmental duties and helping in arrangements for seminar and defense presentations.

I wish to thank the system administration of ITC (Information and Technology Centre) for use of the computing facilities particularly Mr. Mohammed Abdul Raheem and Mr. Saleh Al-Shaiban for their help and guidance. Thanks also to Mr. Farooq Ashraf and Mr. Shahid Ali of the system administration at CCSE (College of Computer Science and Engineering) for cooperation. Special thanks to Mr. Mutlaq Al-Mutlaq, in charge of 'NEXT' lab and his supporting staff for help and assistance. I also appreciate the help provided by Mr. Husain Ali and Mr. Mohammed Ghouseuddin of the PC administration at CCSE.

An expression of gratitude for all friends at North Compound, particularly my house-mates Mr. Rehan Sadiq and Mr. Irfan Ahmed Ilyas for being cooperative.

Finally, I am grateful to my family for their extreme moral support, encouragement and patience during the course of my studies here.

Contents

List of Tables

List of Figures

Nomenclature

D_h	hydraulic diameter of annulus $2(r_{io} - r_{oi})$
e	eccentricity (distance between axes of the two tubes)
E	dimensionless eccentricity, $e/(r_{io} - r_{oi})$
h	coordinate transformation scale factor
H	dimensionless coordinate transformation scale factor
	$\mathrm{h}/D_h = \frac{0.5\sinh(\eta_o)}{(1-NR_2)(\cosh(\eta)-\cos(\zeta))}$
i	index for the bi-polar grid in the η-diection
	and the cylindrical grid in the radial direction
j	index for the bi-polar grid in the ζ-direction
	and the cylindrical grid in the tangential direction
k_f	thermal conductivity of fluid
k_s	thermal conductivity of solid
KR	solid-fluid conductivity ratio, k_s/k_f
M	number of intervals in each of the ζ and ϕ-directions

N	number of intervals in the η-direction
NR_1	ratio between inner radius of core tube and inner radius of outer tube, r_{ii}/r_{io}
NR_2	ratio between outer radius of core tube and inner radius of outer tube, r_{oi}/r_{io}
NR_3	dimensionless inner radius of outer tube = 1
NR_4	ratio between outer radius of outer tube and inner radius of outer tube, r_{oo}/r_{io}
NSO	number of radial intervals in the outer tube wall
NSI	number of radial intervals in the inner tube wall
q_{in}	local heat flux on the inner interface at the narrowest gap
q_{iw}	local heat flux on the inner interface at the widest gap
q_{on}	local heat flux on the outer interface at the narrowest gap
q_{ow}	local heat flux on the outer interface at the widest gap
Q_{II}	average heat flux on the inner interface
Q_{OI}	average heat flux on the outer interface
r_{ii}	inner radius of core tube
r_{oi}	outer radius of core tube
r_{io}	inner radius of external tube
r_{oo}	outer radius of external tube

r	first transverse cylindrical coordinate
R	dimensionless radial coordinate, r/r_{io}
ΔR	numerical grid mesh size in R-direction
ΔR_i	value of ΔR for the inner wall
ΔR_o	value of ΔR for the outer wall
T	temperature at any point
T_m	mixing-cup (mixed-mean) temperature at any cross-section
T_o	ambient or entrance temperature
T_w	isothermal temperature of heated wall
u	axial velocity component
u_{fd}	fully developed axial velocity component
$\bar{u}$	average (mean) axial velocity
U	dimensionless axial velocity, $u/\bar{u}$
U_{fd}	dimensionless fully developed axial velocity, $u_{fd}/\bar{u}$
v	η-direction velocity component
V	dimensionless η-velocity component, vD_h/γ
w	ζ-direction velocity componet
W	dimensionless ζ-velocity component, wD_h/γ
X	first transverse direction in the Cartesian coordinate system
Y	second transverse direction in the Cartesian coordinate system

z	axial coordinate (measured from the annulus entrance)
Z	dimensionless axial coordinate, $z/(D_h Re)$
Z^*	modified dimensionless axial coordinate, $z/(D_h RePr)$

Greek Letters

η	first transverse bi-polar coordinate
η_i	value of η on the inner interface
η_o	value of η on the outer interface
$\Delta\eta$	numerical grid mesh size in the η-direction
θ	dimensionless temperature, $(T - T_o)/(T_w - T_o)$
θ_{fd}	fully developed value of θ
θ_{in}	value of θ on the inner interface at the narrowest gap
θ_{iw}	value of θ on the inner interface at the widet gap
θ_m	dimensionless value of mixing-cup temperature at any cross-section
$\theta_{m,fd}$	fully developed value of θ_m
θ_{on}	value of θ on the outer interface at the narrowest gap
θ_{ow}	value of θ on the outer interface at the widest gap
θ_{si}	value of θ in the inner solid wall
θ_{so}	value of θ in the outer solid wall
ν	kinematic viscosity of fluid

ζ	second transverse bi-polar coordinate
$\Delta\zeta$	numerical grid mesh size in ζ-direction
ϕ	second transverse cylindrical coordinate
$\Delta\phi$	numerical grid mesh size in ϕ-direction
ψ	normalized value of ζ, $\psi=\zeta/\pi$

THESIS ABSTRACT

Name: SAIYED AIJAZ HAIDER

Title: CONJUGATE FORCED CONVECTION HEAT TRANSFER IN ECCENTRIC ANNULI

Degree: MASTER OF SCIENCE

Major Field: MECHANICAL ENGINEERING

Date of Degree: MAY 1999

Conjugate laminar forced convection heat transfer in the entry region of eccentric annuli is numerically investigated. Heat transfer parameters are presented for a fluid of Pr=0.7 flowing in an annulus of radius ratio 0.5 for four values of dimensionless eccentricity ranging from 0.1 to 0.7. Solid-fluid conductivity ratio (KR) is varied to cover the range for practical cases with commonly encountered inner and outer tube thicknesses. Limits for KR above which the conjugation can be neglected are obtained. For solid-fluid conductivity ratio (KR) equal to 10, the inner and outer tube thicknesses are varied to obtain the limits of wall thickness below which the conjugation can be neglected. Boundary conditions applied are isothermal heating of the inner surface of the core tube while the outer surface of the external tube is maintained at the inlet fluid temperature. Results indicate that the conjugate effect is significant for systems with low values of KR and thick-walled tubes. Moreover, this effect increases with invreasing the eccentricity (E) and thus conjugation must be taken into consideration particularly at high values of E.

King Fahd University of Petroleum and Minerals
Dhahran, Saudi Arabia
May 1999

" الخلاصه "

الاسم : سيد اعجاز حيدر

العنوان : انتقال الحرارة المترافق بالحمل القسرى فى أنبوب حلقى لامركزى

الدرجه : الماجستير

المجال : الهندسة ميكانيكية

تم دراسة انتقال الحرارة الطبقى بالحمل القسرى فى مدخل انبوب حلقى لامركزى باستحدام طريقة عددية. وقد تم عرض متغيرات انتقال الحرارة لمائع ذو رقم برانتل يساوى ٧,. يسرى فى انبوب حلقى ذو نسبة نصف قطر تقدر بنصف و ذلك لأربعة قيم للامركزية من ١,. الى ٧,. وقد تم تغيير نسبة معامل انتقال الحرارة بالتوصيل بين سطح الصلب والمائع بحيث تغطى المدى الموجود فى الحالات العملية لسماكات الأنابيب الموجودة كما تم حساب حدود تلك النسبة والتى يمكن بعدها اهمال الترافق. وقد تم تغيير سمك الأنبوب الداخلى و الخارجى و ذلك لنسبة معاملات توصيل تساوى ١٠ لحساب الحد الذى يمكن عنده اهمال الترافق.

و فى تلك الدراسة أيضا تم تطبيق قيم المتغيرات عند الحدود بحيث تكون درجة الحرارة ثابتة للسطح الداخلى للأنبوب الداخلى بينما كانت درجة الحرارة الخارجية للانبوب الخارجى ثابتة عند قيمة درجة حرارة المائع عند دخوله إلى الأنبوب. وقد اظهرت النتائج أن تأثير الترافق يكون واضحا للحالات التى تكون فيما نسبة معامل انتقال الحرارة بالتوصيل صغيرة و كذلك فى حالة زيادة سمك الأنابيب. وبالاضافة الى ذلك يزداد ذلك التأثير بزيادة اللامركزية وبالتالى يجب اخذ تأثير الترافق فى الاعتبار عند القيمة العالية للامركزية.

جامعة الملك فهد للبترول والمعادن

الظهران - المملكة العربية السعودية

مايو ١٩٩٩

Chapter 1

INTRODUCTION

Analysis of fluid flow and heat transfer in eccentric annuli provides a useful model for many practical applications. Practical examples of forced convection in annuli include flow and heat transfer in double pipe heat exchangers, nuclear fuel element cooling system, absorber and glass envelope assembly in parabolic-cylindrical solar collectors. Manufacturing tolerances and/or the assembly process or the operating conditions lead to eccentricity. Also, since eccentricity results in an increase in heat transfer [1] and a simultaneous decrease in the presssure drop [2], it can be intentionally provided to achieve enhanced performance of heat exchange equipment.

In conventional heat transfer analyses, it is common practice to prescribe the temperature or the heat flux at the fluid-wall interface. Consequently, the energy equation for the fluid alone has to be solved. The results thus obtained are good only for heat transfer in flows bounded by walls having extremely small thermal

resistance, i.e. very high thermal conductivity and/or very small thickness.

However, in actual practice, the wall thermal resistance is finite and the thermal conditions at the the fluid-wall interface are different from their counterparts imposed at the other surface of the the solid walls. Thus, the thermal conditions at the fluid-wall interface, which are not known a priori, depend on the thermal properties and flow characteristics of the fluid as well as the dimensions and properties of the solid wall. Such type of problems, where heat conduction in the solid is coupled with convective heat transfer in the fluid, are often referred to as conjugate problems. If the bounding cylinder walls are thick and have low thermal conductivity, the heat transfer can be significantly affected and conjugation (i.e., coupling of conduction and convection) must be taken into account.

The present work aims at obtaining a solution for the conjugate laminar forced convection heat transfer in the entrance region of eccentric annuli. Solution for this problem has not been reported in the literature. Results of this investigation determine limits for solid-fluid conductivity ratio, above which, and wall thickness, below which, the conjugate effect can be neglected for practical purposes. The results presented are expected to be of practical value in the design and analysis of heat exchange equipment. Design engineers need data to decide whether or not the conjugate effect should be taken into account for system design. Also, the present results can be used to refine the available conventional results to account for the coupling of conduction and convection for sytems with low values of KR and /

or thick walls, particularly at high eccentricities. The results clearly highlight the significant role of eccentricity in enhancing the conjugate effect.

Chapter 2 summarizes the literature review. Mathematical model and problem formulation is discussed in Chapter 3. Numerical approach and the method of solution are described in Chapter 4. Validation of the present work by comparisons with the available conventional solutions is presented in Chapter 5. Results and discussions are compiled in Chapters 6 and 7 for the critical conductivity ratio and critical tube thickness, respectively. Finally, conclusions are listed in Chapter 8.

Chapter 2

LITERATURE REVIEW

2.1 Introduction

Considerable work has been done to study the problem of flow and heat transfer in annuli, both concentric and eccentric. However, this literature review will focus on forced flow in annuli and on conjugate heat transfer in ducts of various geometries. The conventional (i.e., neglecting the conjugate effect) cases for annuli are discussed first followed by the available conjugate solutions.

2.2 Conventional solutions for Concentric Annuli

Reynolds et al. [3], presented for the first time a general formulation of the fully developed forced convection problem in concentric annuli for arbitrarily prescribed wall temperatures or heat fluxes. Four fundamental thermal boundary conditions were established as listed below:

First Kind: One boundary is isothermally heated while the other is kept at the inlet fluid temperature.

Second Kind: Contant heat flux at one boundary while the other is adiabatic.

Third Kind: One Boundary is isothermally heated while the other is adiabatic.

Fourth Kind: Contant heat flux at one boundary while the other is kept at the inlet fluid temperature.

Combinations of solutions corresponding to these fundamental boundary conditions may be used to obtain solutions for more complicated boundary conditions found in practice. Using an approximate integral method **Reynolds et al.** [4] solved the governing equations for the heat transfer in annular passages for simultaneously developing velocity and temperature profiles in laminar forced flow.

Sparrow and Lin [5] provided the axial velocity distribution and the axial pressure drop for laminar forced flow in the entrance region of concentric annuli. **Shumway and McEligot** [6] obtained a numerical solution for laminar gas flow in

concentric annuli. They employed a finite-difference method to solve the combined entry-length problem for constant and variable physical properties. The fundamental solutions of the first, third and fourth kinds were obtained for an annulus of radius ratio 0.25 and fluid of Pr=0.72.

Based on a simple linearized finite-difference scheme, **Coney and El-Shaarawi [7]** presented a numerical solution for the simplified Navier-Stokes equations for a hydrodynamically developing laminar flow with constant physical properties in the the entrancce region of concentric annuli with rotating inner walls. **Coney and El-Shaarawi [8]** investigated laminar forced convection heat tranfer in concentric annuli with simultaneously developing hydrodynamic and thermal boundary layers. The hydrodynamic entry length problem was solved first to obtain the velocity profiles; then the energy equation was solved for the temperature profiles.

2.3 Conventional solutions for Eccentric Annuli

Using the bi-polar coordinates, **Caldwell [9] and Piercy et al. [10]** showed that the Macdonald's equation for the torsion moment is comparable to the equation for the volumetric flow rate of a fully developed forced laminar flow through an eccentric annulus.

Snyder and Goldstein [11] obtained analytically, the velocity distribution for the fully developed forced laminar flow through eccentric annuli using the bi-polar

coordinates. **Redberger and Charles [12]**, also using the bi-polar coordinates, numerically solved the same problem. The differential equation was replaced by a finite difference representation and an iterative method was used to solve the resultant set of algebraic equations. Without using the bi-polar coordinates, **Cheng and Hwang [13]** obtained a solution for the energy equation in cylindrical coordinates for the fully developed laminar forced convection in eccentric annular ducts with heat sources and constant wall temperature gradient (i.e., constant heat flux). Using the method introduced by **Cheng and Hwang [13]**, **Trombetta [14]** obtained an approximate analytical solution for the energy equation in cylindrical coordinates for the hydrodynamically and thermally fully developed forced convection in eccentric annuli under other boundary conditions.

Fully developed forced convection in eccentric annuli has been treated numerically by **Suzuki et al. [15]**. The finite difference equivalents of the governing equations of velocity and temperature fields written in bi-polar coordinates were solved using an iterative procedure. **Patankar et al. [16]** presented a numerical study for fully developed laminar mixed convection in vertical eccentric annular ducts. They solved the equations governing the velocity and temperature using a body conforming grid and finite volume technique.

Feldman et al. [17,18] analyzed the hydrodynamic and thermal entry region for forced convection in straight eccentric ducts. The absence of axisymmetry gives rise to three velocity components in this entrance region. They derived two gov-

erning equations for the hydrodynamic problem, the continuity and the streamwise momentum equation; the two transverse momentum equation have been dropped through an order of magnitude analysis. To complete their hydrodynamic model, they developed an additional relation between the two transverse velocity components.

El-Shaarawi et al. [1] presented a boundary-layer model describing the laminar forced convection heat transfer in eccentric annuli and a finite-difference numerical algorithm was developed for solving this model. The main objective was to introduce a mathematically well-posed model, i.e. a model capable of describing the forced flow and convection heat transfer in the entry region of eccentric annuli without need of assumptions dependent on prior knowledge of the mechanism of transverse flows in such a region. Numerical results were presented for the developing velocity profiles and the pressure drop in annuli of radius ratio 0.5 and 0.9 with dimensionless eccentricity ranging from 0.1 to 0.8. Heat transfer parameters were tabulated for a fluid of Pr=0.7 with the boundary conditions of an isothermally heated inner wall and an outer wall maintained at the inlet fluid temperature.

2.4 Conjugate solutions

Literature until 1976, pertinent to conjugate heat transfer in ducts of various geometrical shapes, has been reviewed by **Shah and London** [19]. **Mori et al.** [20, 21]

considered the problem of steady conjugate heat transfer with fully developed laminar flow between parallel plates when there is internal heat generation in the fluid. Using the finite-difference method, **Faghri and Sparrow [22]** solved numerically the steady conjugate heat transfer with hydrodynamically fully developed laminar flow in a thick-walled circular tube. **Pagliarini [23]** considered the same problem with the exception that the flow is hydrodynamically developing. **Sakakibara et al. [24]** analytically investigated the steady conjugate heat transfer problem in an annulus with a heated core and an insulated outside tube when the laminar flow is hydrodynamically fully developed.

Using Laplace transform techniques, **Kirshan [25]** analytically solved the transient conjugate problem for hydrodynamically and thermally fully developed laminar pipe flow with viscous dissipation. **Olek et al. [26]** considered the same problem by means of a method of separation of variables and concluded that the degree of conjugation and viscous dissipation may have a great impact on the temperature distribution in the fluid. **El-Shaarawi et al. [27]** presented a finite-difference scheme to solve the transient conjugate heat transfer problem in a concentric annulus with simultaneously developing hydrodynamic and thermal boundary layers. The annular forced flow was taken as laminar with constant physical properties and thermal transient was initiated by a step change in the prescribed isothermal temperature of the inner surface of the inside tube while the outer surface of the external tube was kept adiabatic. They concluded that it is not advisable to use the conventional

assumption of extremely thin walls with infinite thermal conductivities and diffusivities particularly for systems with small solid-fluid conductivity and diffusivity ratios and/or very thick walls.

To the best of the writer's knowledge and as is evident from this review, solution for the problem of conjugate forced convection heat transfer in eccentric annuli has not been reported in the literature.

Chapter 3

MATHEMATICAL MODEL and PROBLEM FORMULATION

3.1 Introduction

Figure 3.1 shows a two-dimensional cross-section for the geometry of the problem under consideration. The axes of the two eccentric cylinders are perpendicular to the plane of the paper. Fluid is forced to flow axially in the annular space between the two eccentric cylinders. Figure 3.2 illustrates the numerical meshes, with a bipolar grid in the fluid annulus and cylindrical grids in the two solid walls.

The present work aimed at obtaining a solution for the conjugate heat transfer problem with laminar forced convection in the entry region of eccentric annuli. The bi-polar coordinate system is used to express the partial differential equations

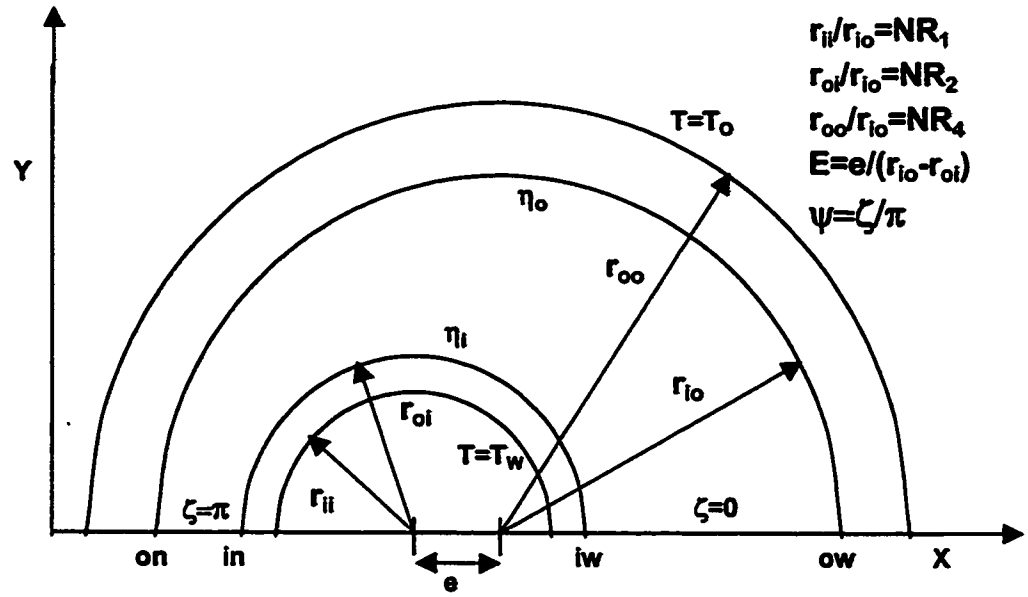

FIG. 3.1: Two-dimensional cross-section of the geometry under consideration.

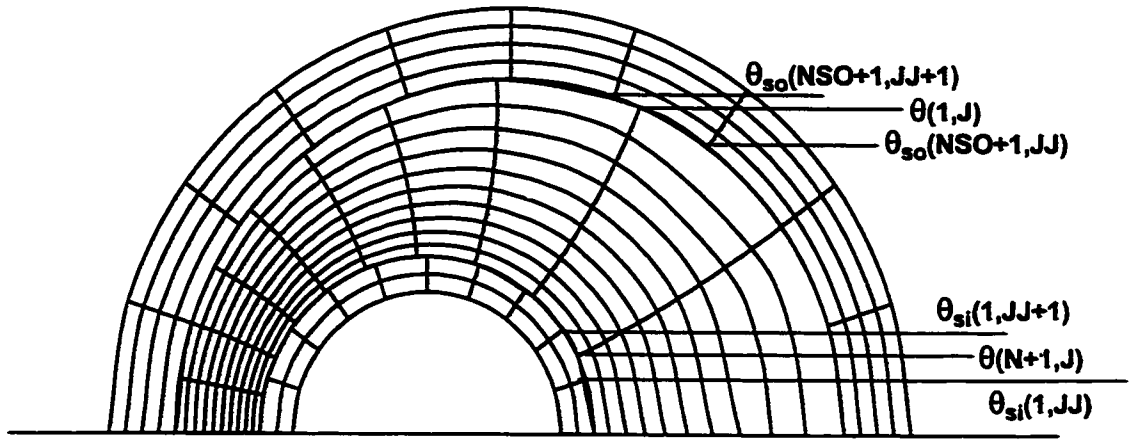

FIG. 3.2: Sample of numerical grid mesh for N=M=10, NSO=4 and NSI=2. Computations were done using a mesh with N=M=20, NSO=16 and NSI=8

describing the flow and heat transfer in the eccentric fluid annulus. This coordinate system consists of a set of eccentric cylinders such that the boundary surfaces of the annulus can be taken as one of the coordinates and the other coordinate will be the set of eccentric cylinders which orthogonally intersect the boundaries. Details of the bi-polar coordinate sytem and transformation of the governing partial differential equations are given in [28, 29, 30]. However, since the cylinder walls have uniform thickness, the cylindrical coordinate system is more appropriate for the solid walls. Therefore, the governing equations for fluid in the annulus will be written in bi-polar coordinates, whereas the energy equations for the solid cylinder walls will be expressed in cylindrical coordinates. Continuity of temperature and heat flux at the solid-fluid interfaces provide the necessary link.

3.2 Governing Equations

To develop an appropriate model for the said problem, the following simplifying assumptions were made [31, 32]:

1. The flow is steady.

2. The fluid is Newtonian with constant properties.

3. Body forces, viscous dissipation, internal heat generation and radiation heat transfer are absent.

4. Pressure is a function of the axial coordinate only.

5. Axial diffusion of momentum in the fluid and that of energy in both fluid and solid are neglected (i.e., $\frac{\partial^2}{\partial Z^2}$ terms omitted).

6. Momentum equation in the η-direction (i.e. the radial-like direction) is dropped, since the η-velocity component (v) is much smaller than the ζ- and z-velocity components (w and u).

Under these assumptions and using the appropriate dimensionless parameters given in the nomenclature we obtain the following six dimensionless equations [1, 2, 28]:

Continuity Equation

$$\frac{\partial(HW)}{\partial\zeta} + \frac{\partial(HV)}{\partial\eta} + \frac{\partial(H^2U)}{\partial Z} = 0 \tag{3.1}$$

ζ - Momentum Equation

$$\begin{aligned} &\frac{W}{H}\frac{\partial W}{\partial\zeta} + \frac{V}{H^2}\frac{\partial HW}{\partial\eta} + U\frac{\partial W}{\partial Z} - \frac{V^2}{H^2}\frac{\partial H}{\partial\zeta} \\ &= \frac{1}{H^3}\left(\frac{\partial^2 HW}{\partial\eta^2} + \frac{\partial^2 HW}{\partial\zeta^2}\right) - \frac{2}{H^4}\left(\frac{\partial HW}{\partial\eta} - \frac{\partial HV}{\partial\zeta}\right)\frac{\partial H}{\partial\eta} + \frac{2}{H^2}\frac{\partial H}{\partial\zeta}\frac{\partial U}{\partial Z} \end{aligned} \tag{3.2}$$

Axial, Z - Momentum Equation

$$\frac{W}{H}\frac{\partial U}{\partial\zeta} + \frac{V}{H}\frac{\partial U}{\partial\eta} + U\frac{\partial U}{\partial Z} = -\frac{dP}{dZ} + \frac{1}{H^2}\left(\frac{\partial^2 U}{\partial\zeta^2} + \frac{\partial^2 U}{\partial\eta^2}\right) \tag{3.3}$$

Energy Equation for the Fluid

$$\frac{W}{H}\frac{\partial\theta}{\partial\zeta}+\frac{V}{H}\frac{\partial\theta}{\partial\eta}+U\frac{\partial\theta}{\partial Z}=\frac{1}{Pr.H^2}\left(\frac{\partial^2\theta}{\partial\zeta^2}+\frac{\partial^2\theta}{\partial\eta^2}\right) \tag{3.4}$$

Integral Form of the Continuity Equation

$$\bar{U}=\frac{8(1-N_2)}{\pi(1+N_2)}\int_0^{\pi}\int_{\eta_o}^{\eta_i}UH^2d\eta d\zeta=1.0 \tag{3.5}$$

Energy Equation for the Solid

$$\frac{\partial^2\theta_s}{\partial R^2}+\frac{1}{R}\frac{\partial\theta_s}{\partial R}+\frac{1}{R^2}\frac{\partial^2\theta_s}{\partial\phi^2}=0 \tag{3.6}$$

Equation (3.6) is applied twice, once for the outer wall with $\theta_s=\theta_{so}$ and R varying from $NR_3=1$ to NR_4 and then for the inner wall with $\theta_s=\theta_{si}$ and R varying from NR_1 to NR_2.

3.3 Boundary Conditions

Equations (3.1) through (3.6) are subject to the following boundary conditions:

$$
\left.
\begin{array}{l}
for\ Z = 0\ and\ \eta_o < \eta < \eta_i,\ V = W = P = 0\ and\ U = 1 \\
for\ Z \geq 0\ and\ \eta = \eta_i,\ U = V = W = 0 \\
for\ Z \geq 0\ and\ \eta = \eta_o,\ U = V = W = 0 \\
for\ Z \geq 0\ and\ R = NR_1, \theta_{si} = 1\ (T = T_w) \\
for\ Z \geq 0\ and\ R = NR_4, \theta_{so} = 0\ (T = T_o) \\
for\ Z > 0\ and\ \zeta = 0\ and\ \pi\ (the\ line\ of\ symmetry): \\
\frac{\partial V}{\partial \zeta} = \frac{\partial W}{\partial \zeta} = \frac{\partial U}{\partial \zeta} = \frac{\partial \theta}{\partial \zeta} = \frac{\partial \theta_s}{\partial \phi} = 0 \\
for\ Z > 0\ and\ R = NR_2\ and\ R = 1\ (i.e.,\ the\ interfaces) \\
\theta = \theta_s,\ continuity\ of\ temperature \\
k_f \left(\frac{1}{H} \frac{\partial \theta}{\partial \eta} \mathbf{i} + \frac{1}{H} \frac{\partial \theta}{\partial \zeta} \mathbf{j} \right) = k_s \left(\frac{\partial \theta_s}{\partial R} \mathbf{i} + \frac{\partial \theta_s}{\partial \phi} \mathbf{j} \right),\ continuity\ of\ heat\ flux \\
\mathbf{i},\ unit\ vector\ in\ the\ \eta\ and\ R\ directions \\
\mathbf{j},\ unit\ vector\ in\ the\ \zeta\ and\ \phi\ directions
\end{array}
\right\} \quad (3.7)
$$

The hydrodynamically fully developed flow, which occurs if the channel is sufficiently long, provides an analytical check on the numerical solution to be obtained. For this case, V=W=0, $\partial U/\partial Z = 0$, dP/dZ=constant, the ζ-momentum equation and the inertia terms on left hand side of the axial momentum equation vanish and the axial momentum equation reduces to

$$\frac{\partial^2 U_{fd}}{\partial \zeta^2} + \frac{\partial^2 U_{fd}}{\partial \eta^2} = H^2 \left(\frac{dP}{dZ}\right)_{fd} \tag{3.8}$$

This equation is identical to the equation of steady-state heat conduction with internal heat generation which was solved by **El-Saden [33]**. The solution of this equation is

$$U_{fd} = A^* \eta + B - \frac{C^*}{2} \coth \eta + \sum_{n=1}^{\infty} \cos n\zeta [C e^{n\eta} + (D - C^* \coth \eta) e^{-n\eta}] \tag{3.9}$$

Applying the boundary conditions the constants of integration A^*,B,C,C^* and D can be determined **[1]**.

There is no analytical means to solve the set of equations (3.1) through (3.6) and hence they will be treated numerically using a finite-difference technique.

Chapter 4

NUMERICAL ANALYSIS AND METHOD OF SOLUTION

4.1 Introduction

The six dimensionless equations (3.1) through (3.6) listed in the previous chapter were expressed in finite-difference forms. A numerical algorithm has been used to solve for the three velocity components, pressure and temperature in the fluid and the temperatures in the solid cylinders. The existing computer program which was used to obtain the results reported in [1, 2, 28] was modified to incorporate the inner and outer tube wall thickness and the solid-fluid conductivity ratio.

Since the governing equations for the fluid are in bi-polar coordinates whereas the energy equations for the solids are in cylindrical coordintes. the two grids are

linked by applying the principles of the continuity of temperature (using an interpolation procedure) and the continuity of heat flux at the two interfaces.

4.2 Finite-Difference Equations

Using backward differences to express all first derivatives with respect to Z and the first derivative of (HV) with respect to η in the continuity equation and replacing the second and other first order derivatives in η and ζ directions by central finite-differences, equations (3.1) to (3.6) can be written in the following forms respectively:

Continuity Equation

$$\frac{H(i,j+1)W(i,j+1) - H(i,j-1)W(i,j-1)}{2\Delta\zeta}$$
$$+\frac{H(i,j)V(i,j) - H(i-1,j)V(i-1,j)}{\Delta\eta} + H^2(i,j)\frac{U(i,j) - U^*(i,j)}{\Delta Z} = 0 \quad (4.1)$$

ζ - Momentum Equation

$$\frac{W^*(i,j)}{H(i,j)}\frac{W(i,j+1)-W(i,j-1)}{2\Delta\zeta}$$
$$+\frac{V^*(i,j)}{(H(i,j))^2}\frac{H(i+1,j)W(i+1,j)-H(i-1,j)W(i-1,j)}{2\Delta\eta}$$
$$+U^*(i,j)\frac{W(i,j)-W^*(i,j)}{\Delta Z}-\frac{(V^*(i,j))^2}{(H(i,j))^2}\frac{H(i,j+1)-H(i,j-1)}{2\Delta\zeta}$$
$$=\frac{1}{(H(i,j))^3}\left(\begin{array}{l}\frac{H(i-1,j)W(i-1,j)-2H(i,j)W(i,j)+H(i+1,j)W(i+1,j)}{(\Delta\eta)^2}\\ +\frac{H(i,j-1)W(i,j-1)-2H(i,j)W(i,j)+H(i,j+1)W(i,j+1)}{(\Delta\zeta)^2}\end{array}\right)$$
$$-\frac{2}{(H(i,j))^4}\left(\frac{H(i+1,j)-H(i-1,j)}{2\Delta\eta}\right)\left(\begin{array}{l}\frac{H(i+1,j)W(i+1,j)-H(i-1,j)W(i-1,j)}{2\Delta\eta}\\ -\frac{H(i,j+1)V^*(i,j+1)-H(i,j-1)V^*(i,j-1)}{2\Delta\zeta}\end{array}\right)$$
$$+\frac{2}{(H(i,j))^2}\frac{H(i,j+1)-H(i,j-1)}{2\Delta\zeta}\frac{U(i,j)-U^*(i,j)}{\Delta Z} \qquad (4.2)$$

Axial, Z - Momentum Equation

$$\frac{W^*(i,j)}{H(i,j)}\frac{U(i,j+1)-U(i,j-1)}{2\Delta\zeta}+\frac{V^*(i,j)}{H(i,j)}\frac{U(i+1,j)-U(i-1,j)}{2\Delta\eta}$$
$$+U^*(i,j)\frac{U(i,j)-U^*(i,j)}{\Delta Z}=\frac{P(i,j)-P^*(i,j)}{\Delta Z}$$
$$+\frac{1}{(H(i,j))^2}\left(\begin{array}{l}\frac{U(i-1,j)-2U(i,j)+U(i+1,j)}{(\Delta\eta)^2}\\ +\frac{U(i,j-1)-2U(i,j)+U(i,j+1)}{(\Delta\zeta)^2}\end{array}\right) \qquad (4.3)$$

Energy Equation for the Fluid

$$\frac{W^*(i,j)}{H(i,j)}\frac{\theta(i,j+1)-\theta(i,j-1)}{2\Delta\zeta}+\frac{V^*(i,j)}{H(i,j)}\frac{\theta(i+1,j)-\theta(i-1,j)}{2\Delta\eta}$$
$$+U^*(i,j)\frac{\theta(i,j)-\theta^*(i,j)}{\Delta Z}=\frac{1}{Pr(H(i,j))^2}\left(\begin{array}{c}\frac{\theta(i-1,j)-2\theta(i,j)+\theta(i+1,j)}{(\Delta\eta)^2}\\ +\frac{\theta(i,j-1)-2\theta(i,j)+\theta(i,j+1)}{(\Delta\zeta)^2}\end{array}\right) \tag{4.4}$$

Integral Form of the Continuity Equation

$$\frac{8(1-NR_2)}{\pi(1+NR_2)}\left(0.5\sum_{i=2}^{N}U(i,1)(H(i,1))^2+U(i,M+1)(H(i,M+1))^2\right.$$
$$\left.\sum_{j=2}^{M}\sum_{i=2}^{N}U(i,j)(H(i,j))^2\right)\Delta\eta\Delta\zeta=1 \tag{4.5}$$

Energy Equation for the Solid

$$\frac{\theta_s(i+1,j)-2\theta_s(i,j)+\theta_s(i-1,j)}{(\Delta R)^2}+\frac{1}{[NR_*-(i-1)\Delta R]}\frac{\theta_s(i+1,j)-\theta_s(i-1,j)}{2\Delta R}$$
$$+\frac{1}{[NR_*-(i-1)\Delta R]^2}\frac{\theta_s(i,j+1)-2\theta_s(i,j)+\theta_s(i,j-1)}{(\Delta\phi)^2}=0 \tag{4.6}$$

Equation (4.6) will be applied for the inner and the outer solid walls by making the following replacements:

For the outer wall, $\theta_s=\theta_{so}$, $\Delta R=\Delta R_o$, $NR_*=NR_4$ and for the inner wall $\theta_s=\theta_{si}$, $\Delta R=\Delta R_i$, $NR_*=NR_2$.

4.3 Boundary Conditions

Boundary conditions are expressed as follows:

$$
\left.
\begin{array}{l}
for\ Z = 0\ and\ \eta_o < \eta < \eta_i \\
V(i,j) = W(i,j) = P = 0\ and\ U = 1 \\
for\ Z \geq 0,\ \eta = \eta_i\ and\ \eta = \eta_o \\
U(i.j) = V(i,j) = W(i,j) = 0 \\
for\ Z \geq 0\ and\ R = NR_1,\ \theta_{si}(NSI+1,j) = 1 \\
for\ Z \geq 0\ and\ R = NR_4,\ \theta_{so}(1,j) = 0 \\
for\ Z > 0\ and\ \zeta = 0 \\
U(i,2) = U(i,0), V(i,2) = V(i,0), W(i,2) = W(i,0) \\
\theta(i,2) = \theta(i,0), \theta_s(i,2) = \theta_s(i,0) \\
for\ Z > 0\ and\ \zeta = \pi \\
U(i.M) = U(i.M+2). V(i.M) = V(i.M+2). W(i.M) = W(i.M+2) \\
\theta(i,M) = \theta(i,M+2), \theta_s(i,M) = \theta_s(i,M+2)
\end{array}
\right\} \quad (4.7)
$$

Since the temperature field comprises three separate grids, for the outer tube 'i' varies from i=1 at the outer boundary to i=NSO+1 at the outer interface: for the fluid annulus, from i=1 at the outer interface to i=N+1 at the inner interface: and for the inner tube from i=1 at the inner interface to i=NSI+1 at the inner boundary. Thus, i=NSO+1 of the cylindrical grid in the outer wall is coincident with i=1 of

the bi-polar grid in the eccentric fluid annulus. Similarly, i=N+1 of the bipolar grid coincides with i=1 of the cylindrical grid in the inner wall. The boundary conditions are imposed at i=1 of the outer cylindrical grid and i=NSI+1 of the inner cylindrical grid.

With the boundary conditions imposed at the inner surface of the inner tube and the outer surface of the outer tube, the interface conditions are unknown. Also, the eccentric annulus is fitted with a bi-polar mesh whereas the walls have cylindrical ones resulting in 2M+2 mesh points at both interfaces. Therefore, the three grids are linked by applying the principle of continuity of temperature at all points on both interfaces and the continuity of heat flux at only the four points on the intersection of the the interfaces with the line of symmetry.

For the four points at the intersection of the interfaces with the line of symmetry, continuity of temperature and continuity of heat flux can be expressed as follows:

$$\left.\begin{array}{l} at\ R = NR_2\ and\ \zeta = 0 \\ \theta(N+1,1) = \theta_{si}(1,1) \\ KR * H(N+1,1)\frac{\theta_{si}(2,1)-\theta_{si}(1,1)}{\Delta R_i} = \frac{\theta(N+1,1)-\theta(N,1)}{\Delta\eta} \\ where.\ H(N+1,1) = \frac{\sinh(\eta_o)}{\cosh(\eta_i)-1} \end{array}\right\} \qquad (4.8)$$

$$
\left.
\begin{aligned}
&at\ R = NR_2\ and\ \zeta = \pi \\
&\theta(N+1, M+1) = \theta_{si}(1, M+1) \\
&KR * H(N+1, M+1)\frac{\theta_{si}(2,M+1)-\theta_{si}(1,M+1)}{\Delta R_i} = \frac{\theta(N+1,M+1)-\theta(N,M+1)}{\Delta\eta} \\
&where,\ H(N+1, M+1) = \frac{\sinh(\eta_o)}{\cosh(\eta_i)+1}
\end{aligned}
\right\} \quad (4.9)
$$

$$
\left.
\begin{aligned}
&at\ R = 1\ and\ \zeta = 0 \\
&\theta(1,1) = \theta_{so}(NSO+1, 1) \\
&KR * H(1,1)\frac{\theta_{so}(NSO+1,1)-\theta_{so}(NSO,1)}{\Delta R_o} = \frac{\theta(2,1)-\theta(1,1)}{\Delta\eta} \\
&where,\ H(1,1) = \frac{\sinh(\eta_o)}{\cosh(\eta_o)-1}
\end{aligned}
\right\} \quad (4.10)
$$

$$
\left.
\begin{aligned}
&at\ R = 1\ and\ \zeta = \pi \\
&\theta(1, M+1) = \theta_{so}(NSO+1, M+1) \\
&KR * H(1, M+1)\frac{\theta_{so}(NSO+1,M+1)-\theta_{so}(NSO,M+1)}{\Delta R_o} = \frac{\theta(2,M+1)-\theta(1,M+1)}{\Delta\eta} \\
&where,\ H(1, M+1) = \frac{\sinh(\eta_o)}{\cosh(\eta_o)+1}
\end{aligned}
\right\} \quad (4.11)
$$

The linking of the three grids is completed by applying two-way interpolation at both interfaces for the mesh points other than the above four. At both interfaces temperature at every mesh point of the bi-polar grid is evaluated using the temperatures at the two neighbouring mesh points of the cylindrical grid and at every point of the cylindrical grid using the temperatures at the two adjacent bi-polar

grid points. The X-coordinates of the grid points are used for this purpose. This interpolation can be expressed as follows (see Fig. 3.2):

fluid temperature at the outer interface :

$$\theta(1,J) = (\theta_{so}(NSO+1,JJ+1) - \theta_{so}(NSO+1,JJ))/(XSO(JJ+1) - XSO(JJ))*$$

$$(XFO(J) - XSO(JJ)) + \theta_{so}(NSO+1,JJ)$$

fluid temperature at the inner interface :

$$\theta(N+1,J) = (\theta_{si}(1,JJ+1) - \theta_{si}(1,JJ))/(XSI(JJ+1) - XSI(JJ))*$$

$$(XFI(J) - XSI(JJ)) + \theta_{si}(1,JJ)$$

solid temperature at the outer interface :

$$\theta_{so}(NSO+1,J) = (\theta(1,JJ+1) - \theta(1,JJ))/(XFO(JJ+1) - XFO(JJ))*$$

$$(XSO(J) - XFO(JJ)) + \theta(1,JJ)$$

solid temperature at the inner interface :

$$\theta_{si}(1,J) = (\theta(N+1,JJ+1) - \theta(N+1,JJ))/(XFI(JJ+1) - XFI(JJ))*$$

$$(XSI(J) - XFI(JJ)) + \theta(N+1,JJ)$$

where,

XFO *is the* $X-$*coordinate of bipolar grid points on the outer interface,*

XFI *is the* $X-$*coordinate of bipolar grid points on the inner interface,*

XSO *is the* $X-$*coordinate of cylindrical grid points on the outer interface.*

XSI *is the* $X-$*coordinate of cylindrical grid points on the inner interface.*

(4.12)

4.4 Method of Solution

The finite-difference equations (4.1) through (4.6) are linearized by assuming that where the product of two unknowns occurs one of them is given approximately by its value at the previous axial step, the variable superscripted with an asterisk (*). Moreover, in the finite-difference representation of the ζ-momentum equation, all the values of V have been deliberately taken at the previous axial step in order to make the equation locally (i.e. within one axial step) uncoupled from the continuity equation. Thus the finite-difference equations (4.1) to (4.6) represent a complete mathematical model of six equations in six unknowns (U,V,W,P,θ and θ_s) and are numerically solved in the manner described hereinafter. Due to symmetry, these equations need to be solved in only half the domain, i.e. for $0 \leq \zeta \leq \pi$. The variables U,V,W,θ and θ_s are computed, for a given axial location (Z), at the intersections of the grid lines, i.e., the mesh points.

For a fluid of a given Pr flowing in an annulus of given N and E, numerical solution of this set of equations is obtained by first calculating the corresponding values of η_i and η_o [1]. The inner radius of the outer tube is used as reference and hence $NR_3 = 1$. By selecting the number of increments in the η and ζ directions (N and M, respectively) the values of $\Delta\eta$ and $\Delta\zeta$ can be computed. Similarly, for the solid walls, by selecting the values of NR_1 and NR_4 and the number of radial (R) increments in the outer and inner walls and the number of increments in the

tangential (ϕ) directions (NSO, NSI and M, respctively) the values of ΔR_o, ΔR_i and $\Delta\phi$ can be determined.

Details of the numerical solution in the fluid annulus are given in [1]. However, they are summarized hereinafter. To solve for the two unknowns, P and U, at the first plane after the inlet cross section, the integral form of the continuity equation (4.5) and the finite-difference form of the axial momentum equation (4.3) are used. An extension to a special form of the Gauss-Jordan elimination scheme has been applied to solve the obtained matrix. The ζ - momentum equation (4.2) is then solved for W using Gauss-Seidel iteration and the continuity equation (4.1) is used to solve for V. Finally, the energy equations for the fluid (4.4) and solid (4.6) are simultaneously solved for the temperatures using Gauss-Seidel iteration. The simultaneous solution of equations (4.4) and (4.6) results in obtaining the unknown values of θ, θ_{so} and θ_{si} at the second cross-section. Repeating this procedure, we proceed downstream in the Z-direction until the flow becomes fully developed. Execution of the computer program is stopped when the maximum developing velocity becomes equal to 99 % of the maximum fully developed velocity as given by the analytical solution (eq. (3.9)).

Chapter 5

VALIDATION OF PRESENT COMPUTER CODE

To check the adequacy of the present computer code, special runs were made with very large values of conductivity ratio (KR) and very thin walls. For a typical large value of solid-fluid conductivity ratio (KR)=1000 and very thin walls corresponding to $NR_4 = 1.002$, $NR_1 = 0.499$, and $NR_2 = 0.5$ the results of the present computer code with E=0.5 and 0.6, for the fully developed heat transfer parameters, are in excellent agreement with the conventional case results [1, 14, 18]. The maximum deviation between the present results and those of [1], [14] and [18] are 0.05 %, 0.3 % and 1.4 %, respectively. Moreover, results for the fully developed heat transfer parameters, obtained by setting E=0.01 with the above-mentioned values of KR and NR_4 but with $NR_1 = 0.249$ and $NR_2 = 0.25$, are in good agreement with the

conventional solutions for the concentric case as reported in the literature [19]; the maximum deviation is about 2 %. Tables 5.1 and 5.2 give comparisons between the present numerical solutions and other corresponding conventional solutions available in the literature.

Results have been obtained using a grid of 20 segments in each of the η and ζ directions in the fluid annulus. For the solids, 20 segments were used in the tangential (ϕ) direction and 16 and 8 segments in the radial (R) direction for the outer and inner walls, respectively; the outer tube thickness being taken twice that of the inner one. Since very large gradients exist near the entrance, computations were made with very small axial steps near the entrance ($\Delta Z = 10^{-10}$); the axial step size being gradually increased several times as the flow moves downstream to reach a maximum value of $\Delta Z = 10^{-3}$ near full development. At 20% CPU share the time required for one run was about two hours and a half on an IBM RISC mainframe computer with AIX operating system. The machine has a RAM of 256 MB and a speed of 71.5 MHz.

To improve the agreement with the available solutions in the developing region and investigate the effect of mesh size on the results, special runs were done with N=M=30. Since M is the number of increments in both the ζ and the ϕ directions, higher value of M results in a finer mesh in both the fluid annulus and the solid walls. Due to memory limitations, N=M=30 with NSO=16 and NSI=8 is the finest mesh that can be used. With the finer mesh, N=M=30, the time increased eight-

TABLE 5.1 COMPARISONS WITH AVAILABLE CONVENTIONAL SOLUTIONS FOR CONCENTRIC ANNULI, NR1=0.249, NR2=0.25, NR4=1.002, KR=1000, E=0.01, Pr=0.72

RESULTS OF SHUMWAY AND McELIGOT [6]

	HFI		HFO		θm	
Z*	Ref.[6]	Present	Ref.[6]	Present	Ref.[6]	Present
0.01	8.05	7.555	0.0088	0.0227	0.0948	0.1041
0.05	5.31	5.268	0.641	0.6606	0.2533	0.2579
0.1	4.567	4.566	0.9735	0.977	0.312	0.3142

	NUII		NUOI	
Z*	Ref.[6]	Present	Ref.[6]	Present
0.01	8.892	8.432	0.0936	0.2179
0.05	7.112	7.098	2.53	2.562
0.1	6.639	6.658	3.12	3.109

FULLY DEVELOPED AXIAL PRESSURE GRADIENT (DPDZFD)

Ref.[19]	Present	
	Analatical	Numerical
46.604	46.917	45.983

RESULTS OF LUNDBERG ET. AL. AND WORSE-SCHMIDT AS REPORTED BY [19]

HFIFD		NUIFD		NUOFD		θm,fd	
Ref.[19]	Present	Ref.[19]	Present	Ref.[19]	Present	Ref.[19]	Present
4.328	4.414	6.471	6.553	3.267	3.204	0.3312	0.3264

HFI	HEAT FLUX ON THE INNER INTERFACE
HFO	HEAT FLUX ON THE OUTER INTERFACE
NUII	NUSSELT NUMBER ON THE INNER INTERFACE
NUOI	NUSSELT NUMBER ON THE OUTER INTERFACE
θm	MIXED-MEAN TEMPERATURE
θm,fd	FULLY DEVELOPED MIXED-MEAN TEMPERATURE
HFIFD	FULLY DEVELOPED VALUE OF HFI
NUIFD	FULLY DEVELOPED VALUE OF NUII
NUOFD	FULLY DEVELOPED VALUE OF NUOI

TABLE 5.2 COMPARISONS WITH AVAILABLE RESULTS FOR ECCENTRIC ANNULI, NR1=0.499, NR2=0.5, NR4=1.002, KR=1000

RESULTS OF TIEDT AS REPORTED BY [19] FOR E=0.6, Pr=0.7

DPDZFD		
Tiedt	Present	
	Analytical	Numerical
31.818	31.963	32.207

RESULTS OF TROMBETTA [14] FOR E=0.6, Pr=0.7

HFIFD		NUIFD		NUOFD	
Trombetta	Present	Trombetta	Present	Trombetta	Present
3.582	3.593	5.746	5.738	4.754	4.762

RESULTS OF FELDMAN ET AL. [18] FOR E=0.5, Pr=1.0

DPDZFD		
Feldman	Present	
	Analytical	Numerical
35.34	35.49	35.73

θm,fd		NUIFD		NUOFD	
Feldman	Present	Feldman	Present	Feldman	Present
0.3848	0.3793	5.39	5.383	4.308	4.318

	θm		NUII		NUOI	
Z*	Feldman	Present	Feldman	Present	Feldman	Present
0.001	0.0362	0.0416	13.08	15.119	0.00042	0.00008
0.01	0.1319	0.1526	6.858	7.668	3.46	1.537
0.1	0.3209	0.3517	5.184	5.35	4.601	4.334

HFI	HEAT FLUX ON THE INNER INTERFACE
HFO	HEAT FLUX ON THE OUTER INTERFACE
NUII	NUSSELT NUMBER ON THE INNER INTERFACE
NUOI	NUSSELT NUMBER ON THE OUTER INTERFACE
θm	MIXED-MEAN TEMPERATURE
θm,fd	FULLY DEVELOPED MIXED-MEAN TEMPERATURE
HFIFD	FULLY DEVELOPED VALUE OF HFI
NUIFD	FULLY DEVELOPED VALUE OF NUII
NUOFD	FULLY DEVELOPED VALUE OF NUOI

fold requiring 24 hours at the same (20 %) CPU share. However, the difference in the values of the results for the two mesh sizes was not significant for the fully developed heat transfer parameters (maximum 3 %) and therefore the former mesh (N=M=20) was used for all computations Tables 5.3 and 5.4 give comparisons with available results for simultaneously developing flow for the two mesh sizes.

Table 5.3 clearly demonstrates that the agreement with the results of **Shumway and McEligot [6]** is significantly improved with the finer mesh. However, Table 5.4 indicates that there is no improvemnt in agreement with the results of **Feldman et.al [18]**. It seems that the two-equation hydrodynamic model of Feldman et. al, which uses a hypothesis to relate the radial-like and tangential-like velocity components, is not accurately describing the hydrodynamics in the developing flow region.

TABLE 5.3 COMPARISON WITH RESULTS OF SHUMWAY & McELIGOT [6] FOR DEVELOPING FLOW IN CONCENTRIC ANNULI NR1=0.249, NR2=0.25, NR4=1.002, KR=1000, E=0.01, Pr=0.72

HFI

		Shumway	Present for two mesh sizes			
Z	Z*	McEligot	20 X 20	% DIFF.	30 X 30	% DIFF.
0.0072	0.01	8.05	7.555	6.15	7.837	2.65
0.018	0.025	6.383	6.251	2.07	6.346	0.58
0.036	0.05	5.31	5.268	0.79	5.326	0.30

HFO

		Shumway	Present for two mesh sizes			
Z	Z*	McEligot	20 X 20	% DIFF.	30 X 30	% DIFF.
0.0072	0.01	0.0088	0.0227	157.95	0.0181	105.68
0.018	0.025	0.2294	0.2671	16.43	0.2463	7.37
0.036	0.05	0.641	0.6606	3.06	0.6405	0.08

θm

		Shumway	Present for two mesh sizes			
Z	Z*	McEligot	20 X 20	% DIFF.	30 X 30	% DIFF.
0.0072	0.01	0.0948	0.1041	9.81	0.0995	4.96
0.018	0.025	0.1744	0.1824	4.59	0.1773	1.66
0.036	0.05	0.2533	0.2579	1.82	0.2535	0.08

NUII

		Shumway	Present for two mesh sizes			
Z	Z*	McEligot	20 X 20	% DIFF.	30 X 30	% DIFF.
0.0072	0.01	8.892	8.432	5.17	8.703	2.13
0.018	0.025	7.731	7.646	1.10	7.714	0.22
0.036	0.05	7.112	7.098	0.20	7.135	0.32

NUOI

		Shumway	Present for two mesh sizes			
Z	Z*	McEligot	20 X 20	% DIFF.	30 X 30	% DIFF.
0.0072	0.01	0.0936	0.217	131.84	0.1817	94.12
0.018	0.025	1.315	1.464	11.33	1.389	5.63
0.036	0.05	2.53	2.562	1.26	2.526	0.16

HFI	HEAT FLUX ON THE INNER INTERFACE
HFO	HEAT FLUX ON THE OUTER INTERFACE
NUII	NUSSELT NUMBER ON THE INNER INTERFACE
NUOI	NUSSELT NUMBER ON THE OUTER INTERFACE
θm	MIXED-MEAN TEMPERATURE

**TABLE 5.4 COMPARISON WITH RESULTS OF FELDMAN [18]
FOR DEVELOPING FLOW IN ECCENTRIC ANNULI
NR1=0.499, NR2=0.5, NR4=1.002, KR=1000 E=0.5, Pr=1.0**

θm					
	Feldman	Present for two mesh sizes			
Z*		20 X 20	% DIFF.	30 X 30	% DIFF.
0.001	0.0362	0.0416	14.92	0.0433	19.61
0.01	0.1313	0.1526	16.22	0.1495	13.86
0.1	0.3203	0.3517	9.80	0.3486	8.84
NUII					
	Feldman	Present for two mesh sizes			
Z*		20 X 20	% DIFF.	30 X 30	% DIFF.
0.001	13.08	15.119	15.59	14.959	14.37
0.01	6.858	7.668	11.81	7.776	13.39
0.1	5.184	5.35	3.20	5.34	3.01
NUOI					
	Feldman	Present for two mesh sizes			
Z*		20 X 20	% DIFF.	30 X 30	% DIFF.
0.001	0.00042	0.00008	80.95	0.00007	83.33
0.01	3.46	1.537	55.58	1.504	56.53
0.1	4.601	4.334	5.80	4.35	5.46

θm	MIXED-MEAN TEMPERATURE
NUII	NUSSELT NUMBER ON THE INNER INTERFACE
NUOI	NUSSELT NUMBER ON THE OUTER INTERFACE
z	AXIAL DISTANCE MEASURED FROM THE INLET
Z	DIMENSIONLESS AXIAL COORDINATE = z/(ReDh)
Z*	MODIFIED Z = Z/Pr = z/(ReDhPr)

Chapter 6

RESULTS AND DISCUSSION FOR CRITICAL CONDUCTIVITY RATIO

6.1 Introduction

Six controlling parameters are explicitly required to solve the problem under consideration. These are: the annulus radius ratio (NR_2), the dimensionless eccentricity (E), the outer wall radius ratio (NR_4), the inner wall radius ratio (NR_1), the solid-fliud conductivity ratio (KR) and the Prandtl number (Pr). In this part of the study, computations were carried out for a fluid of Pr=0.7 in an annulus of radius ratio $NR_2 = 0.5$ with $NR_4 = 1.2$ and $NR_1 = 0.4$ for values of E=0.1, 0.3, 0.5 and 0.7

and KR=1, 10, 50, 100 and 1000. The reason for the selection of $NR_2 = 0.5$ is that most of the results in the literature for the conventional problem (i.e., neglecting the effect of conjugation) are reported for this particular value, which represents a typical annular geometry. The selected values of NR_4 and NR_1 are typical practical values as can be seen from Table 6.1 which lists some values of radius ratios for possible combination of inner / outer standard steel pipes. Table 6.2 indicates practical values of the solid-fluid conductivity ratio KR and displays the wide possible range.

Results and discussion for the heat transfer parameters are given in the following sections. Since the annulus radius ratio is fixed ($NR_2 = 0.5$), the hydrodynamics is unaffected for a given eccentricity as KR is varied. Effect of varying the eccentricity on the hydrodynamics is discussed in detail in [28] and will not be given here. However, the effect of eccentricity and KR on the heat transfer parameters is presented hereinafter. The chapter concludes with results for the critical conductivity ratio beyond which the conjugate effect can be neglected, presented both graphically and in the form of a table.

6.2 Results and Discussion

6.2.1 Temperature profiles across the annulus

Figures 6.1 and 6.2 show the developing temperature profiles, corresponding to different values of Z, across the narrowest and the widest gaps, respectively, for KR=1

TABLE 6.1 RADIUS RATIOS FOR STANDARD STEEL PIPES

NOMINAL SIZE (INCH)		RADIUS RATIOS				DIMENSIONLESS TUBE THICKNESS	
INNER	OUTER	ASTM Schedule #	NR1	NR2	NR4	INNER	OUTER
1/4	1	Sch. 40	0.35	0.51	1.25	0.17	0.25
		Sch. 80	0.32	0.56	1.37	0.25	0.37
3/8	1 1/4	Sch. 40	0.36	0.49	1.20	0.13	0.20
		Sch. 80	0.33	0.53	1.30	0.20	0.30
1/2	1 1/2	Sch. 40	0.39	0.52	1.18	0.14	0.18
		Sch. 80	0.36	0.56	1.27	0.20	0.27
3/4	2	Sch. 40	0.40	0.51	1.15	0.11	0.15
		Sch. 80	0.38	0.54	1.22	0.16	0.22
1	2 1/2	Sch. 40	0.42	0.53	1.16	0.11	0.16
		Sch. 80	0.41	0.57	1.24	0.15	0.24
1 1/2	4	Sch. 40	0.40	0.47	1.12	0.07	0.12
		Sch. 80	0.39	0.50	1.18	0.10	0.18

TABLE 6.2 COMMON VALUES OF KR

MATERIAL	THER. CONDUCTIVITY (W/M-°C)
AIR @ 300 K	0.02624
CARBON STEEL (1% C)	43
WATER - SATURATED @ 300 K	0.613
CAST IRON (4% C) @ 293 K	52
ENGINE OIL (SAE 50) @ 293 K	0.145
ALUMINUM METAL @ 293 K	236
ASBESTOS @ 273 K	0.154
PLASTIC	0.48

SOLID - FLUID CONDUCTIVITY RATIO - KR			
	AIR	WATER	OIL
ALUMINUM	8993.90	384.99	1627.59
CAST IRON	1981.71	84.83	358.62
STEEL	1638.72	70.15	296.55
PLASTIC	18.29	0.78	3.31
ASBESTOS	5.87	0.25	1.06

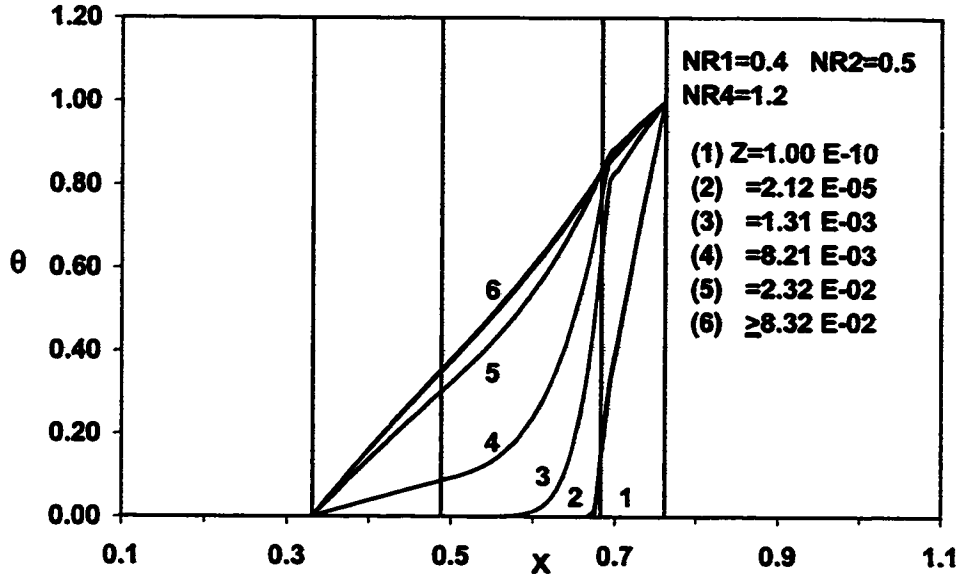

FIG. 6.1: Developing temperature profiles across the narrowest gap. E=0.5 and KR=1.

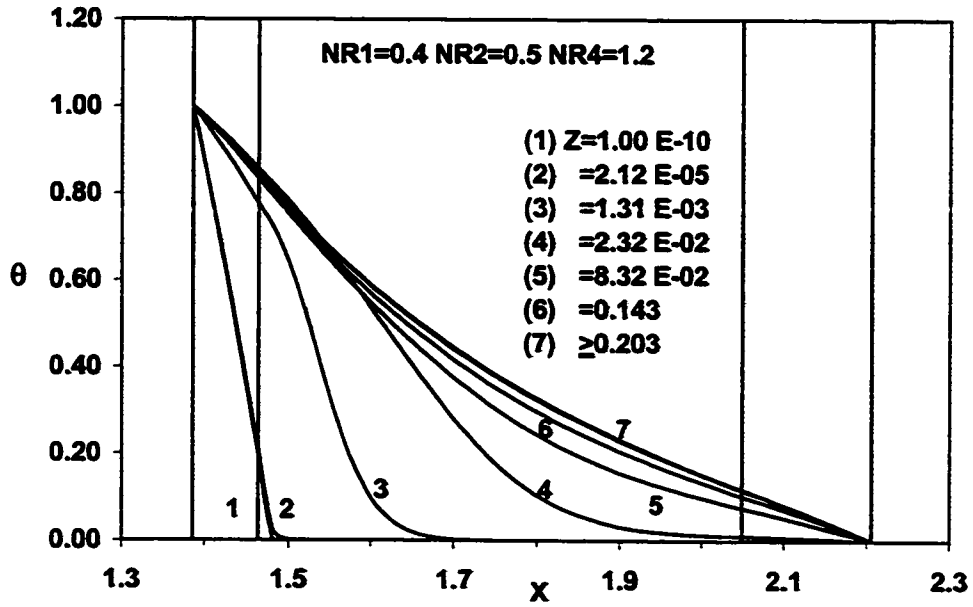

FIG. 6.2: Developing temperature profiles across the widest gap. E=0.5 and KR=1.

and E=0.5. It is noticed that full development is reached significantly faster across the narrowest gap (Z=0.0832) as compared to the widest gap (Z=0.203). This is expected because the eccentricity leads to a reduced overall thermal resistance across the narrowest gap resulting in the heat signal being sensed relatively earlier. Figures 6.3 and 6.4 show the developing temperature profiles for KR=10 and Figs. 6.5 and 6.6 for KR=100. The increase in the value of KR results in lower temperature drop across the solid walls. Also, the increase in KR accelerates heating of the fluid adjacent to the inner interface near the entrance but fluid adjacent to the outer wall remains unaffected. It can also be noticed from these figures, particularly at the widest gap, that the fluid temperature near the inner wall reaches a maximum before full development is attained and then decreases slightly. This is because close to the entrance heat loss through the ambient wall is absent with the adjacent fluid also at ambient temperature which results in more heat being gained by the fluid. Further downstream, as heat loss through the outer wall initiates with rise in the the adjacent fluid temperature, the temperature of fluid close to the inner wall is pulled down slightly. This can also be seen in Fig. 6.23 which gives the axial distribution of temperatures at the inner interface.

Each pair of Figs. 6.7-6.14 displays the variation with KR, of the fully developed temperature profile across the narrowest and the widest gaps in the same annulus ($NR_1 = 0.4$, $NR_2 = 0.5$ and $NR_4 = 1.2$) but for E=0.1, 0.3, 0.5 and E=0.7, respectively. It is obvious that increasing the value of KR results in smaller

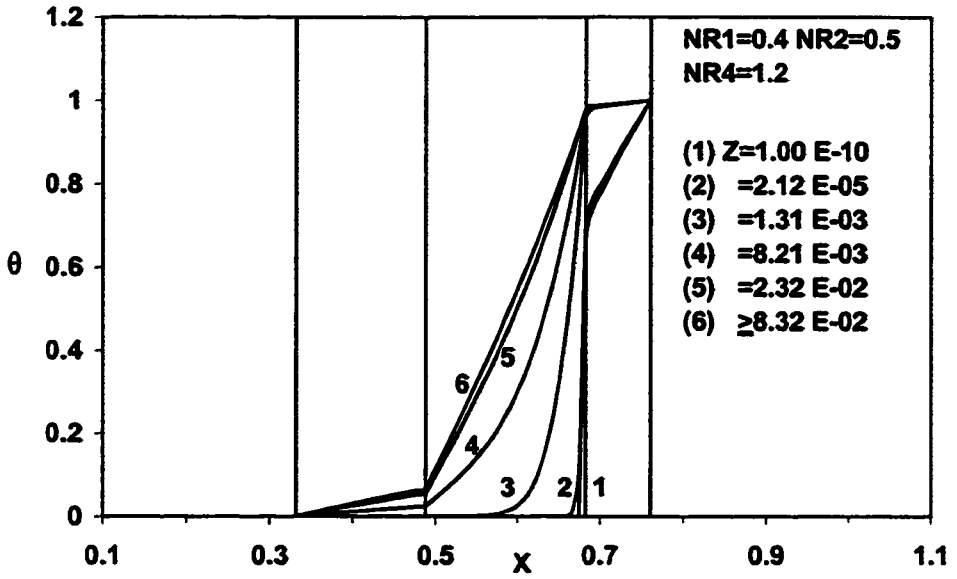

FIG. 6.3: Developing temperature profiles across the narrowest gap. E=0.5 and KR=10.

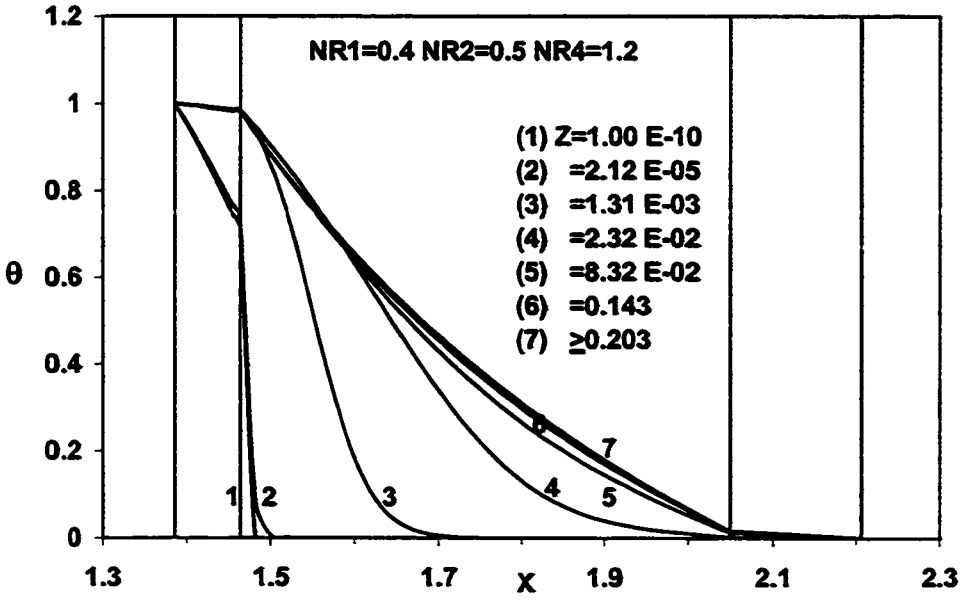

FIG. 6.4: Developing temperature profiles across the widest gap. E=0.5 and KR=10.

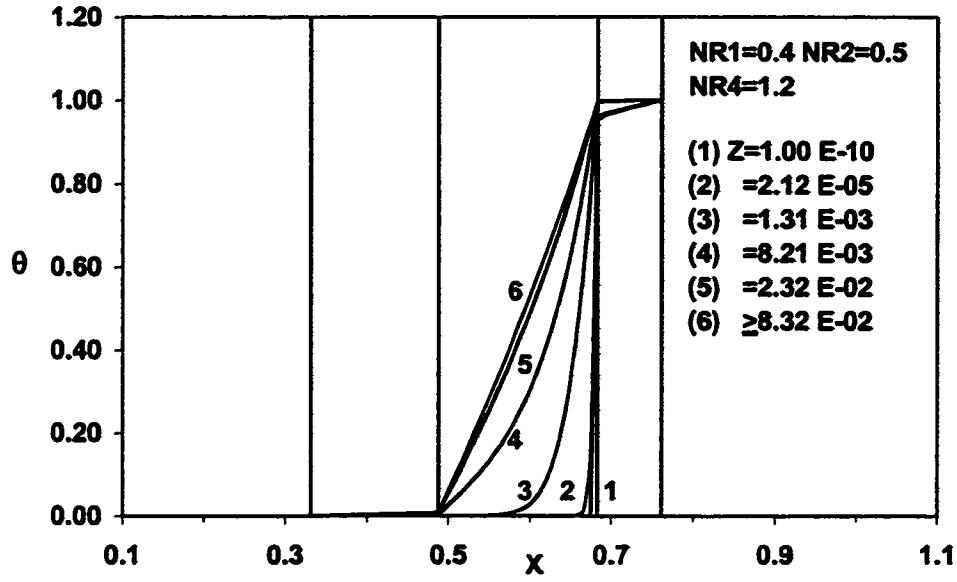

FIG. 6.5: Developing temperature profiles across the narrowest gap. E=0.5 and KR=100.

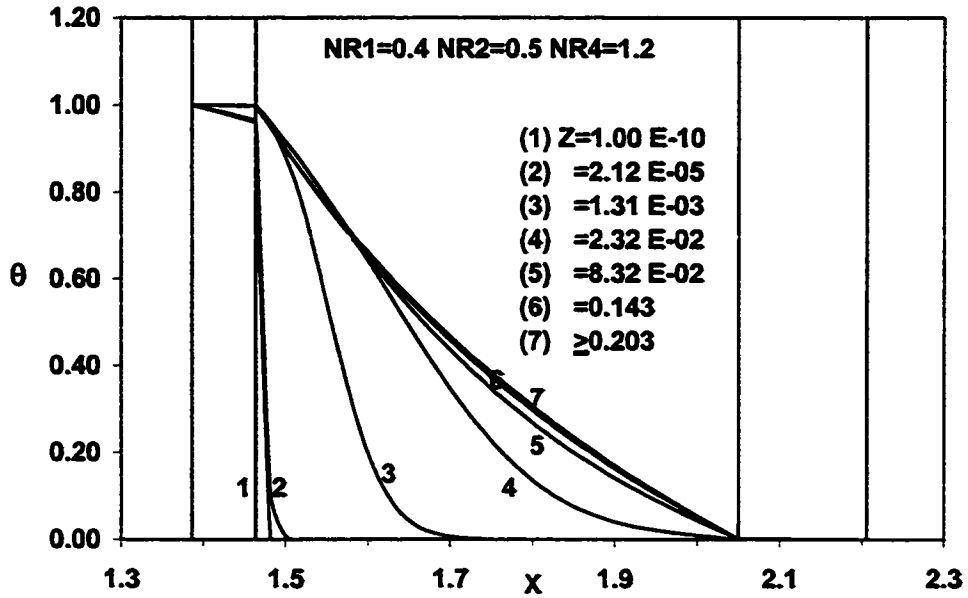

FIG. 6.6: Developing temperature profiles across the widest gap. E=0.5 and KR=100.

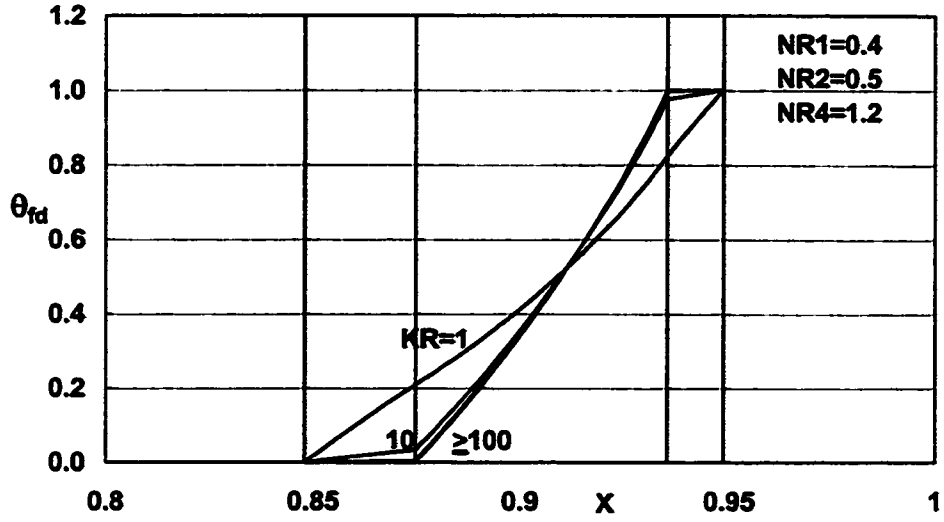

FIG. 6.7: Effect of KR on the fully developed temperature profile across the narrowest gap for E=0.1.

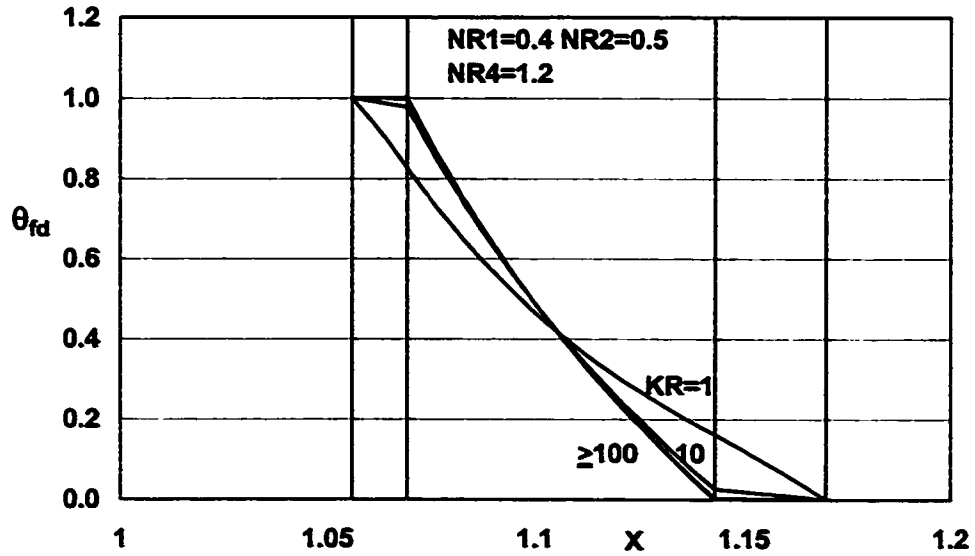

FIG. 6.8: Effect of KR on the fully developed temperature profile across the widest gap for E=0.1.

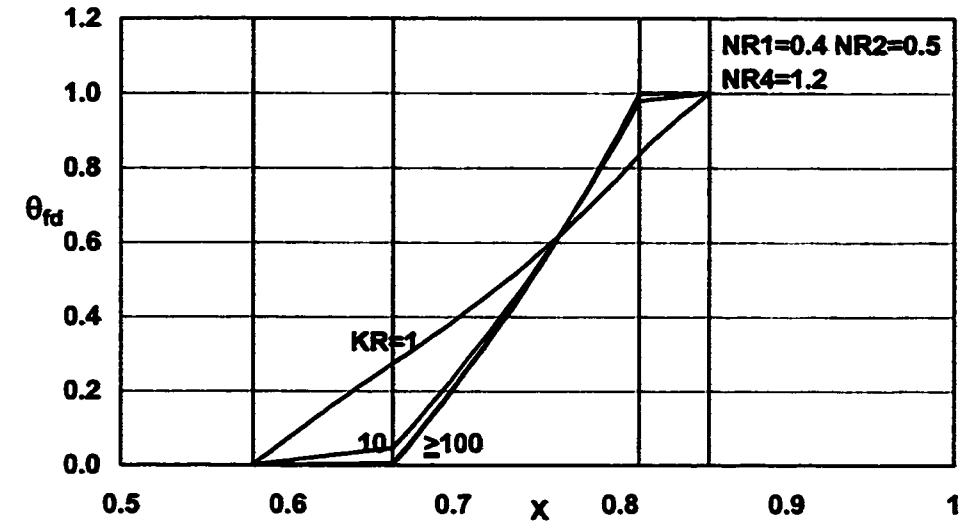

FIG. 6.9: Effect of KR on the fully developed temperature profile across the narrowest gap for E=0.3.

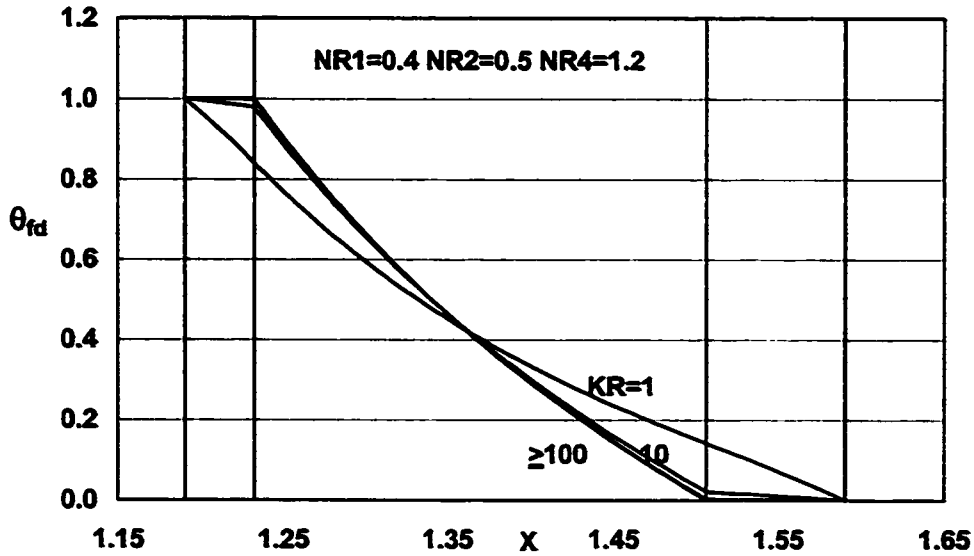

FIG. 6.10: Effect of KR on the fully developed temperature profile across the widest gap for E=0.3.

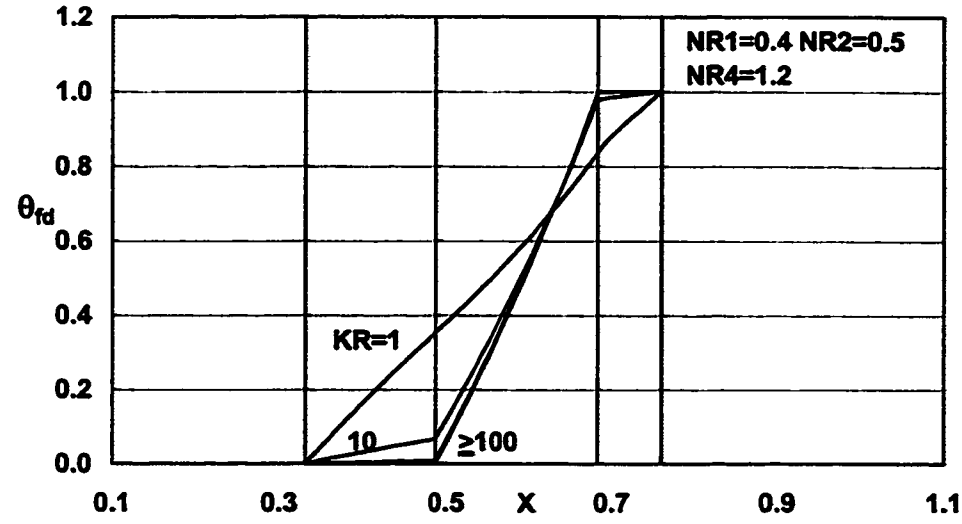

FIG. 6.11: Effect of KR on the fully developed temperature profile across the narrowest gap for E=0.5.

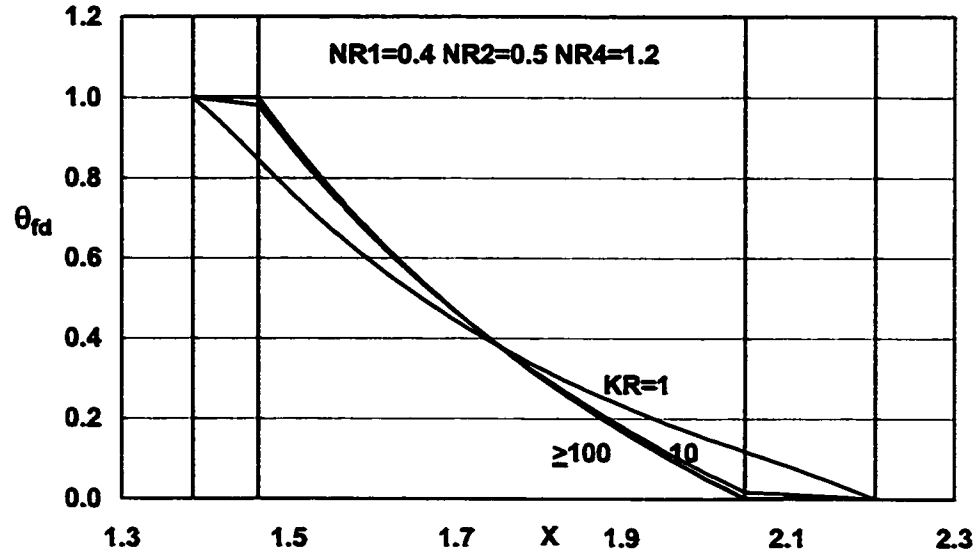

FIG. 6.12: Effect of KR on the fully developed temperature profile across the widest gap for E=0.5.

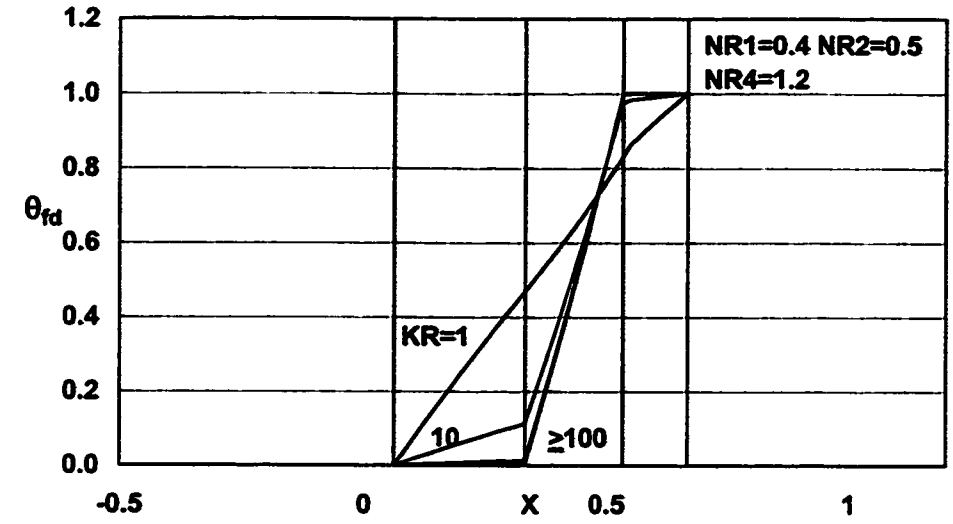

FIG. 6.13: Effect of KR on the fully developed temperature profile across the narrowest gap for E=0.7.

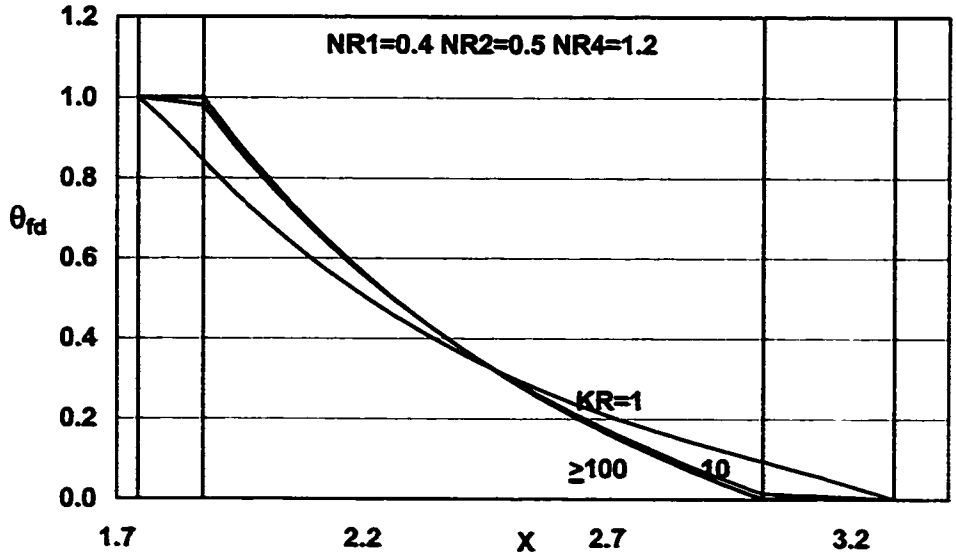

FIG. 6.14: Effect of KR on the fully developed temperature profile across the widest gap for E=0.7.

temperature drop across the solid walls. The effect of increasing eccentricity is a steeper temperature profile across the narrowest gap and a flatter one across the widest gap. For a given value of KR, increasing the eccentricity results in increase in the temperature on the outer interface at the narrowest gap and vice versa at the widest gap, thus leading to greater circumferential temperature variation. The effect on the temperature at the inner interface is not appreciable in these figures and will be shown in the following section.

6.2.2 Interfacial temperatures

Figures 6.15 and 6.16 give the effect of eccentricity, at KR=10, on the fully developed circumferential temperature variations at the outer and the inner interface respectively. The figures indicate how the increase in the value of the eccentricity enhances the circumferential variation of temperature. The increased circumferential temperature variation at the interfaces results in increased deviation from the conventional case with isothermal boundaries; thus consideration of conjugation is more important at higher eccentricities. It can be observed from Figs. 6.15 and 6.16 that the higher the value of E, the higher the temperature at the narrowest gap (Ψ=1) on the outer interface, and at the widest gap (Ψ=0) on the inner interface. Moreover, the higher the value of E, the higher the circumferential variation of temperature on either interface (i.e., higher circumferential temperature gradient). Consequently, the higher the value of E, the larger the circumferential heat flow.

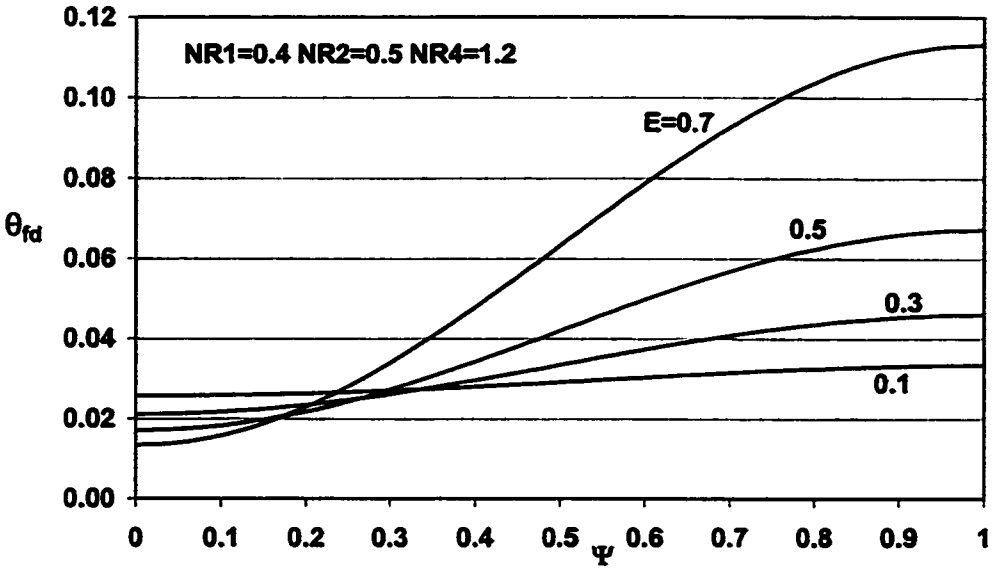

FIG. 6.15: Effect of the eccentricity on the circumferential temperature variation at the outer interface for KR=10.

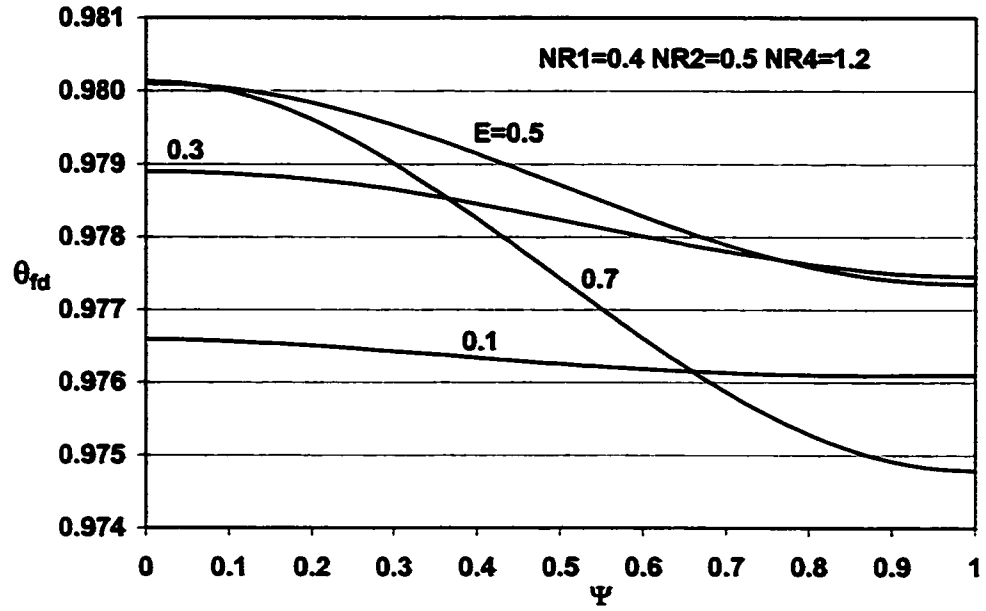

FIG. 6.16: Effect of the eccentricity on the circumferential temperature variation at the inner interface for KR=10.

The circumferential heat flow on the inner interface is in the positive ζ-direction (i.e., from the widest to the narrowest gap side). However, it is in the opposite direction (the negative ζ-direction) on the outer interface.

Figures 6.17 and 6.18 also show the effect of eccentricity on the circumferential temperature distributions at the outer and the inner interface, respectively, for KR=100. The trend is the same as for the previous two figures except that the higher value of KR results in higher temperatures (but smaller circumferential variation) at the inner interface and lower temperatures (and smaller circumferential variation) at the outer interface.

Figure 6.19 gives the effect of KR, for E=0.3 and 0.7, on the fully developed circumferential temperature variation at the outer interface and Fig. 6.20 shows such an effect at the inner interface for E=0.3. The figures indicate how the decrease in the value of KR enhances the circumferential variation of temperature at both interfaces in addition to raising the temperature at the outer interface and vice versa on the inner interface. The increased circumferential temperature variation at the interfaces results in increased deviation from the conventional case with isothermal boundaries. Figures 6.21 and 6.22 show the effect of KR, on the fully developed circumferential temperature variation at the outer and the inner interface, respectively, for E=0.5. The increase in circumferential variation of temperature with the decrease in the value of KR, as discussed earlier, can be noticed.

The above discussion is further supplemented by observing the effect of the

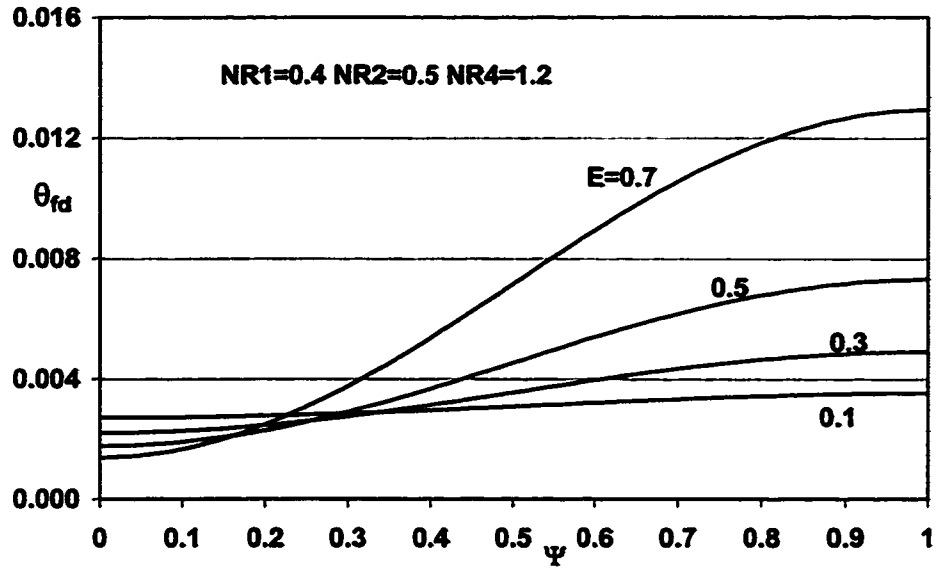

FIG. 6.17: Effect of the eccentricity on the circumferential temperature variation at the outer interface for KR=100.

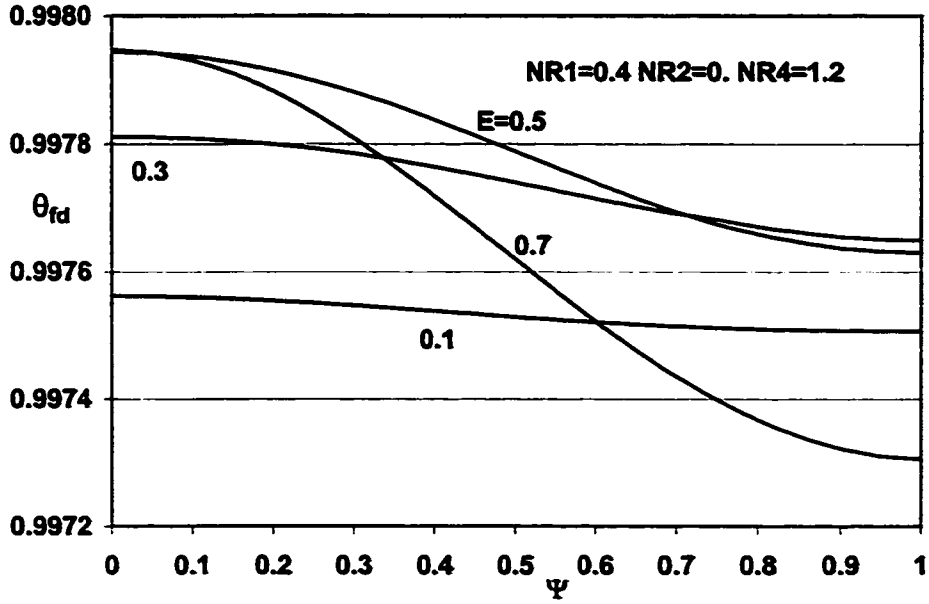

FIG. 6.18: Effect of the eccentricity on the circumferential temperature variation at the inner interface for KR=100.

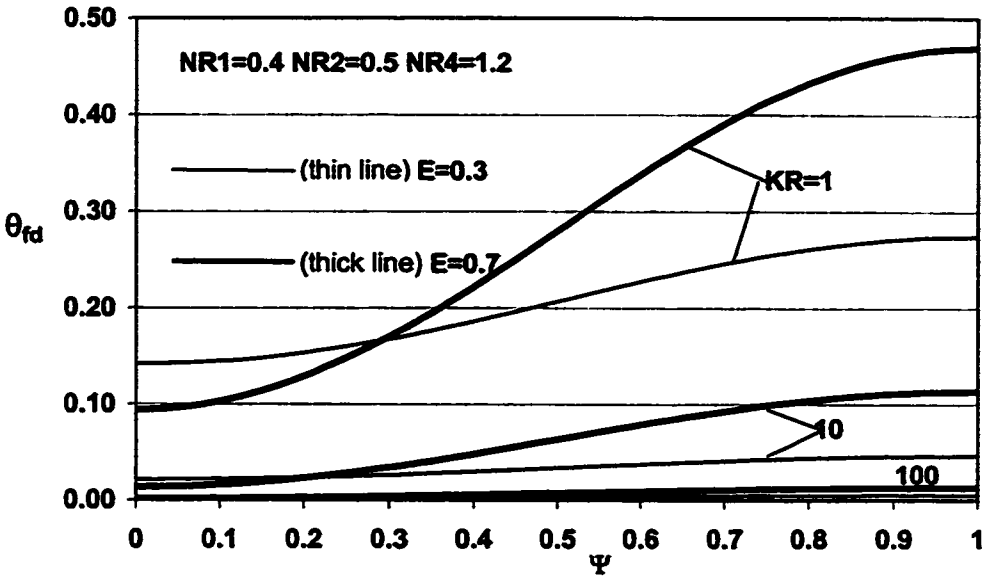

FIG. 6.19: Effect of KR on the circumferential temperature variation at the outer interface for two selected values of E.

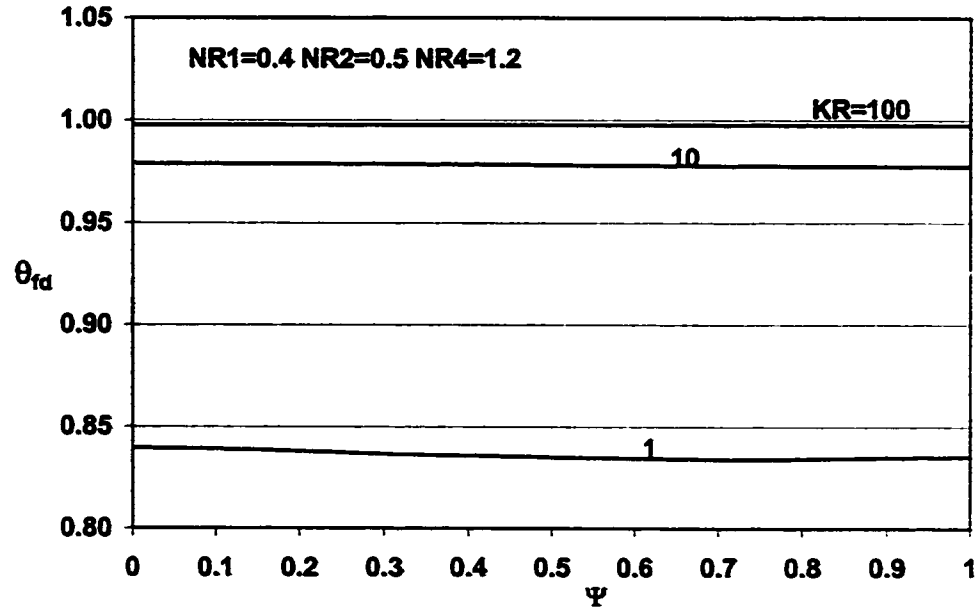

FIG. 6.20: Effect of KR on the circumferential temperature variation at the inner interface for E=0.3.

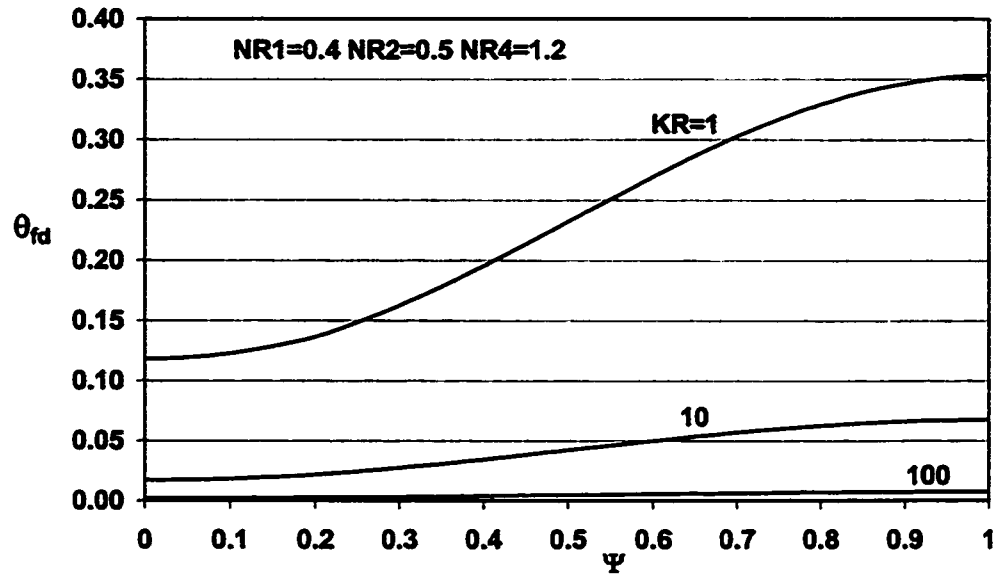

FIG. 6.21: Effect of KR on the circumferential temperature variation at the outer interface for E=0.5.

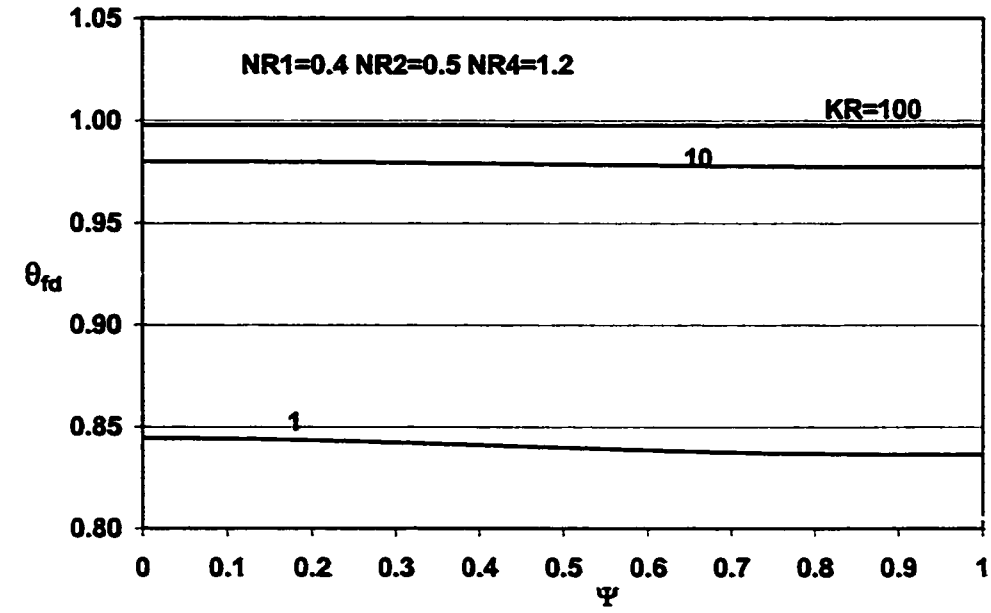

FIG. 6.22: Effect of KR on the circumferential temperature variation at the inner interface for E=0.5.

controlling parameters on the axial distribution of the interfacial temperatures at the four points of intersection of the interfaces with the line of symmetry. Figures 6.23 and 6.24 give this distribution for E=0.5 and both KR=10 and 100, on the inner and outer interface, respectively, at both the narrowest and widest gaps. As discussed in the foregoing paragrahs, the higher value of KR results in higher temperatures but smaller circumferential variation at the inner interface. At the outer interface, increase in the value of KR leads to lower temperatures and smaller circumferential variation. It can be noticed from Fig. 6.23 that at the inner interface temperatures reach a maximum before full development when the fluid near the outer wall is still near ambient temperature. However, with the rise in fluid temperature adjacent to the outer interface, the heat loss through the outer wall initiates, thus pulling down slightly the temperature of fluid close to the inner interface. This phenomenon can also be observed in Figs. 6.1 through 6.6 which depict the developing profiles; particularly the temperature profile number (4) overshoots, near the inner wall, the downstream profiles number (5), (6) and (7), in Figs. 6.2, 6.4 and 6.6.

Figures 6.25 and 6.26 give the axial distribution of the interfacial temperature for KR=10 and two values of the dimensionless eccentricity, at the inner and outer interface, respectively, at both the narrowest and the widest gaps. It can be observed that for the inner interface the temperature, for both values of E, is higher at the widest gap but it is higher at the narrowest gap for the outer interface, thus giving rise to circumferential heat flows in opposing directions as discussed earlier.

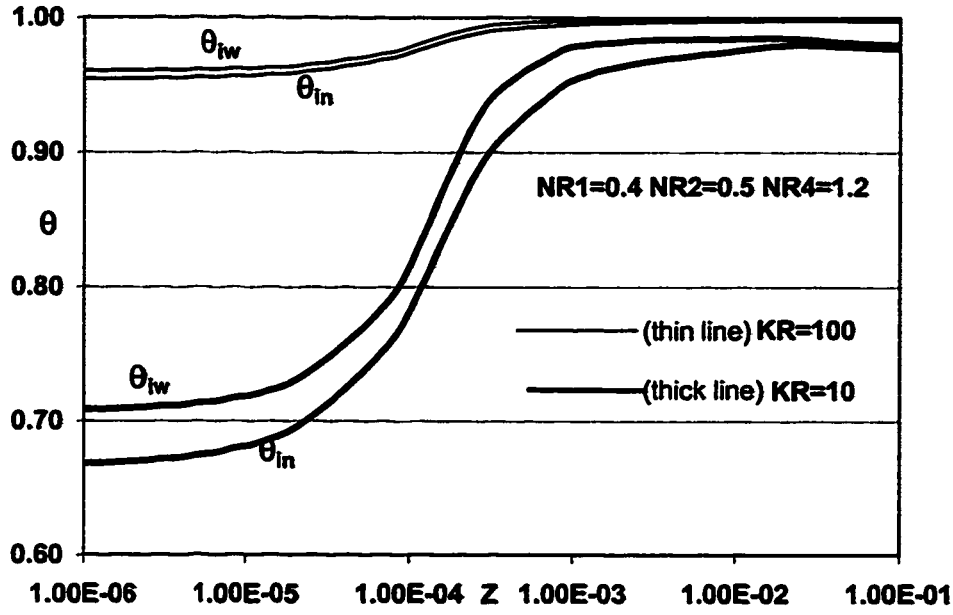

FIG. 6.23: Effect of KR on the axial variation of the temperature on the inner interface at the narrowest and widest gaps for E=0.5.

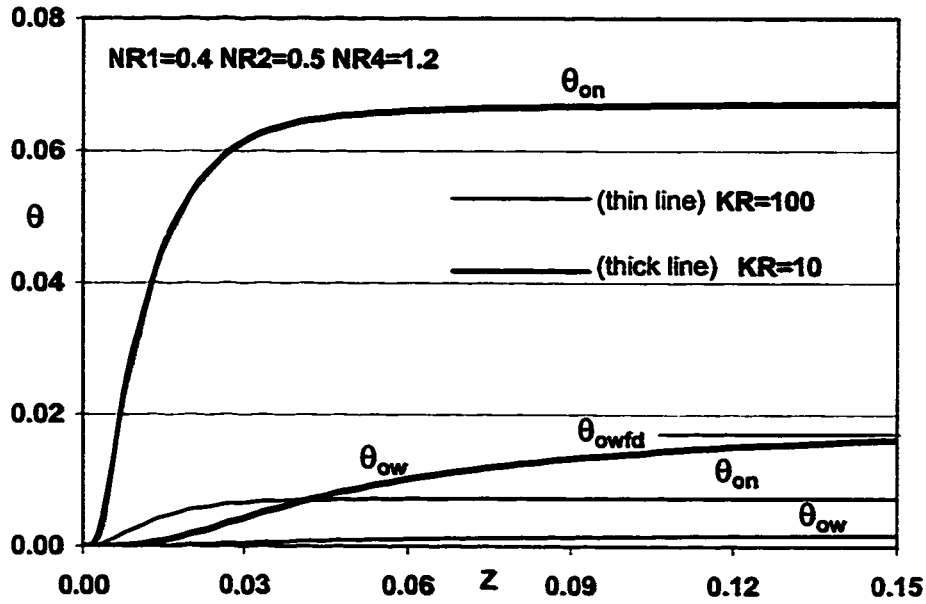

FIG. 6.24: Effect of KR on the axial variation of the temperature on the outer interface at the narrowest and widest gaps for E-0.5.

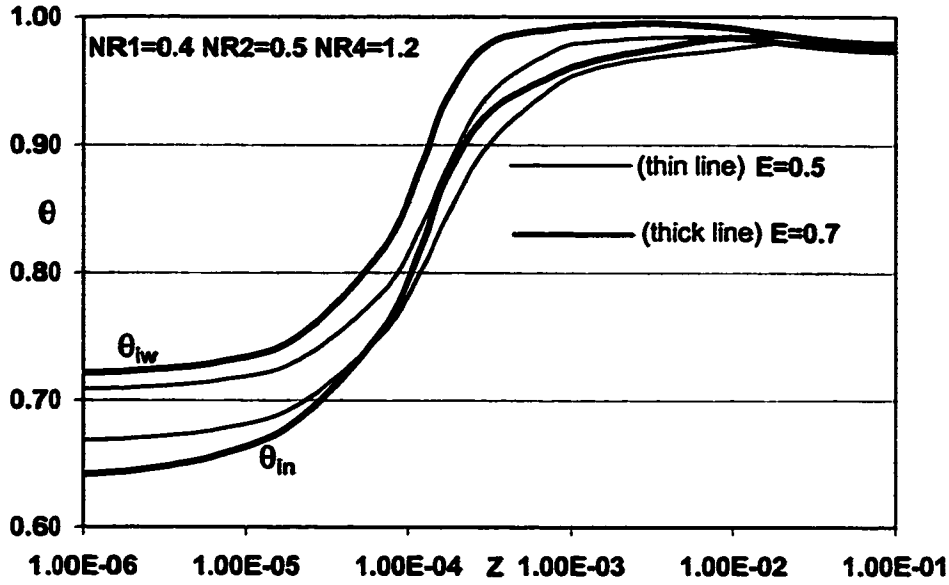

FIG. 6.25: Effect of the eccentricity on the axial variation of the temperature on the inner interface at the narrowest and widest gaps for KR=10.

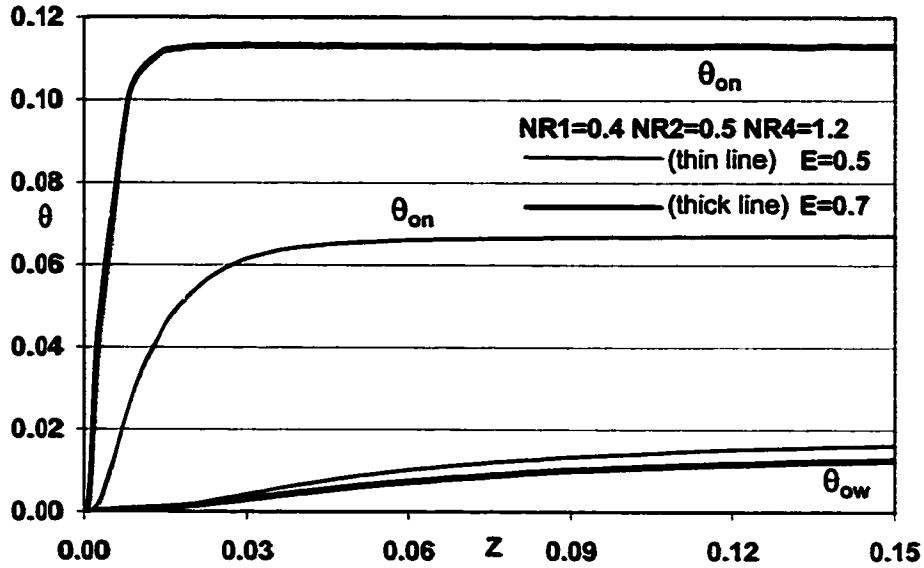

FIG. 6.26: Effect of the eccentricity on the axial variation of the temperature on the outer interface at the narrowest and widest gaps for KR=10.

Further more, the increase in the value of the eccentricity results in the inner interface temperature being raised at the widest gap and lowered at the narrowest gap, thus enhancing the circumferential variation and making the conjugate effect more significant. Circumferential temperature variation is also enhanced at the outer interface with increase in the eccentricity but with a rise in temperature at the narrowest gap and a decrease in the temperature at the widest gap.

6.2.3 Interfacial heat flux

Figures 6.27 and 6.28 show, respectively, the effect of KR (at E=0.5) and the eccentricity (at KR=10 and 100) on the axial distribution of the peripherally averaged heat flux on the inner interface. Figure 6.23 indicates that increasing KR results in an increase in the values of the heat flux, approaching almost the corresponding values of the conventional case at KR=100 (with a maximum deviation of 0.5 % based on the conventional case results). Figure 6.28 highlights that the heat flux increases with E and KR.

Figures 6.29 and 6.30 show, respectively, the effect of KR (at E=0.5) and the eccentricity (at KR=10 and 100) on the axial variation of the peripherally averaged heat flux on the outer interface. The negative sign indicates that heat is lost from the fluid at the outer interface. Figure 6.29 indicates that increasing the value of KR results in an increase in the heat lost from the fluid through the outer wall and Fig. 6.30 highlights that such a negative heat flux increases with both E and KR. It

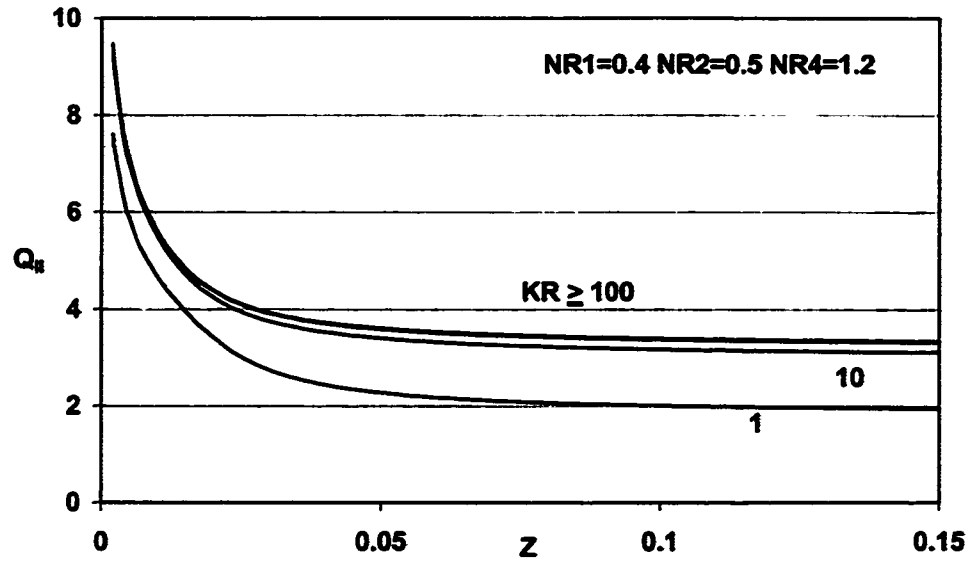

FIG. 6.27: Effect of KR on the axial variation of the circumferentially averaged heat flux at the inner interface for E=0.5.

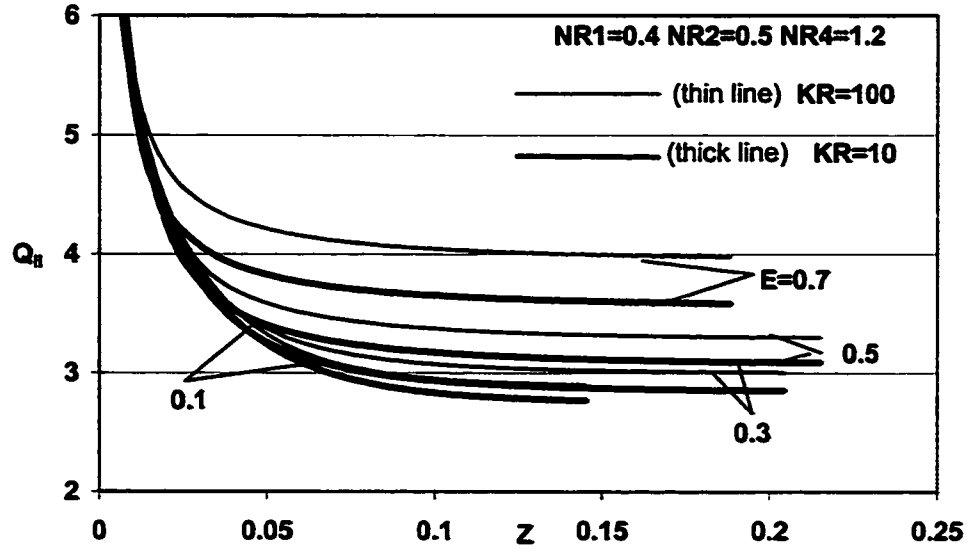

FIG. 6.28: Effect of the eccentricity on the axial variation of the circumferentially averaged heat flux at the inner interface for KR=10 and KR=100.

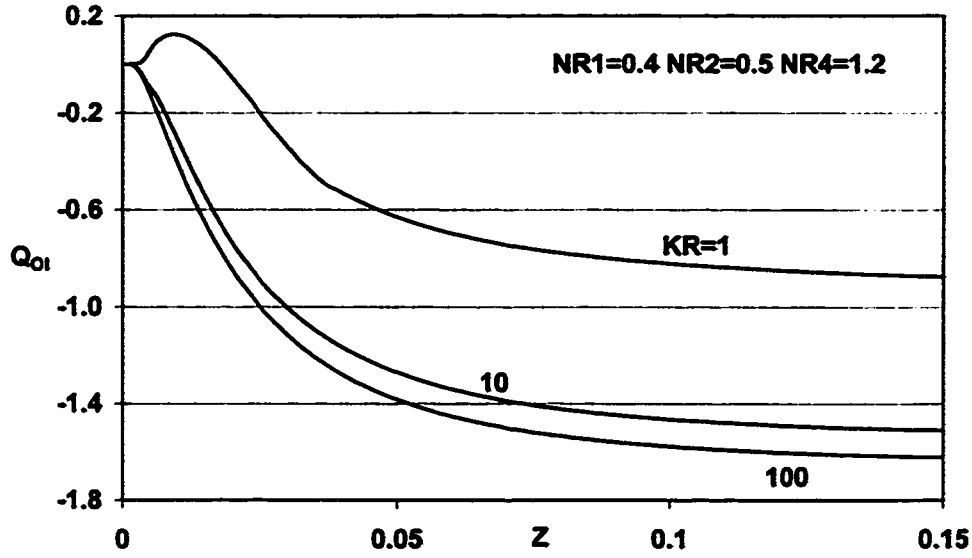

FIG. 6.29: Effect of KR on the axial variation of the circumferentially averaged heat flux on the outer interface for E=0.5.

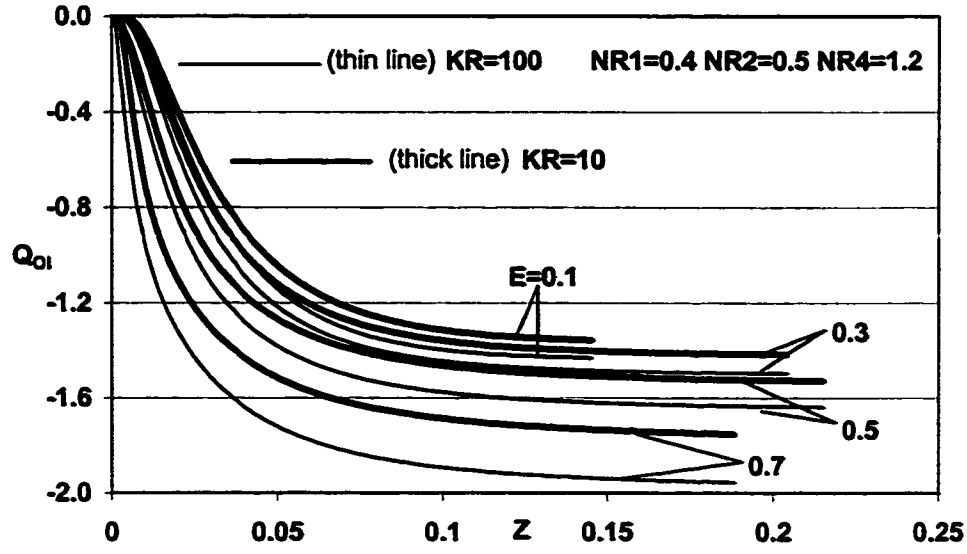

FIG. 6.30: Effect of the eccentricity on the axial variation of the circumferentially averaged heat flux on the outer interface for KR=10 and KR=100.

can be seen from Fig. 6.29 that close to the entrance the heat flux is zero because the fluid near the outer interface has not sensed the heat signal yet and is still at the ambient temperature. Just a little downstream the heat loss initiates due to the rise in the fluid temperature. It can be observed that for KR=1 the heat flux is positive for a short axial length. This is because the heat crossing the narrowest gap has been transmitted circumferentially within the outer wall to the widest gap side thus raising the outer interface temperature above ambient while the adjacent fluid is still at the ambient temperature. This results in a positive value of the circumferentially averaged heat flux. Further downstream, with convection in the fluid becoming dominant, the fluid temperature rises above the outer interface temperature near the widest gap and the heat flux becomes negative. For higher values of KR ($\geq$ 10), i.e., lower fluid conductivity, the heat diffusion across the narrowest gap within the fluid is reduced and convection becomes dominant thus the phenomenon observed for KR=1 is suppressed.

Figures 6.31 and 6.32 show the axial distribution of the local heat flux for E=0.5 and both KR=10 and 100, at the intersections of the symmetry line with the inner and the outer interface, respectively. At both interfaces, the local heat flux is of a higher magnitude at the narrowest gap. This is because the temperature profile is much steeper across the narrowest gap as compared to that across the widest gap. Moreover, the increase in the value of KR leads to higher local heat flux at the narrowest gap but the local heat flux at the widest gap is almost unaffected.

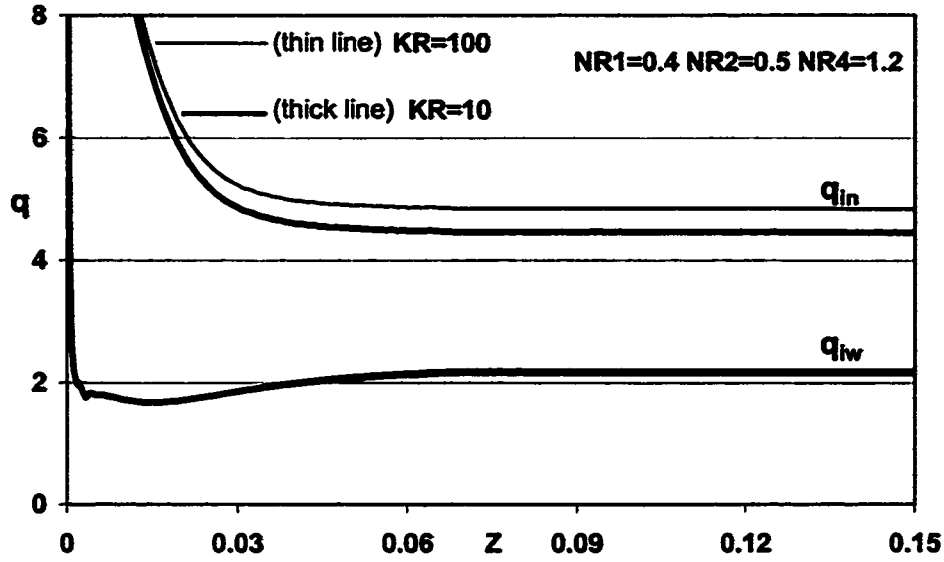

FIG. 6.31: Effect of KR on the axial variation of the local heat flux on the inner interface at the narrowest and widest gaps for E=0.5.

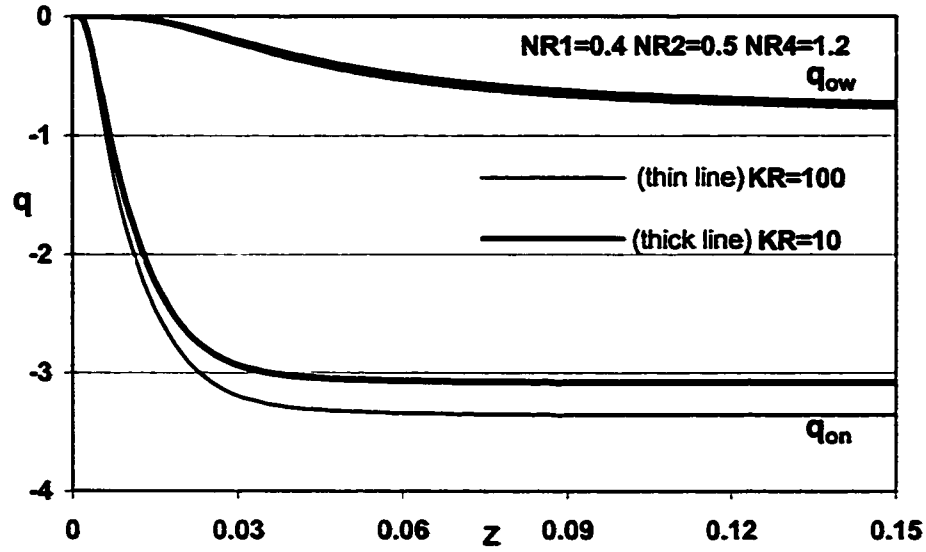

FIG. 6.32: Effect of KR on the axial variation of the local heat flux on the outer interface at the narrowest and widest gaps for E=0.5.

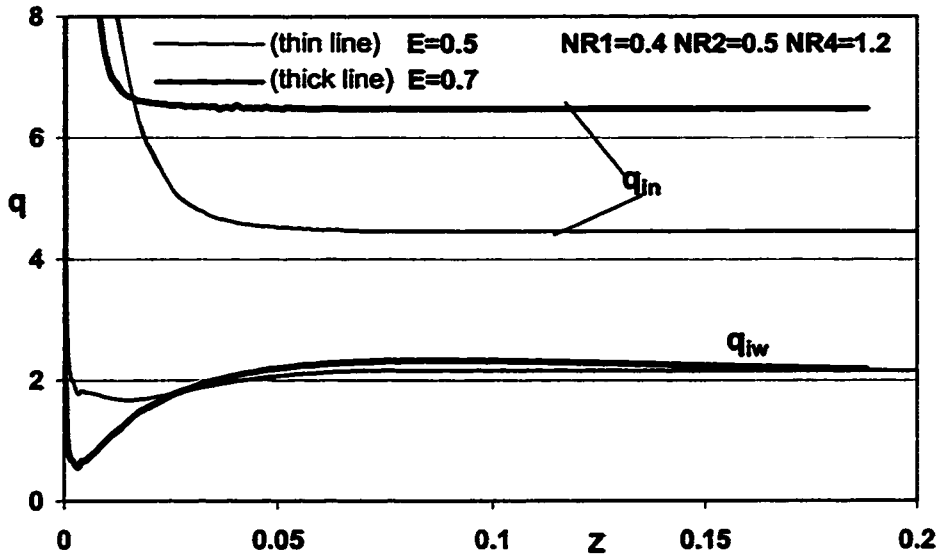

FIG. 6.33: Effect of the eccentricity on the axial variation of the local heat flux at the inner interface at the narrowest and widest gaps for KR=10.

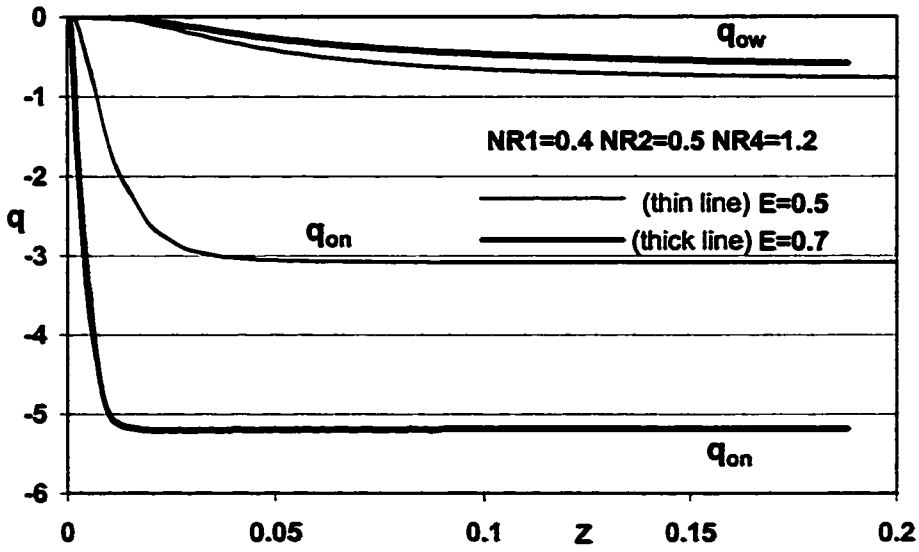

FIG. 6.34: Effect of the eccentricity on the axial variation of the local heat flux at the outer interface at the narrowest and widest gaps for KR=10.

Figures 6.33 and 6.34 indicate the effect of the eccentricity at KR=10, on the axial distribution of the local heat flux at the inner and the outer interface, respectively. As can be oberved from these figures, the increase in the value of the eccentricity leads to increased local heat flux at the narrowest gap on both interfaces due to the temperature profile getting steeper. However, the local heat flux at the widest gap is slightly decreased at the outer interface due to flattening of the temperature profile. At the inner interface, higher eccentricity (E=0.7) causes a decrease in the local heat flux at the widest gap near the entrance, but it increaees further downstream slightly above the value for E=0.5 and then converges to the same. It can be observed from Figs. 6.31 and 6.33 that the local heat flux on the inner interface at the widest gap reaches a minimum before rising to the fully developed value (=2.16) as the flow moves downstream. The reason is the same as discussed earlier; the fluid temperature adjacent to the inner wall, particularly at the widest gap, reaches a maximum before full development due to the absence of heat loss through the outer wall near the entrance. This reduces the slope of the temperature profile close to the inner wall thus reducing the local heat flux. However, further downstream, as the fluid temperature near the inner interface is decreased, the local heat flux increases to reach a constant value (=2.16). Figure 6.33 indicates that this phenomenon is enhanced by increasing the eccentricity.

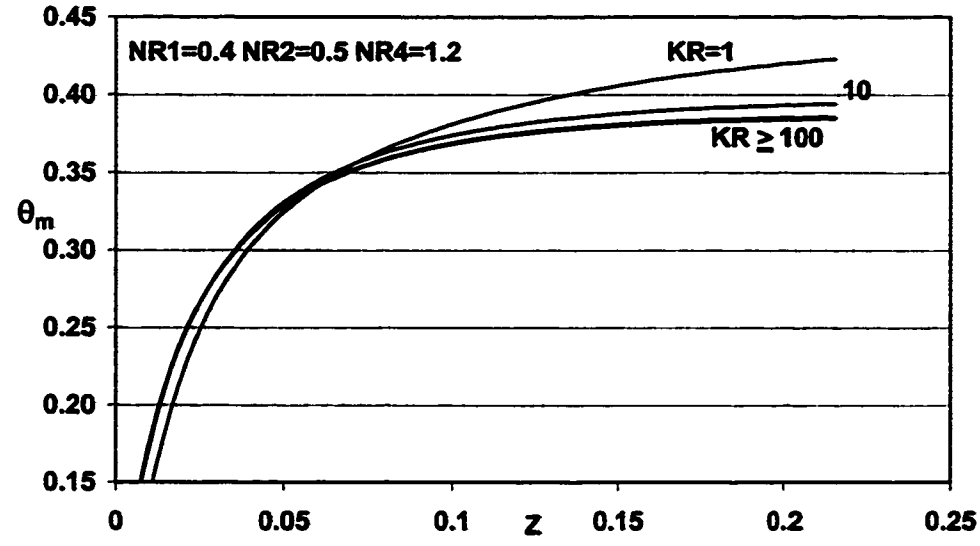

FIG. 6.35: Effect of KR on the axial variation of the mixing-cup temperature for E=0.5.

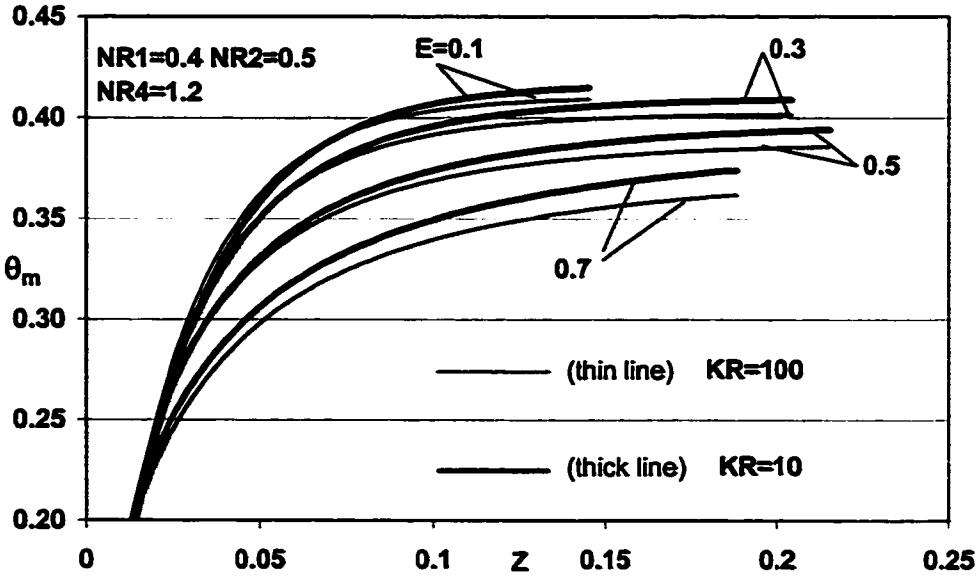

FIG. 6.36: Effect of the eccentricity on the axial variation of the mixing-cup temperature for KR=10 and 100.

6.2.4 Mixing-cup temperature

Engineers are not frequently concerned with the temperature profiles but with the mixed-mean (mixing-cup) temperature. The importance of the mixed-mean temperature comes from the fact that it can be directly used to obtain the heat gained by the fluid. Figures 6.35 and 6.36 present, respectively, the effect of KR (at E=0.5) and eccentricity (at KR=10 and 100) on the axial distribution of the mixing-cup temperature θ_m.

Away from the entrance, the lower values of θ_m at higher values of KR, as shown in Fig. 6.35, indicate an increased local heat flux due to the reduced wall resistance. This is because the local heat flux is directly proportional to the difference between the wall temperature and the fluid mixed-mean temperature ($Q \propto (\theta_w - \theta_m)$). Consequently, with an isothermal boundary ($\theta_w = 1$), the decrease in the value of θ_m will cause an increase in the local value of the wall heat flux (Q). However, it can be noticed that near the entrance, the trend is reversed, i.e., the higher the value of KR the higher the value of θ_m. The reason for this is that, near the entrance, the increase in the value of KR results in more heat being gained by the fluid through the isothermally heated surface than that lost by the fluid through the wall maintained at the ambient temperature. The increase in the heat gained by the fluid near the entrance through the heated boundary is attributed to the presence of the radial-like (η) and tangential-like (ζ) velocity components. These

two velocity components decay as the flow moves away from the entrance and hence the reverse phenomenon occurs as explained before. Moreover, near the entrance, the fluid near the outer wall has not sensed the heat signal and is still at the ambient temperature, resulting in no heat loss through the outer ambient wall. As the flow moves downstream, the heat loss through the outer wall initiates due to the rise in the fluid temperature.

For given values of KR (KR=10 and 100), Fig. 6.36 presents the axial variation of θ_m for various values of E. As can be seen from this figure, for a given Z, the higher the value of E the lower the value of θ_m. The decrease in the value of θ_m with the increase in the value of E is attributed to the associated increase in the mass flow rate through the annulus. Effects of KR similar to those shown before in Fig. 6.35 can also be seen in Fig. 6.36.

6.2.5 Critical solid-fluid conductivity ratio

Finally, it is of practical importance to know the values of KR beyond which the conjugate effect can be neglected. Figure 6.37 shows graphically the results of the present work for the variation of the percentage difference in $\theta_{m.fd}$ from the conventional case with KR for different values of E. This percentage difference is based on the conventional values of $\theta_{m.fd}$. The 'critical' value of KR for a given eccentricity, has been arbitrarily chosen as that value which causes $\theta_{m.fd}$ to differ by no more than one percent from the conventional solution result for a given eccentricity. According

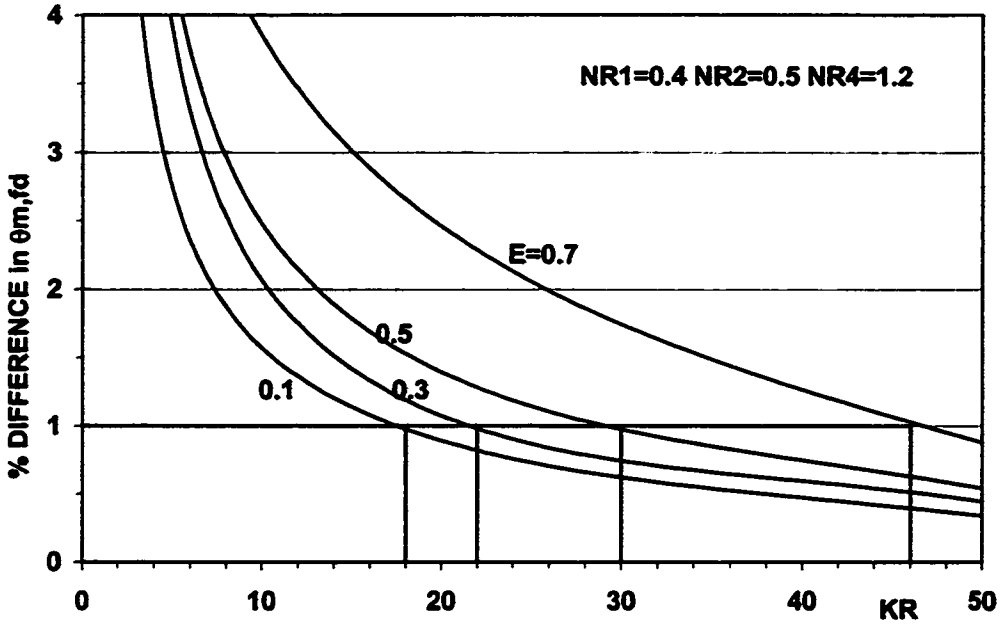

FIG. 6.37: % Difference in θm,fd from the conventional case plotted against solid-fluid conductivity ratio (KR). Critical KR values for a 1 % difference are highlighted.

TABLE 6.3 CRITICAL SOLID-FLUID CONDUCTIVITY RATIO (KR)

FULLY DEVELOPED MIXING-CUP TEMPERATURE (θm,fd)				
KR	E=0.1	E=0.3	E=0.5	E=0.7
1	0.433904678	0.438773572	0.423074216	0.402607769
% DIFF.	6.25	9.53	10.02	11.79
10	0.41480425	0.40887475	0.394055575	0.374003261
% DIFF.	1.57	2.06	2.47	3.85
50	0.409776419	0.402387351	0.386617273	0.363301039
% DIFF.	0.34	0.44	0.54	0.88
100	0.409090549	0.401506364	0.385590166	0.361745119
% DIFF.	0.17	0.22	0.27	0.44
1000	0.408467799	0.400699079	0.384645969	0.360298812
	0.02	0.02	0.03	0.04
INFINITY	0.408396483	0.400613785	0.384539783	0.360143453
θm (1%)	0.412480447	0.404619923	0.388385181	0.363744887
θm @ CKR	0.412098229	0.404556871	0.387951374	0.363566339
% DIFF.	0.91	0.98	0.89	0.95

to this criterion, the critical values of KR given in Table 6.3 are also presented in Fig. 6.37. As can be seen from Table 6.3 and also Fig. 6.37, the higher the value of E the higher the critical KR. Thus, it can be concluded that the conjugate effect increases with eccentricity. However, Fig. 6.37 can also be used to obtain critical KR values for other percentage difference criteria. Moreover, for given E and KR, Fig. 6.37 can be useful in correcting available conventional results to take into account the conjugate effect.

6.2.6 Thermal entrance length

The figures presented in sections 6.2.1 to 6.2.4 indicate that the thermal entrance length is not appreciably affected by varying KR. This is particularly because of the boundary conditions investigated. The increase in the value of KR, while increasing the heat input through the inner wall, simultaneously increases the heat loss through the outer wall. The counteracting effects cancel each other and therefore thermal entrance length is relatively insensitive to changes in KR.

For a fluid of Pr=0.7, thermal entry length is within the hydrodynamic entry length and with forced convection the temperature profile is dependent on the velocity distribution. Therefore, the effect of the eccentricity on the thermal entrance length is in-step with the effect of the eccentricity on the hydrodynamic entrance length which is presented in [2, 28].

Chapter 7

RESULTS AND DISCUSSION FOR CRITICAL TUBE THICKNESS

7.1 Introduction

As stated in Chapter 6, six controlling parameters are explicitly required to solve the problem under consideration. These are: the annulus radius ratio (NR_2), the dimensionless eccentricity (E), the outer wall radius ratio (NR_4), the inner wall radius ratio (NR_1), the solid-fliud conductivity ratio (KR) and the Prandtl number (Pr). For this part of the work, computations were carried out for a fluid of Pr=0.7 in an annulus of radius ratio $NR_2 = 0.5$ with values of NR_4=1.4, 1.2, 1.1, 1.02 and

1.002 and NR_1=0.3, 0.4, 0.45, 0.49 and 0.499 for values of E=0.1, 0.3, 0.5 and 0.7 and KR=10. The reason for the selection of $NR_2 = 0.5$ is, as mentioned in section 6.1, that most of the results in the literature for the conventional problem (i.e., neglecting the effect of conjugation) are reported for this particular value, which represents a typical annular geometry. The maximum values of NR_4 and NR_1 are typical practical values as can be seen from Table 6.1 which lists some values of radius ratios for possible combination of inner / outer standard steel pipes. Table 6.2 shows practical values of the solid-fluid conductivity ratio (KR) and indicates the wide range possible. However, after several runs of the program, it was concluded that the conjugate effect is not appreciable for KR $\geq$ 100, even for thick walls corresponding to $NR_4 = 1.4$, $NR_2 = 0.5$ and $NR_1 = 0.3$ with values of E upto E=0.7; the maximum deviation from the conventional case, obtained with E=0.7, being within 1 %. Even for KR=50, the conjugate effect is not significant upto E=0.7 for standard wall thickness corresponding to NR_4=1.2, $NR_2 = 0.5$ and NR_1=0.4 (see Fig. 6.37 and Table 6.3). Therefore, KR=10 was chosen in this part of the work, as a typical value, to study the effect of varying the wall thickness and to determine the wall thickness limits below which the conjugate effect is negligible for practical purposes.

Following sections give the results and discussion for the heat transfer parameters. The annulus radius ratio is kept fixed ($NR_2 = 0.5$) since the outer tube thickness is varied on the outside and the inner tube thickness on the inside. There-

fore, the hydrodynamics of the problem is not affected by varying the wall thickness at a given eccentricity. Detailed discussion regarding the effect of varying the eccentricity on the hydrodynamics is given in [28]. However, the effect of eccentricity and tube thickness on the heat transfer parameters will be presented here. Results for the critical tube thickness are presented at the end, both graphically and in the form of a table.

7.2 Results and Discussion

7.2.1 Temperature profiles across the annulus

Each pair of Figs. 7.1 to 7.6 shows the developing temperature profiles, corresponding to different values of Z, across the narrowest and the widest gaps, for KR=10, E=0.5 and the indicated wall thickness. It can be noticed that full development is reached significantly faster across the narrowest gap (Z=0.0832) as compared to the widest gap (Z=0.203). This is expected because the eccentricity reduces the thermal resistance across the narrowest gap and consequently the heat signal is sensed relatively earlier. Decreasing the wall thickness results in accelerated heating of the fluid near the inner interface but the fluid near the outer interface remains unaffected. It can be noticed that temperatures near the inner interface reach a maximum before full development and then decrease as the flow approaches full development. This is because near the entrance, heat loss through the outer wall is absent due to the fluid

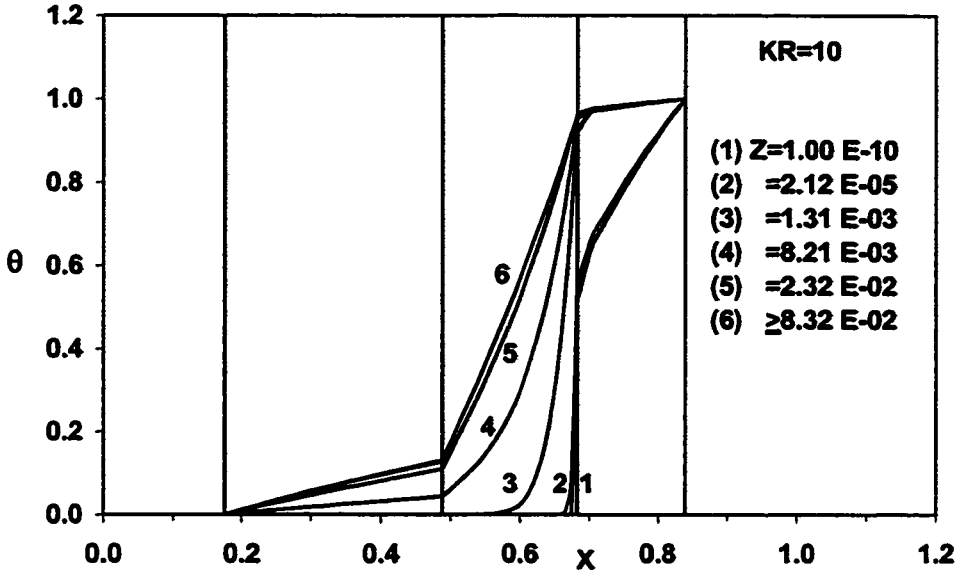

FIG. 7.1: Developing temperature profiles across the narrowest gap for E=0.5, NR1=0.3, NR2=0.5 and NR4=1.4.

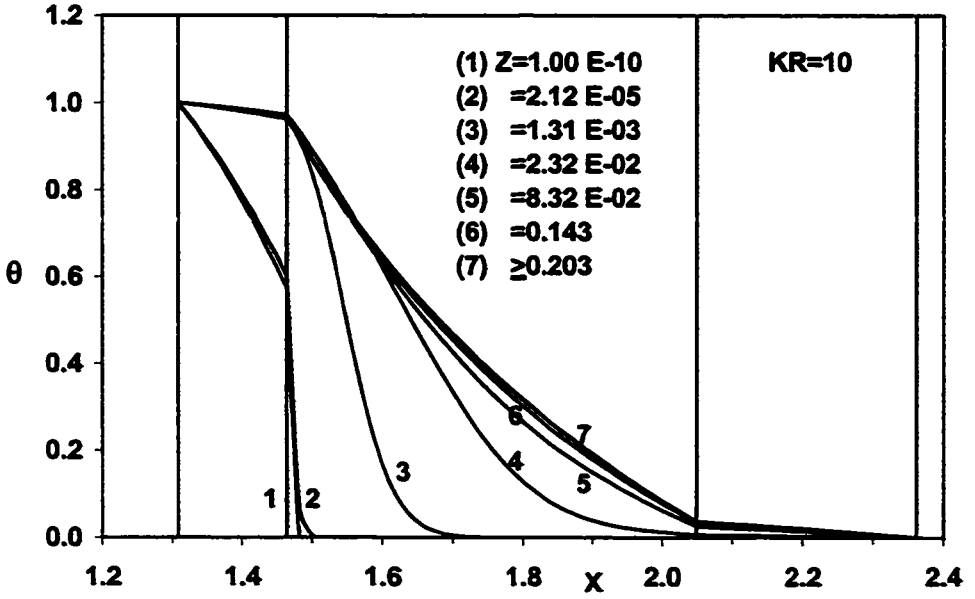

FIG. 7.2: Developing temperature profiles across the widest gap for E=0.5, NR1=0.3, NR2=0.5 and NR4=1.4.

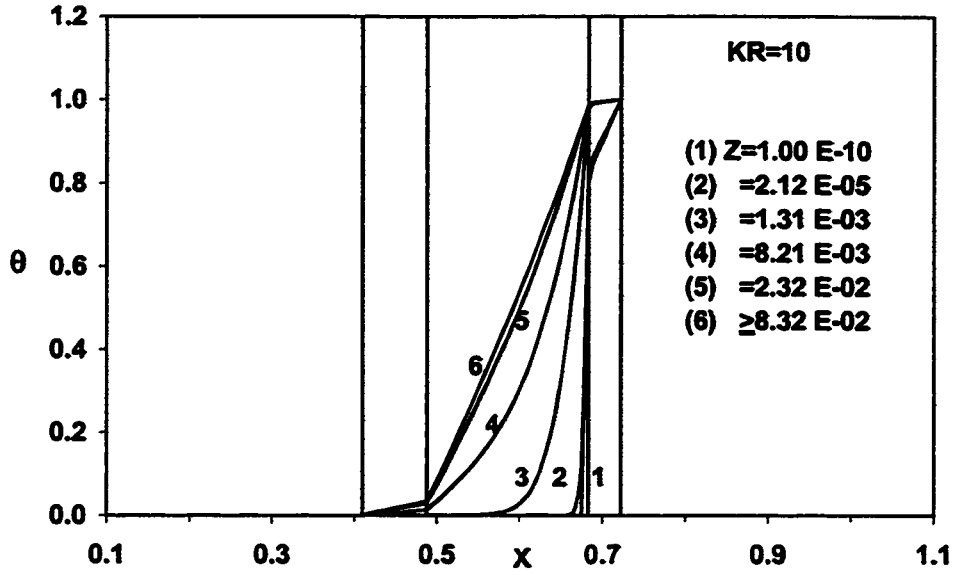

FIG. 7.3: Developing temperature profiles across the narrowest gap for E=0.5, NR1=0.45, NR2=0.5 and NR4=1.1.

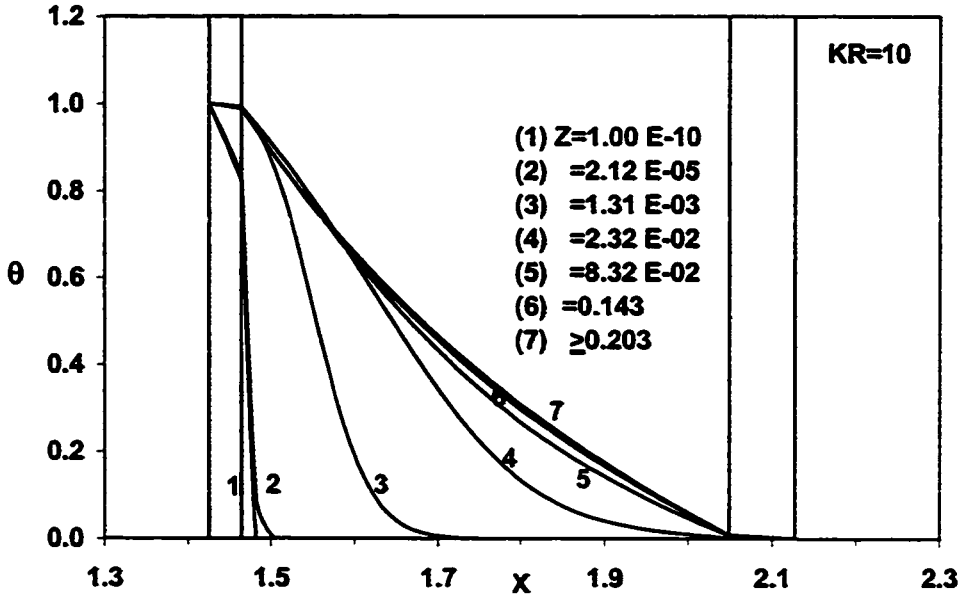

FIG. 7.4: Developing temperature profiles across the widest gap for E=0.5, NR1=0.45, NR2=0.5 and NR4=1.1.

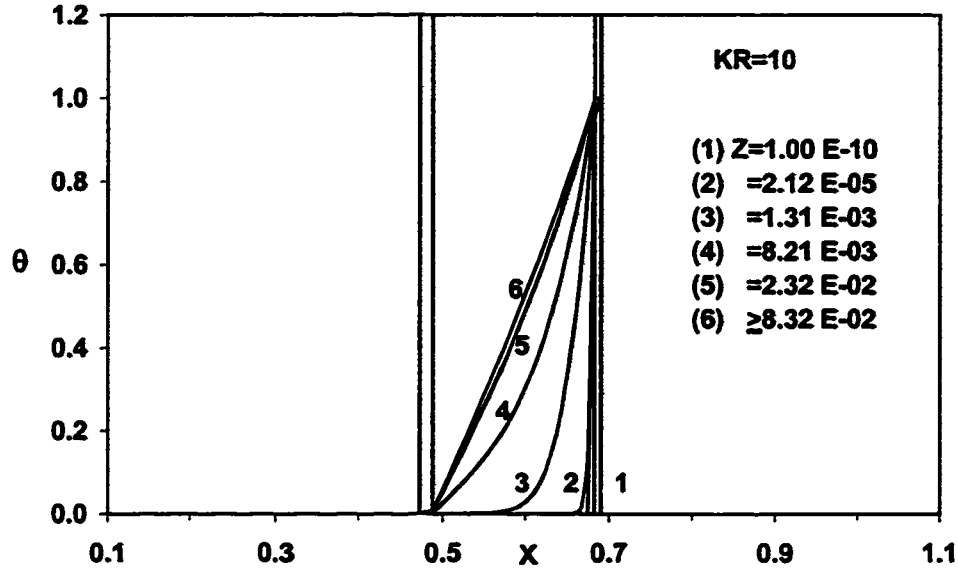

FIG. 7.5: Developing temperature profiles across the narrowest gap for E=0.5, NR1=0.49, NR2=0.5 and NR4=1.02.

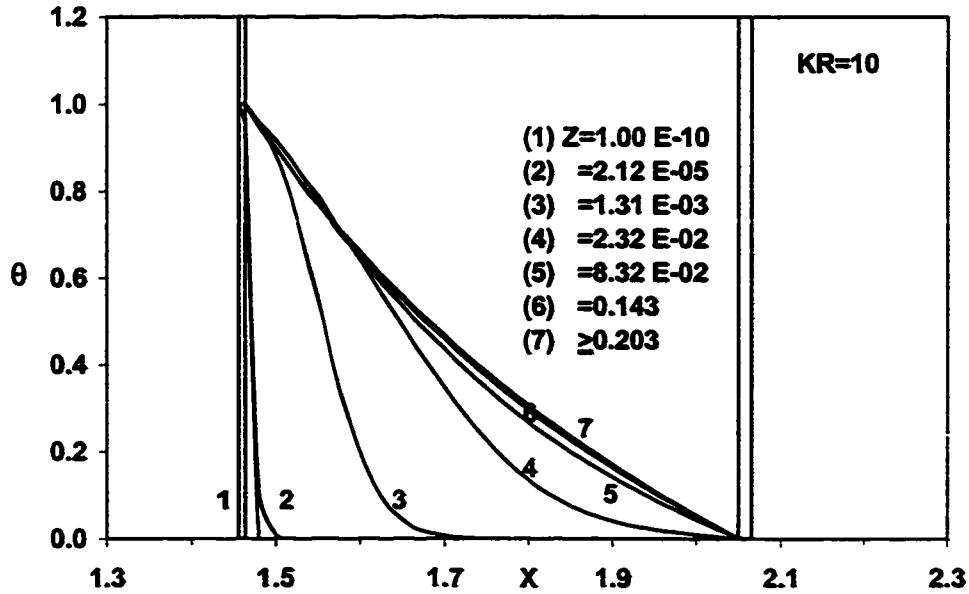

FIG. 7.6: Developong temperature profiles across the widest gap for E=0.5, NR1=0.49, NR2=0.5 and NR4=1.02.

being at ambient temperature. As the flow moves downstream, heat loss through the ambient wall initiates due to rise in the adjacent fluid temperature, thereby slightly decreasing the temperature of the fluid adjacent to the inner wall.

Each pair of Figs 7.7 to 7.10 display the effect of the wall thickness on the fully developed temperature profile across the narrowest and the widest gaps, with NR_1=0.3, 0.4, 0.45, 0.49, NR_2 = 0.5 and NR_4=1.4, 1.2, 1.1, 1.02 and the eccentricity indicated. It is obvious that increasing the wall thickness results in greater temperature drop across the solid walls. The increase in the wall thickness leads to lower temperatures on the inner interface and vice versa on the outer interface.

7.2.2 Interfacial temperature

For E=0.5, Figs. 7.11 and 7.12 show the effect of the wall thickness on the fully developed circumferential temperature variation at the outer and the inner interface, respectively. It is evident from these figures that increasing the wall thickness, besides lowering the temperature at the inner interface and raising it at the outer interface, also leads to greater circumferential variation at both the interfaces. This higher circumferential temperature variation with thicker walls results in further departure from the conventional case with isothermal boundaries, making it necessary to account for the conjugate effect. Also, the circumferenial temperature variation causes a circumferential heat flow on the inner interface in the positive ζ-direction (i.e., from the widest to the narrowest gap side) and in the opposite

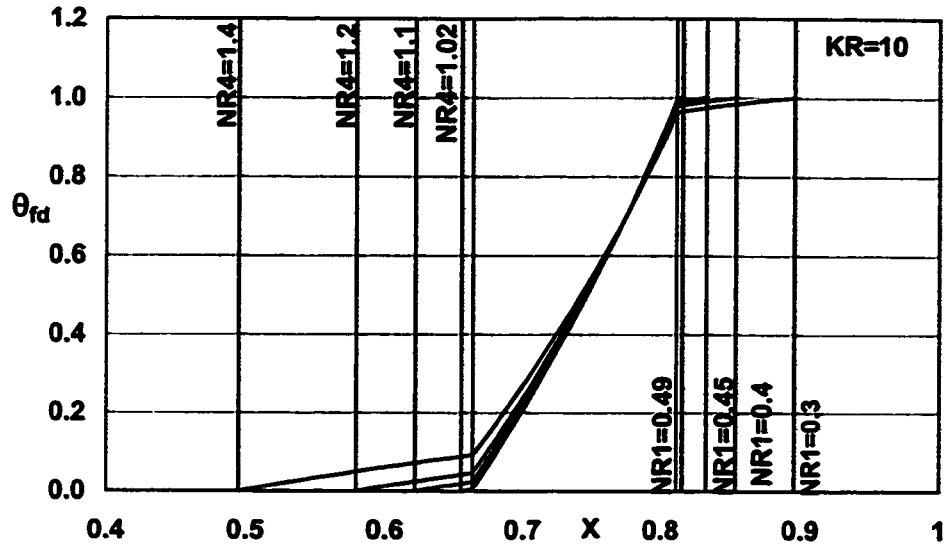

FIG. 7.7: Effect of the wall thickness on the fully developed temperature profile across the narrowest gap for E=0.3.

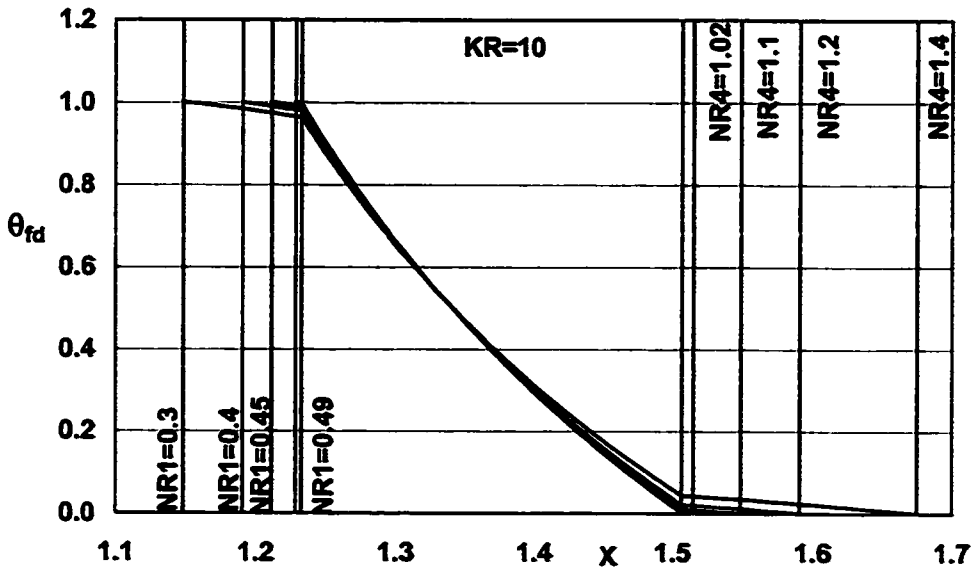

FIG. 7.8: Effect of the wall thickness on the fully developed temperature profile across the widest gap for E=0.3.

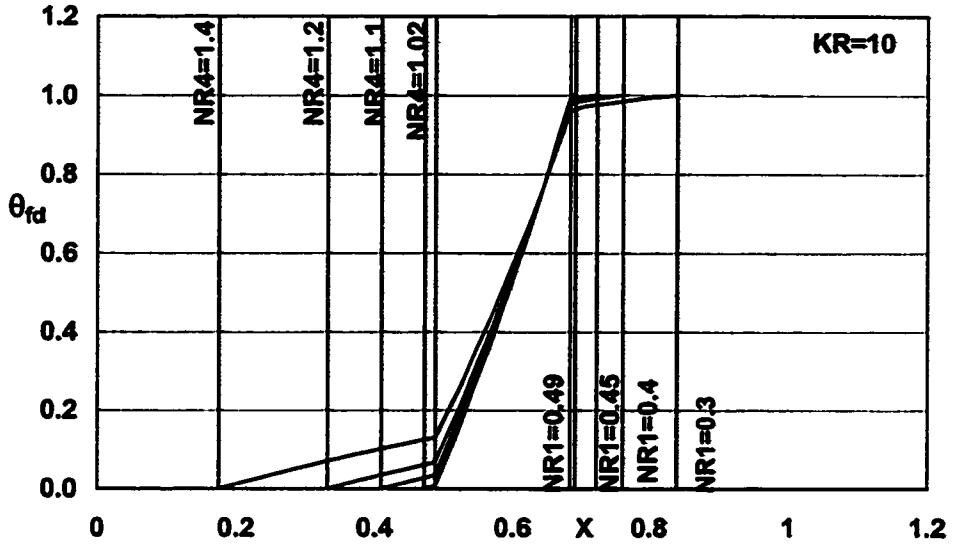

FIG. 7.9: Effect of the wall thickness on the fully developed temperature profile across the narrowest gap for E=0.5.

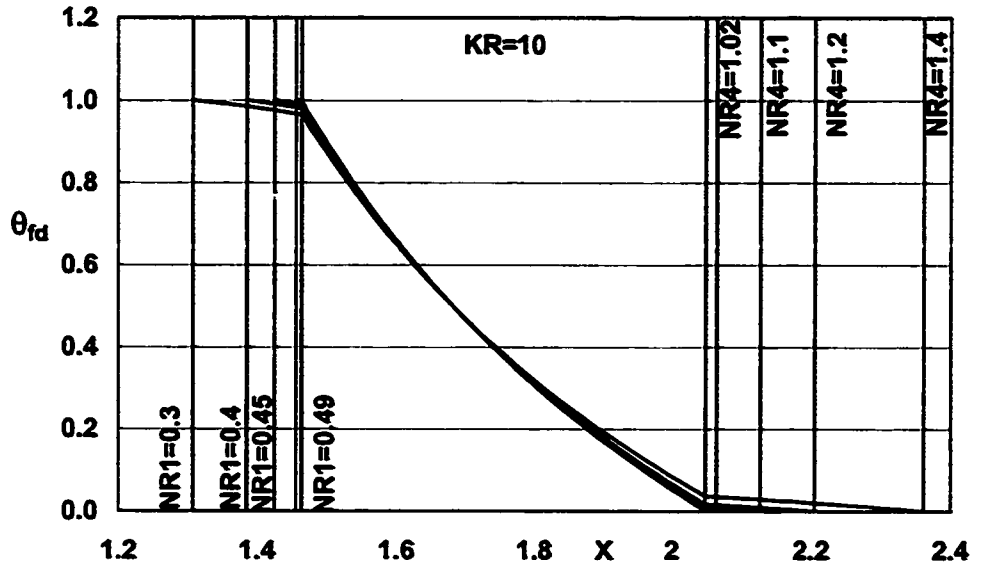

FIG. 7.10: Effect of the wall thickness on the fully developed temperature profile across the widest gap for E=0.5.

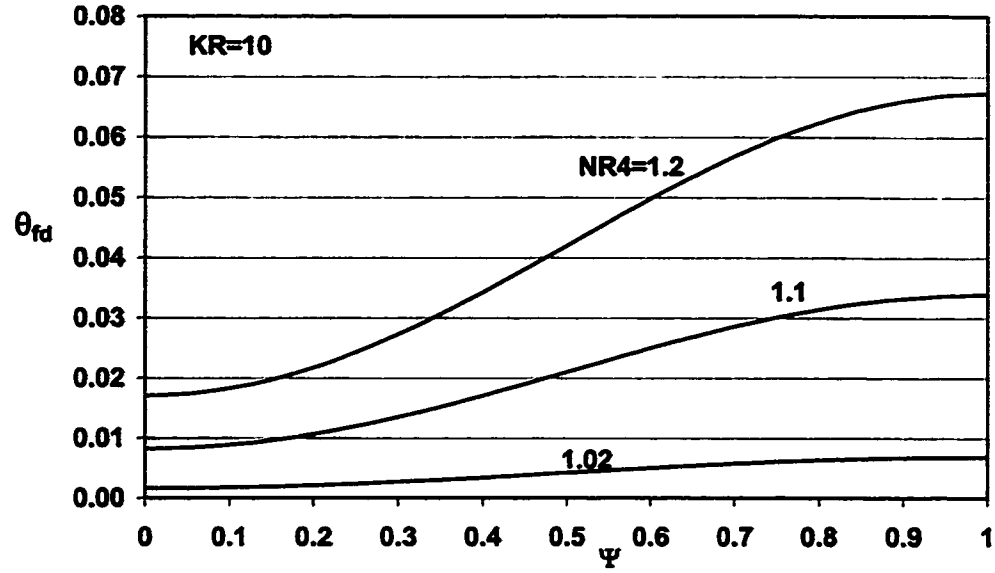

FIG. 7.11: Effect of the wall thickness on the circumferential temperature distribution at the outer interface for E=0.5.

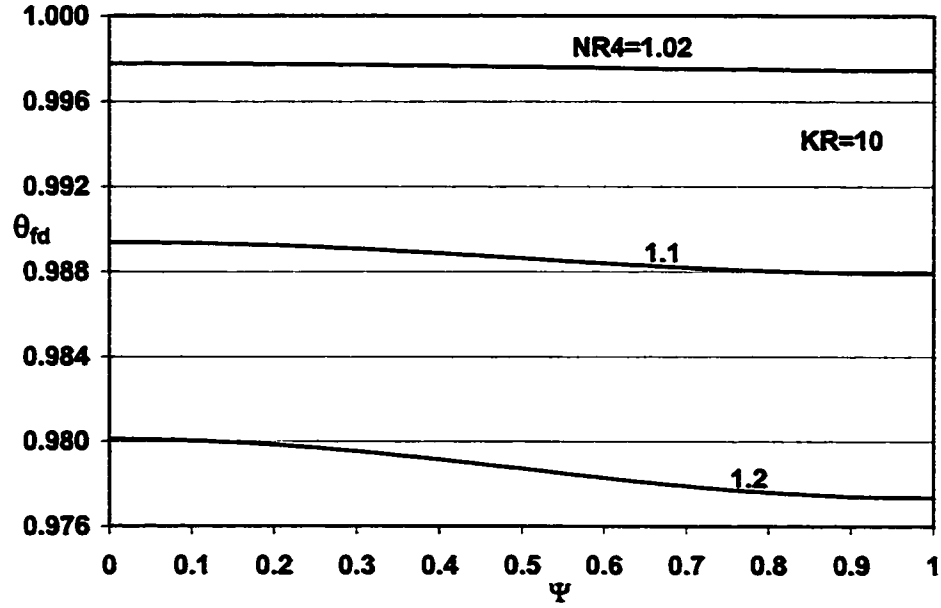

FIG. 7.12: Effect of the wall thickness on the circumferential temperature distribution at the inner interface for E=0.5.

direction (the negative ζ-direction, from the narrowest to the widest gap side) on the outer interface. Thus, increasing the wall thickness, while reducing the radial temperature gradient within the fluid annulus, decreases the dominant radial heat flow and increases the circumferential heat flow.

Figures 7.13 and 7.14 show the effect of eccentricity, for two wall thicknesses, on the fully developed circumferential temperature distributions at the outer and the inner interface, respectively. The figures indicate how the increase in the value of the eccentricity enhances the circumferential variation of temperature. The increased circumferential temperature variation at the interfaces results in increased deviation from the conventional case with isothermal boundaries; thus consideration of conjugation is more important at higher eccentricities. It can be observed from Figs. 7.13 and 7.14 that the higher the value of E the higher the temperature at the narrowest gap (Ψ=1) on the outer interface, and at the widest gap (Ψ=0) on the inner interface. Moreover, the higher the value of E the higher the circumferential variation of temperature on either interface (i.e., higher circumferential temperature gradient). Consequently, the higher the value of E, the larger the circumferential heat flow. The circumferential heat flow on the inner interface is in the positive ζ-direction (i.e., from the widest to the narrowest gap side). However, it is in the opposite direction (the negative ζ-direction) on the outer interface.

The above discussion is further supplemented by observing the effect of the controlling parameters on the axial distribution of the interfacial temperatures at the

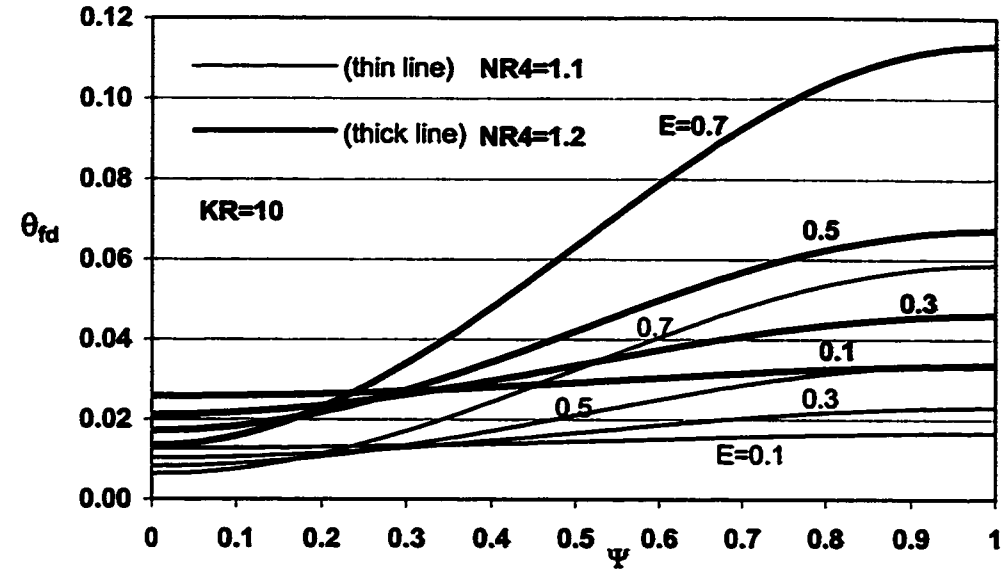

FIG. 7.13: Effect of the eccentricity on the circumferential temperature variation at the outer interface for two values of the wall thickness.

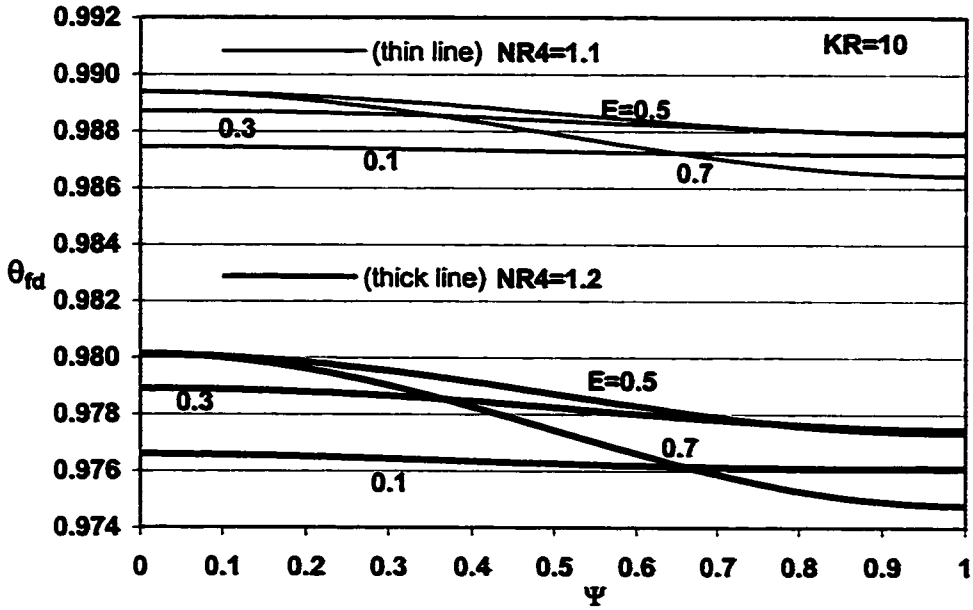

FIG. 7.14: Effect of the eccentricity on the circumferential temperature variation at the inner interface for two values of the wall thickness.

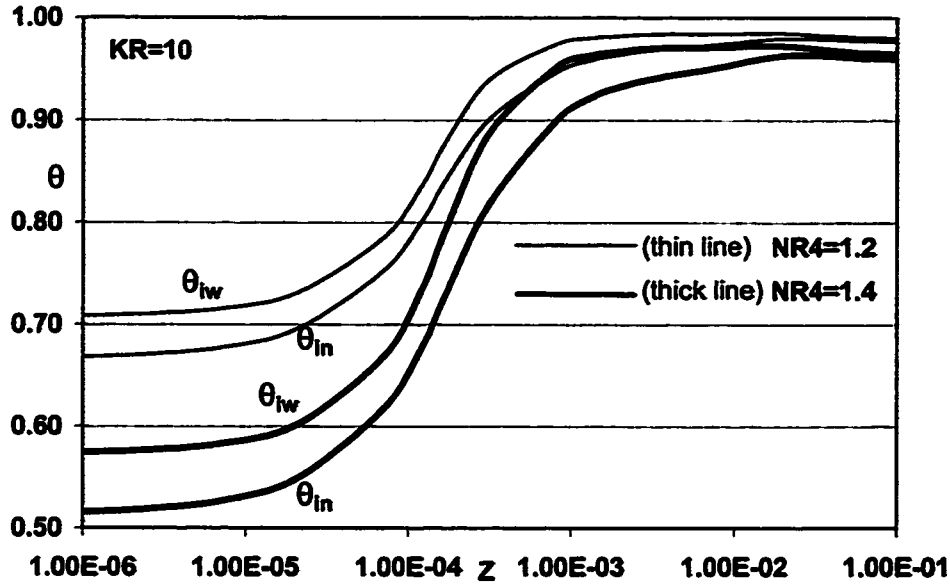

FIG. 7.15: Effect of the wall thickness on the axial variation of the temperature on the inner interface at the narrowest and widest gaps for E=0.5.

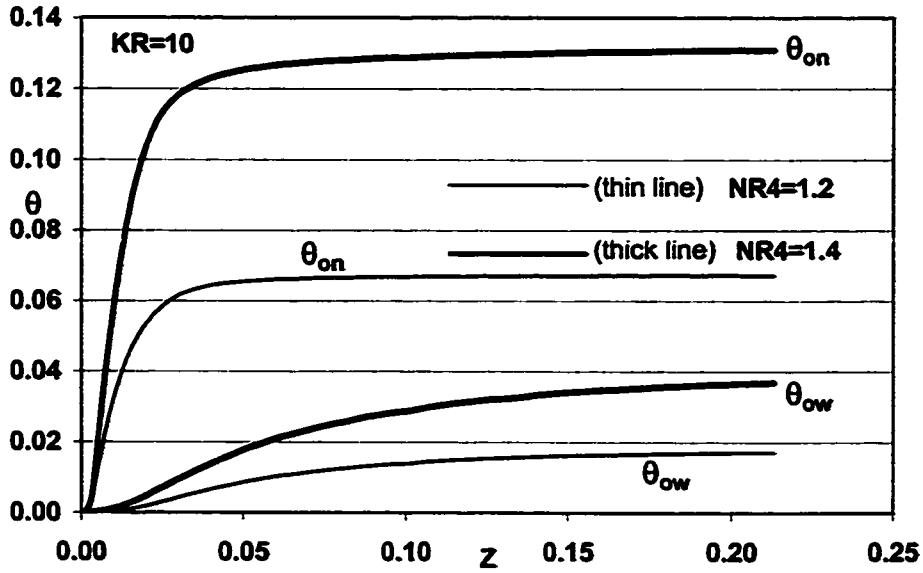

FIG. 7.16: Effect of the wall thickness on the axial variation of the temperature on the outer interface at the narrowest and widest gaps for E-0.5.

four points of intersection of the interfaces with the line of symmetry. Figures 7.15 and 7.16 give this distribution for E=0.5 and both NR4=1.2 and 1.4, at the narrowest and widest gaps on the inner and outer interface, respectively. As discussed in the foregoing paragrahs, the lower value of the wall thickness (i.e., lower values of NR4) results in higher temperatures but smaller circumferential variation at the inner interface. At the outer interface, the decrease in the value of the wall thickness leads to lower temperatures and smaller circumferential variation. It can be noticed from Fig. 7.15 that at the inner interface temperatures reach a maximum before full development when the fluid near the outer wall is still near ambient temperature. However, with the rise in fluid temperature adjacent to the outer interface, the heat loss through the outer wall initiates, thus pulling down slightly the temperature of the fluid close to the inner interface. This phenomenon can also be observed from the figures depicting the developing profiles, particulary across the widest gap (Figs. 7.2, 7.4 and 7.6).

Figures 7.17 and 7.18 give the axial distribution of interfacial temperature for NR4=1.4 and two values of the dimensionless eccentricity, at the narrowest and the widest gaps on the inner and outer interface, respectively. It can be observed that, for the inner interface, the temperature is higher at the widest gap but it is higher at the narrowest gap for the outer interface, thus giving rise to circumferential heat flows in opposing directions as discussed earlier. Furthermore, the increase in the value of the eccentricity results in the inner interface temperature being raised at the widest

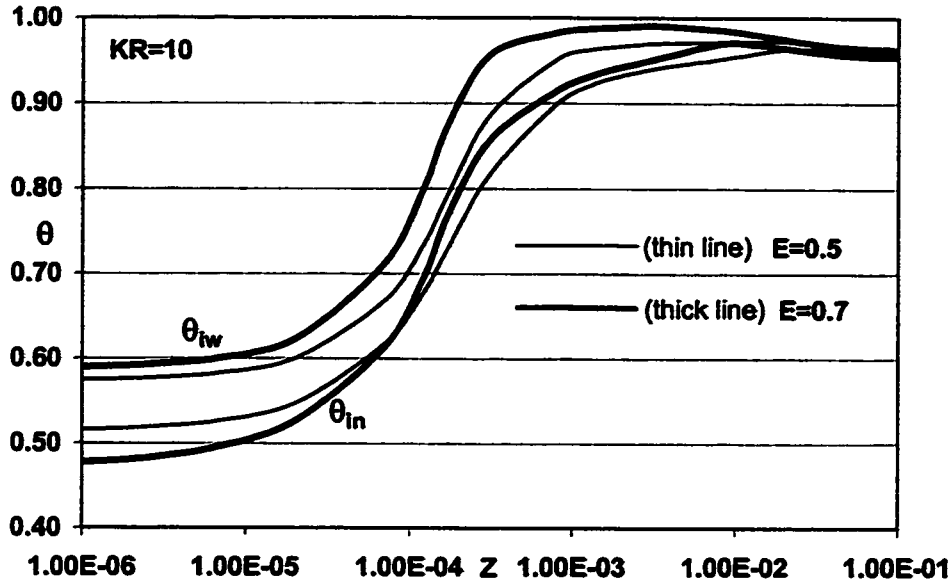

FIG. 7.17: Effect of the eccentricity on the axial variation of the temperature on the inner interface at the narrowest and widest gaps for NR4=1.4.

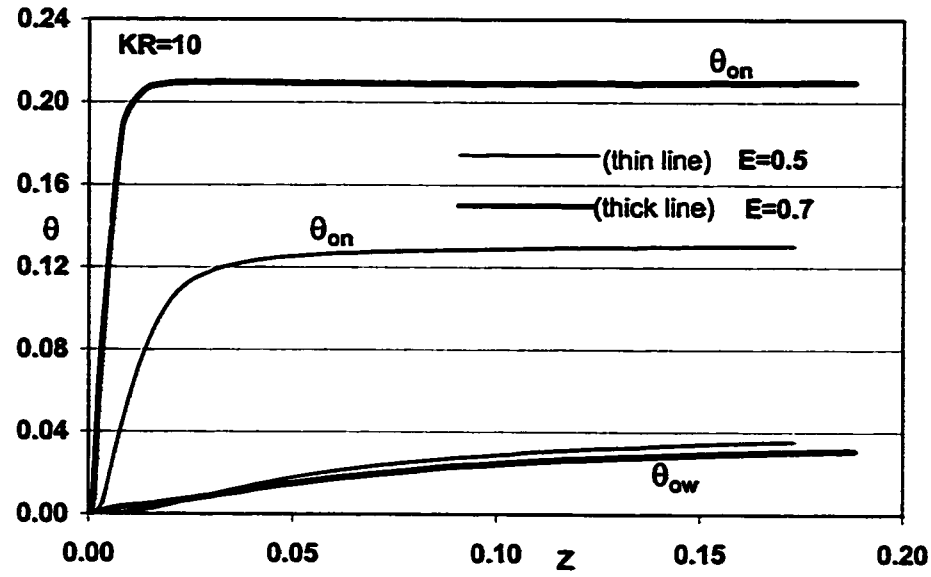

FIG. 7.18: Effect of the eccentricity on the axial variation of the temperature on the outer interface at the narrowest and widest gaps for NR4=1.4.

gap and lowered at the narrowest gap, thus enhancing the circumferential variation and making the conjugate efffect more significant. Circumferential temperature variation is also enhanced at the outer interface with the increase in the eccentricity but with a rise in temperature at the narrowest gap and a decrease at the widest gap.

7.2.3 Interfacial heat flux

Figures 7.19 and 7.20 show, respectively, the effect of the wall thickness (at E=0.5) and the eccentricity (for two wall thicknesses) on the axial variation of the peripherally averaged heat flux at the inner interface (Q_{II}). Fig. 7.19 indicates that, for a given Z, decreasing the wall thickness results in an increase in the value of the heat flux. The values of Q_{II} corresponding to $NR_4 = 1.02$ are almost equal to those of the conventional case; the maximum deviation is about 0.5 % (based on the conventional case results). For a given wall thickness (NR4), Fig. 7.20 highlights that the heat flux, at a given Z, increases with the eccentricity. On the other hand, this figure also shows that the effect of the wall thickness on the axial variation of the circumferentially averaged heat flux is more pronounced for the higher values of E. As can be seen from the figure, the difference between each pair of curves corresponding to NR4=1.02 and NR4=1.2 decreases, for a given Z, as E decreases.

Figures 7.21 and 7.22 show, respectively, the effect of the wall thickness (at E=0.5) and the eccentricity (for two wall thicknesses) respectively on the axial vari-

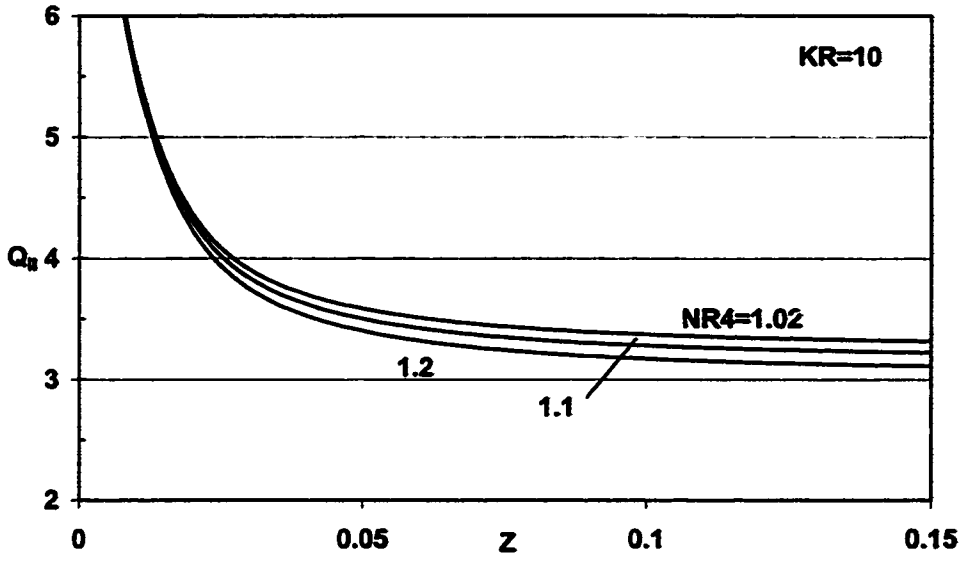

FIG. 7.19: Effect of the wall thickness on the axial variation of the circumferentially averaged heat flux at the inner interface for E=0.5.

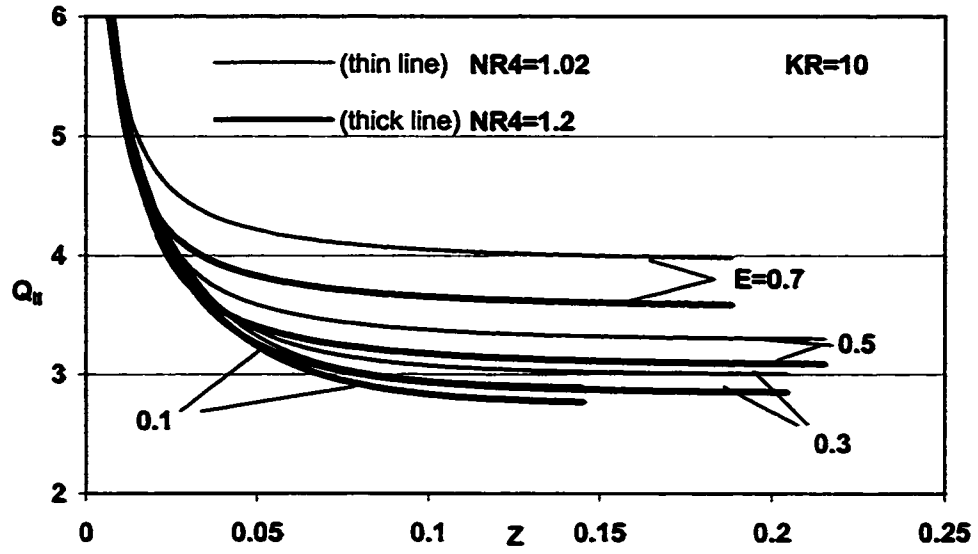

FIG. 7.20: Effect of the eccentricity on the axial variation of the circumferentially averaged heat flux at the inner interface for NR4=1.02 and 1.2.

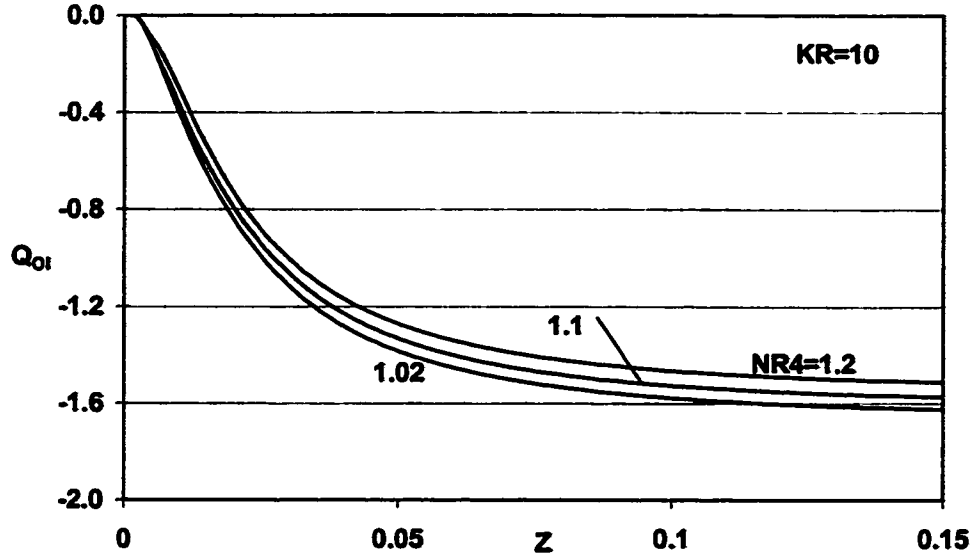

FIG. 7.21: Effect of the wall thickness on the axial variation of the circumferentially averaged heat flux at the outer interface for E=0.5.

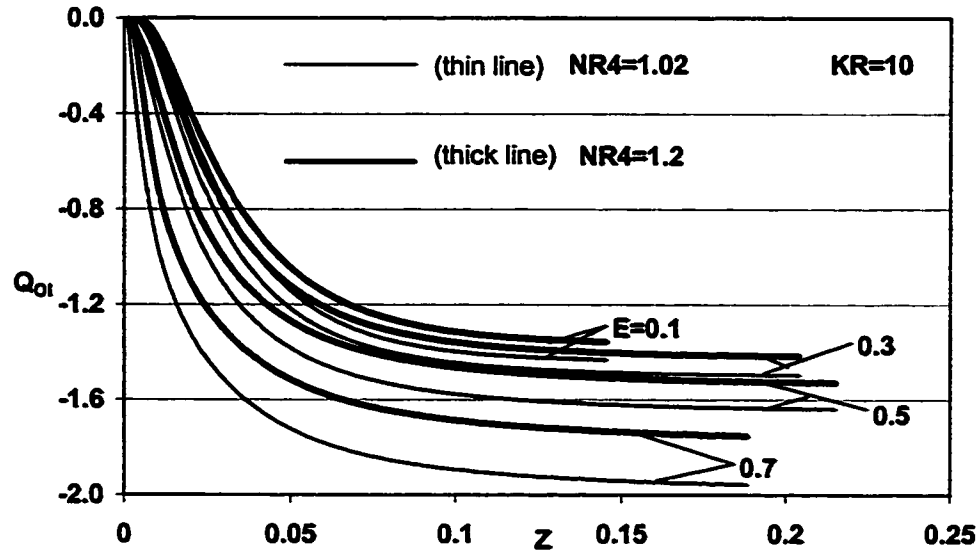

FIG. 7.22: Efect of the eccentricity on the axial variation of the circumferentially averaged heat flux at the outer interface for NR4=1.02 and 1.2.

ation of the peripherally averaged heat flux at the outer interface (Q_{OI}). The negative sign indicates that heat is lost from the fluid at the outer interface. Figure 7.21 indicates that, for a given Z, decreasing the wall thickness results in an increased heat flux. Figure 7.22 highlights that the heat flux, at a given Z, increases with the eccentricity, similar to that at the inner interface.

Figures 7.23 and 7.24 show the axial distribution of the local heat flux for E=0.5 and both NR4=1.2 and 1.4, at the intersections of the symmetry line with the inner and the outer interface, respectively. At both interfaces, the local heat flux is of a higher value at the narrowest gap. This is because the temperature profile is much steeper across the narrowest gap as compared to that across the widest gap. Moreover, the decrease in the value of the wall thickness (i.e., value of NR4) leads to higher local heat flux at the narrowest gap but the local heat flux at the widest gap is almost unaffected. Figures 7.25 and 7.26 indicate the effect of the eccentricity, for NR4=1.4, on the axial distribution of local heat flux at the narrowest and the widest gaps on the inner and the outer interface, respectively. As can be observed from these figures, the increase in the value of the eccentricity leads to an increase in the value of the local heat flux at the narrowest gap on both interfaces due to the temperature profile getting steeper. However, the local heat flux at the widest gap is slightly decreased at the outer interface due to flattening of the temperature profile. At the inner interface, higher eccentricity (E=0.7) causes a decrease in local heat flux at the widest gap near the entrance, but it increases further downstream

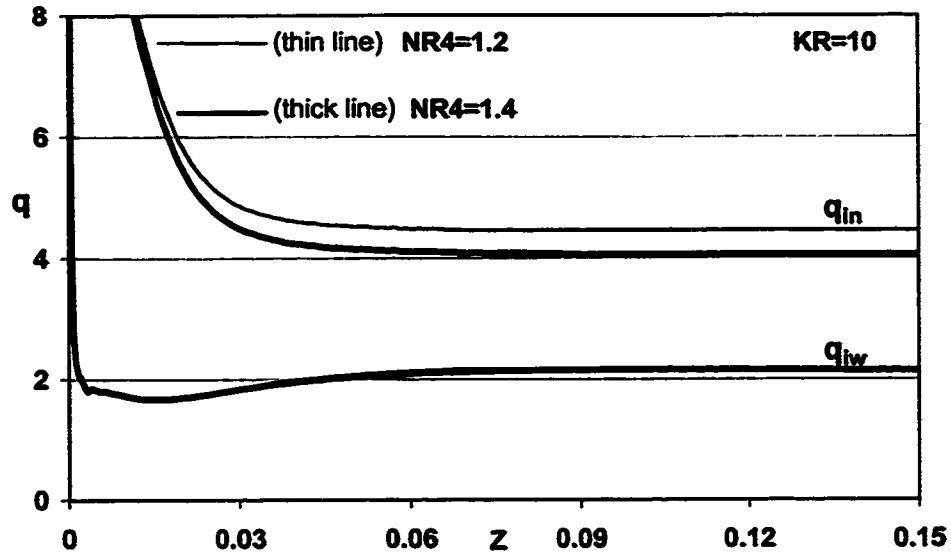

FIG. 7.23: Effect of the wall thickness on the axial variation of the local heat flux at the inner interface at the narrowest and widest gaps for E=0.5.

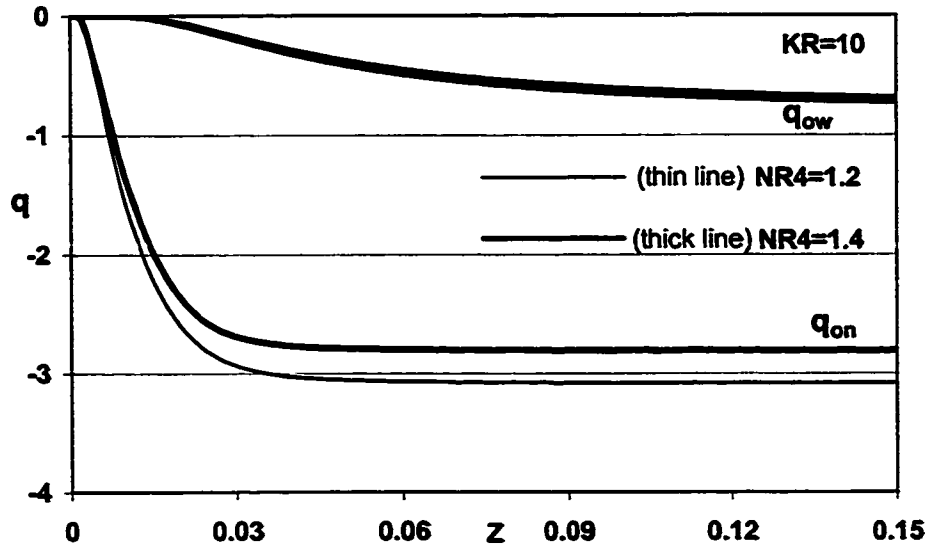

FIG. 7.24: Effect of the wall thickness on the axial variation of the local heat flux at the outer interface at the narrowest and widest gaps for E=0.5.

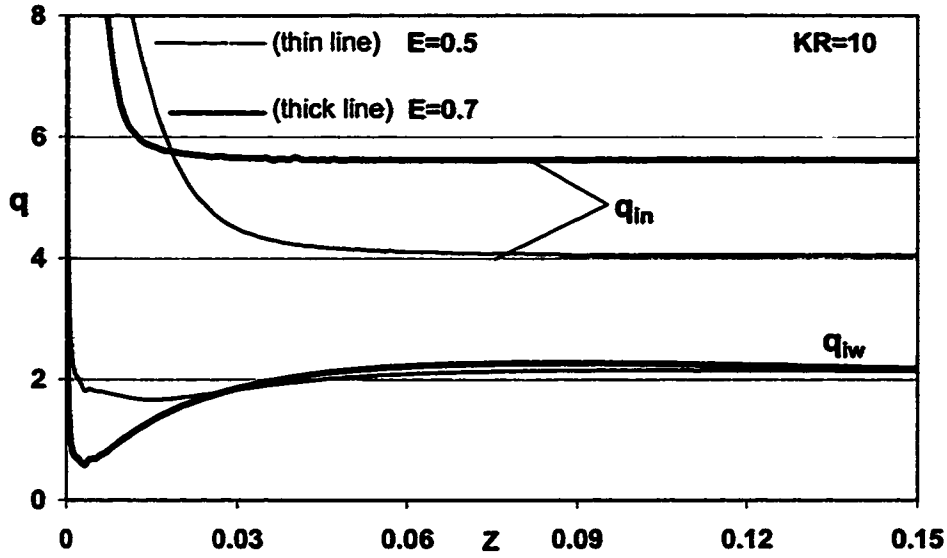

FIG. 7.25: Effect of the eccentricity on the the axial variation of the local heat flux at the inner interface at the narrowest and widest gaps for NR4=1.4.

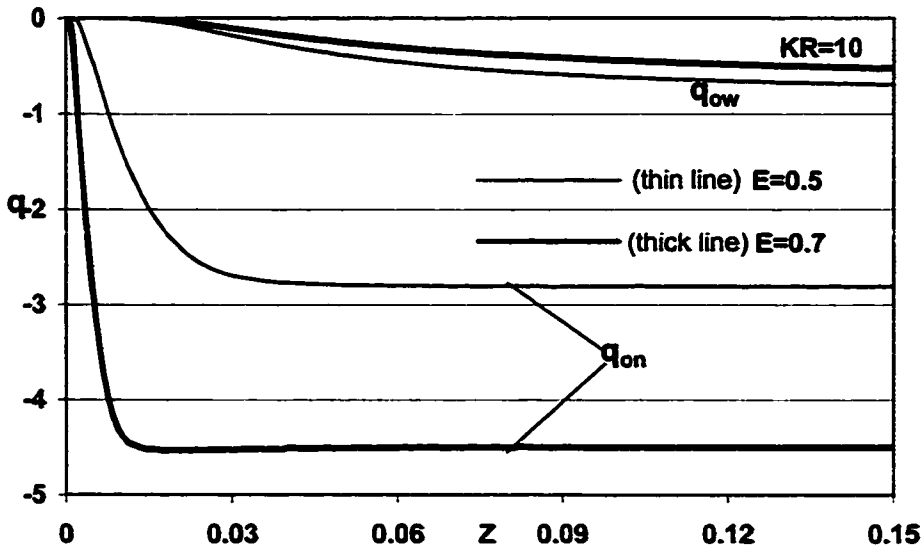

FIG. 7.26: Effect of the eccentricity on the axial variation of the local heat flux at the outer interface at the narrowest and widest gaps for NR4=1.4.

slightly above the value for E=0.5 and then converges to the fully developed value (=2.11).

It can be observed from Fig. 7.23 and 7.25 that the local heat flux on the inner interface at the widest gap reaches a minimum before rising to the fully developed value as the flow moves downstream. The reason is the same as discussed earlier; the fluid temperature adjacent to the inner wall, particularly at the widest gap, reaches a maximum before full development due to the absence of heat loss through the outer wall near the entrance. This reduces the slope of the temperature profile close to the inner wall thus reducing the local heat flux. However, further downstream, as the fluid temperature near the inner interface is decreased, the local heat flux increases to reach a constant value (=2.11). Figure 7.25 indicates that this phenomenon is enhanced by increasing the eccentricity.

7.2.4 Mixing-cup temperature

As was mentioned in section 6.2.4, engineers are not frequently concerned with the temperature profiles but with the mixed-mean (mixing-cup) temperature. Figure 7.27 presents the effect of the wall thickness on the axial distribution of the mixing-cup temperature θ_m. Generally, the effect of decreasing the wall thickness (NR4) on the mixing-cup temperature is qualitatively similar to that corresponding to increasing the thermal conductivity ratio KR, which was explained in section 6.2.4. However, decreasing the wall thickness reduces the thermal resistance to radial heat

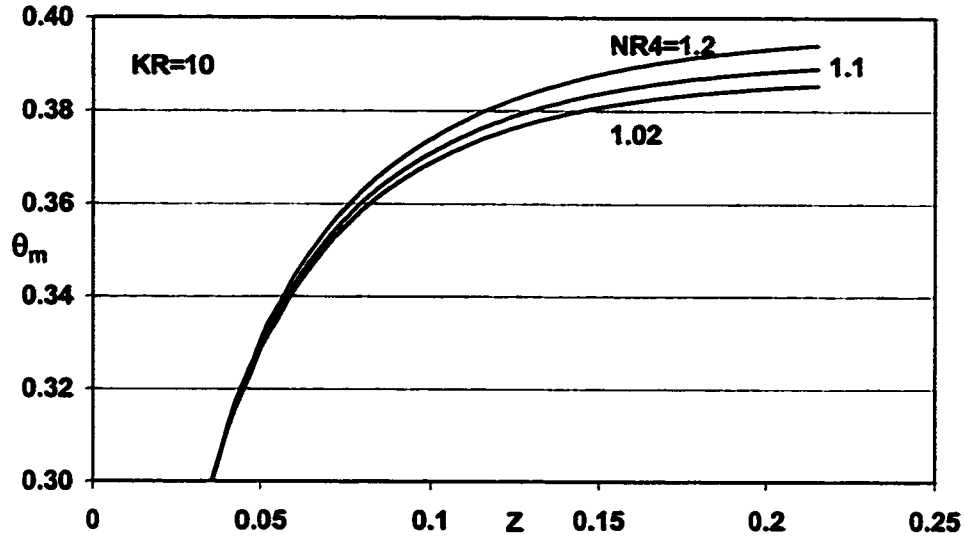

FIG. 7.27: Effect of the wall thickness on the axial variation of the mixing-cup temperature for E=0.5.

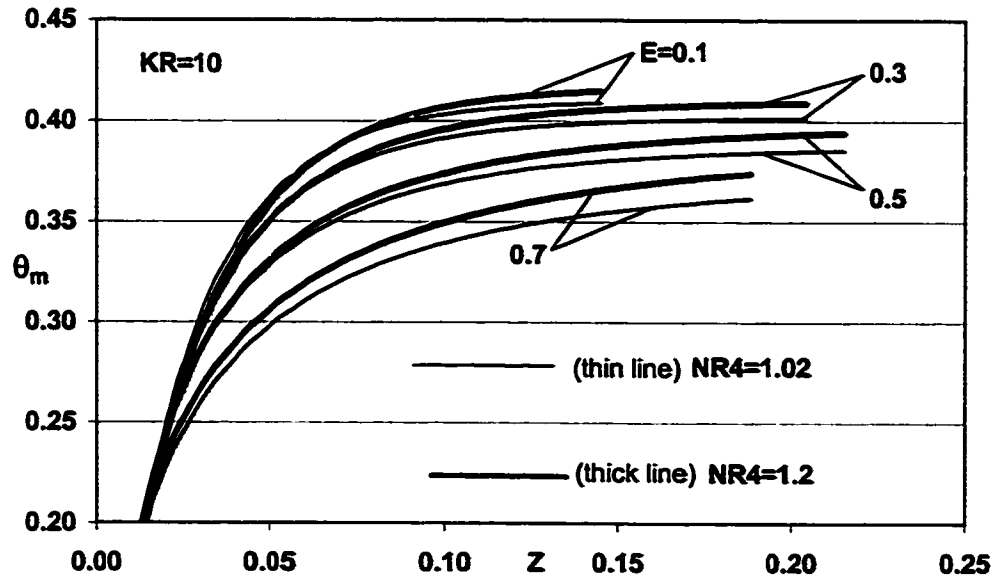

FIG. 7.28: Effect of the eccentricity on the axial variation of the mixing-cup temperature for two values of the wall thickness.

flow and increases this resistance to circumferential heat flow (due to reduction in the circumferential heat flow area). On the other hand, increasing the value of KR reduces the thermal resistance in both the radial and circumferential directions. Probably that is why Fig. 6.37 shows a non-linear variation, whereas Fig. 7.29 indicates a relatively linear trend.

Again, as was mentioned in section 6.2.4, the lower values of θ_m at lower thickness, as shown in Fig. 7.27, imply an increased local heat flux due to the reduced wall resistance. This is because the local heat flux is directly proportional to the difference between the wall temperature and the fluid mixed-mean temperature (Q $\propto (\theta_w - \theta_m)$). Consequently, with an isothermal boundary ($\theta_w = 1$). the decrease in the value of θ_m will cause an increase in the local value of the wall heat flux (Q). Figure 7.28 presents the effect of the eccentricity on the axial variation of θ_m for two wall thicknesses. As can be seen from this figure, for a given Z, the higher the value of E the lower the value of θ_m. The decrease in the value of θ_m with E is attributed to the associated increase in the mass flow rate through the annulus.

7.2.5 Critical tube thickness

Finally, it is of practical importance to know the minimum wall thickness below which the conjugate effect can be neglected. Figure 7.29 shows graphically the results of the present investigation for the variation of the percentage difference in $\theta_{m.fd}$ from the conventional case with the wall thickness for different values of E. This

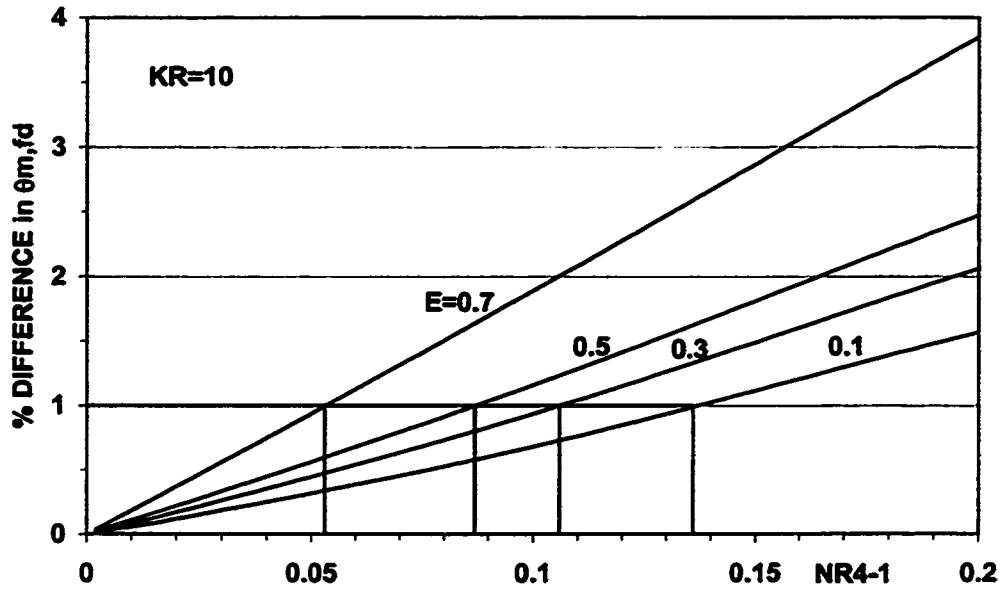

FIG. 7.29: % Difference in θm,fd from the conventional case plotted against outer tube thickness (NR4-1). Critical thickness values for a 1 % difference are highlighted.

TABLE 7.1 CRITICAL TUBE THICKNESS

FULLY DEVELOPED MIXING-CUP TEMPERATURE (θm,fd)				
OUTER TUBE THICKNESS	E=0.1	E=0.3	E=0.5	E=0.7
0.2	0.41480425	0.40887475	0.394055575	0.374003261
% DIFF.	1.57	2.06	2.47	3.85
0.1	0.41116944	0.404357553	0.388989866	0.366949409
% DIFF.	0.68	0.93	1.16	1.89
0.02	0.408877552	0.40129438	0.385377407	0.361481875
% DIFF.	0.12	0.17	0.22	0.37
0.002	0.408441663	0.400673807	0.384621233	0.360270172
% DIFF.	0.01	0.01	0.02	0.04
θm,fd (1%)	0.412480447	0.404619923	0.388385181	0.363744887
Conventional θm,fd	0.408396483	0.400613785	0.384539783	0.360143453
θm @ CTH	0.412403077	0.404585183	0.388309807	0.363515317
% DIFF.	0.98	0.99	0.98	0.94

percentage difference is based on the conventional values of $\theta_{m,fd}$. The 'critical' wall thickness, for a given eccentricity, has been arbitrarily chosen as that value which causes $\theta_{m,fd}$ to differ by no more than one percent from the conventional solution result for a given eccentricity. According to this criterion, the critical values of the wall thickness are given in Table 7.1 and are also presented in Fig. 7.29. As can be seen from Table 7.1 and from Fig. 7.29, the higher the value of E the lower the critical thickness. Thus, it can be concluded that the conjugate effect increases with eccentricity. However, Fig. 7.29 can be used to obtain critical thicknesses for other percentage difference criteria. Moreover, for given wall thickness and E, Fig. 7.29 can be useful in correcting available conventional results to take the conjugate effect into account.

7.2.6 Thermal entrance length

The figures presented in sections 7.2.1 to 7.2.4 indicate that the thermal entrance length is not appreciably affected by varying the wall thickness. As stated in section 6.2.6, this is particularly because of the boundary conditions applied. Decreasing the wall thickness leads to an increase in the heat input through the inner wall with a simultaneous increase in the heat loss through the outer wall. The counteracting effects cancel each other and therefore thermal entrance length is relatively insensitive to changes in the wall thickness.

Chapter 8

CONCLUSIONS

The present work aimed at obtaining a numerical solution for the conjugate laminar forced convection heat transfer in the entry region of eccentric annuli. Thermal boundary conditions applied are isothermal heating of the inner surface of the inner tube while the outer surface of the outer tube is maintained at the inlet fluid temperature. A model using bi-polar grid to fit the eccentric annulus and cylindrical grids in the walls has been presented. A linearized finite-difference algorithm has been developed to solve the model equations which comprise the continuity equation, the axial and tangential-like momentum equations and the fluid and solid energy equations.

Numerical results have been presented for a fluid of Pr=0.7 flowing in an annulus of radius ratio 0.5 for four values of dimensionless eccentricity (0.1, 0.3, 0.5 and 0.7). In the first part of the study the solid-fluid conductivity ratio (KR) was

varied to cover the range for typical practical cases with standard tube thickness. The numerical results indicate that conjugation can have an appreciable effect on the heat transfer parameters at low values of KR and that this effect increases with increasing the eccentricity. Thus, consideration of the the conjugation is more important at higher eccentricities. Based on the results of this investigation, limits for KR are obtained under which the conjugate effect should not be be neglected for practical purposes.

In the second part of the work, for KR equal to 10, the tube thickness was varied to obtain limits for wall thickness above which the conjugate effect should not be neglected. Again, the results indicate that conjugation can appreciably affect the heat transfer parameters in the case of thick-walled tubes and that the conjugate effect increases with eccentricity. Limits for NR4 are obtained below which the conjugate effect is negligible.

From the obtained results the following can be concluded:-

For a given eccentricity (E), decreasing the value of KR and / or increasing the tube thickness, i.e., increasing the thermal resistance of the tube walls results in the following, at a given axial location (Z):

- make the conjugate effect more pronounced.
- lower the temperature at the inner interface and raise the temperature at the outer interface.

- increase the circumferential temperature variation at both interfaces,
- reduce the interfacial heat flux at both interfaces, and
- increase the value of the mixing-cup temperature.

On the other hand, for given KR and NR4, increasing the eccentricity leads to:

- increase in the conjugate effect,
- increase the circumferential temperature variation at both interfaces,
- increase the interfacial heat flux at both interfaces,
- decrease in the value of the mixing-cup temperature due to increase in the mass flow rate through the annulus,
- increase in the value of critical KR above which the conjugate effect can be neglected, and
- decrease in the value of critical thickness below which the conjugate effect can be neglected.

Note: With minor modifications, the computer program can be used to investigate more practical cases such as:

i) different materials for the inner and outer tubes snd

ii) outer tube covered with a layer of insulationg material.

References

1. M.A.I. El-Shaarawi, H.I. Abualhamayel and E.M.A. Mokheimer, "Developing laminar forced convection in eccentric annuli.", Heat and Mass Transfer, Vol. 33, pp. 353-362 (1998).

2. M.A.I. El-Shaarawi, H.I. Abualhamayel and E.M.A. Mokheimer, "Developing laminar flow in eccentric annuli.", Journal of Fluids Engineering, Transactions of the ASME, Vol. 119, pp. 724-728 (1997).

3. W.C. Reynolds, R.E. Lundberg, and P.A. McCuen. "Heat transfer in annular passages. General formulation of the problem for arbitrarily prescribed wall temperatures or heat fluxes.". International Journal of Heat and Mass Transfer. Vol. 6, pp. 483-493 (1963).

4. H.S. Heaton. W.C. Reynolds and W.M. Kays. "Heat transfer in annular passages. Simultaneous development of velocity and temperature fields in laminar flow.", International Journal of Heat and Mass Transfer. Vol. 5. pp. 763-781 (1964).

5. E.M. Sparrow and S.H. Lin, "The developing laminar flow and pressure drop in the entrance region of annular ducts.". Journal of the Basic Engineering

Transactions of the ASME, Vol. 86, pp. 827-834 (1964).

6. R.W. Shumway and D.M. McEligot, "Heated laminar gas flow in annuli with temperature-dependent transport properties.", Nuclear Science Engineering, Vol. 46, pp. 394-407 (1971).

7. J.E.R. Coney and M.A.I. El-Shaarawi, "A contribution to the numerical solution of developing laminar flow in the entrance region of concentric annuli with rotating inner walls.", Journal of Fluid Engineering, Vol. 96, pp. 333-340 (1974).

8. J.E.R. Coney and M.A.I. El-Shaarawi, "Finite difference analysis for laminar flow heat transfer in concentric annuli with simultaneously developing hydrodynamic and thermal boundary layers.", International Journal for Numerical Methods in Engineering, Vol. 9, pp. 17-38 (1975).

9. J. Caldwell, "The hydraulic mean depth as a basis for form comparison in the flow of fluids in pipes.". J.R. Tech. Coll (Glasgow), Vol. 2, pp. 203-220 (1930).

10. N.A.V. Piercy, M.S. Hooper and H.F. Winny, "Viscous flow through pipes with cores.", London Edinburg Dublin, Philos. Mag. J. Sci., Vol. 15, pp. 647-676 (1933).

11. W.T. Snyder and G.A. Goldstein, "An analysis of a fully developed laminar flow in an eccentric annulus.". A.I.Ch.E. Journal , Vol. 11, No.3, pp. 462-469 (1965).

12. P.J. Redberger and M.E. Charles, "Axial laminar flow in a circular pipe containing a fixed eccentric core.". The Canadian Journal of Chemical Engineering, Vol. 40, pp. 148-151 (1962).

13. K.C. Cheng and G.J. Hwang, "Laminar forced convection in eccentric annuli.", A.I.Ch.E. Journal, Vol. 14, No.3, pp. 510-512 (1968).

14. M.L. Trombetta, "Laminar forced convection in eccentric annuli.", International Journal of Heat and Mass Transfer, Vol. 14, pp. 1161-1172 (1972).

15. K. Suzuki, J.S. Szmyd and H. Ohtsuka, "Laminar forced convection heat transfer in eccentric annuli.", originally published in Trans. JASME, Vol. 56, pp. 3445-3450 (1990).

16. P. Sathymurthy, K.C. Karki and S.V. Patankar, "Laminar fully developed mixed convection in a vertcal eccentric annulus.", Numerical Heat Transfer, Part A, Vol. 22, pp. 71-85 (1992).

17. E.E. Feldman, R.W. Hornbeck and J.F. Osterle, "A numerical solution of laminar developing flow in eccentric annular ducts.", "International Journal of Heat and Mass Transfer, Vol. 25, No.2, pp. 231-241 (1982).

18. E.E. Feldman, R.W. Hornbeck and J.F. Osterle, "A numerical solution of temperature for laminar developing flow in eccentric annular ducts.", International Journal of Heat and Mass Transfer, Vol. 25, No.2, pp. 243-253 (1982).

19. R.K. Shah and A.L. London, *Laminar flow forced convection in ducts.*, Academic Press, New York, 1978.

20. S. Mori, T. Inoue and A. Tanimoto, "Heat transfer to laminar flow between parallel plates with interfacial heat generation.", Journal of Chemical Engineering, Japan, Vol. 11, pp. 83-88 (1978).

21. S. Mori, Y. Kawamura and A. Tanimoto, "Conjugated heat transfer to laminar flow with internal heat source in a parallel plate channel.", The Canadian Journal of Chemical Engineering, Vol. 57, pp. 698-703 (1979).

22. M. Faghri and E.M. Sparrow, "Simultaneous wall and fluid axial conduction in laminar pipe-flow heat transfer.", Journal of Heat transfer, Vol. 102, pp. 58-63 (1980).

23. G. Pagliarini, "Conjugate heat transfer for simultaneously developing laminar flow in a circular tube.", Journal of Heat Transfer, Vol. 113, pp. 763-766 (1991).

24. M. Sakakibara, S. Mori and A. Tanimoto, "Conjugate heat transfer with laminar flow in an annulus.", The Canadian Journal of Chemical Engineering, Vol. 65, pp. 541-549 (1987).

25. B. Kirshan, "On conjugated heat transfer in fully developed flow.". International Journal of Heat and Mass Transfer, Vol. 25, pp. 288-289 (1982).

26. S. Olek, E. Ellias, E. Wacholder and S. Kaizerman, "Unsteady conjugated heat transfer in laminar pipe flow.". International Journal of Heat and Mass Transfer, Vol. 34, pp. 1443-1450 (1991).

27. M.A.I. El-Shaarawi, M.A. Al-Nimr and M.A. Hader, "Transient conjugated heat transfer in concentric annuli.". International Journal of Numerical Methods in Heat and Fluid Flow, Vol. 5, pp. 459-473 (1995).

28. E.M.A. Mokheimer, "Heat transfer in eccentric annuli.". PhD disserta-

tion, Mechanical Engineering Department, King Fahd University of Petroleum and Minerals (KFUPM), Dhahran, Saudi Arabia.

29. P. Moon and D.E. Spencer, *Field Theory Handbook*, Springer Verlag, Berlin, Heidlberg, New York, pp. 1-3, 1971.

30. W.F. Hughes and E.W. Gaylord, *Basic Equations of Engineering Science*, Schaum Outline Series, pp. 12-13, 1964.

31. H. Schlichting, *Boundary Layer Theory*, 7th edition, McGraw Hill, New York, pp. 127-149, 1987.

32. M.A.I. El-Shaarawi, "Derivation of Boundary Layer equations for Cases with Curved Boundaries.", International Journal of Engineering Fluid Mechanics, Vol. 3, No. 2, pp. 113-128 (1990).

33. M. R. El-Saden, "Heat conduction in an eccentrically hollow, infinitely long cylinder with internal heat generation.", Journal of Heat Transfer, Vol. 83, pp. 510-512 (1961).

IMAGE EVALUATION
TEST TARGET (QA–3)

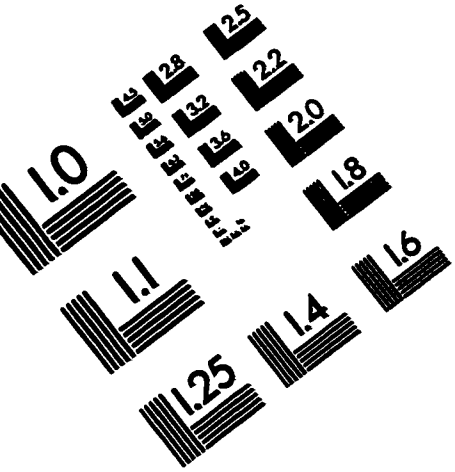

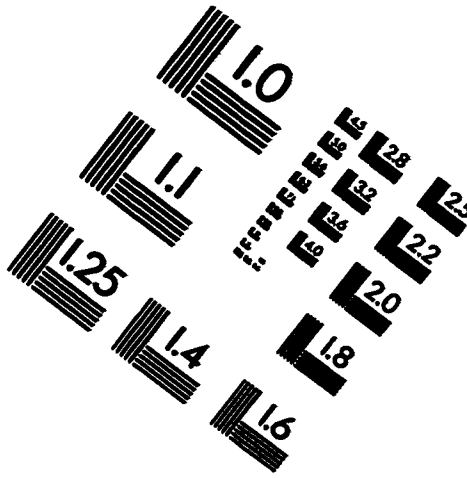

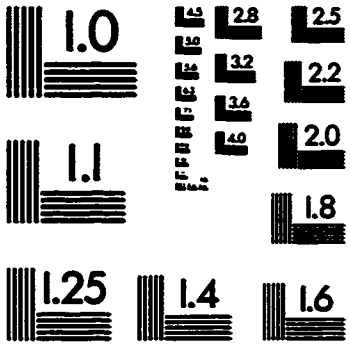

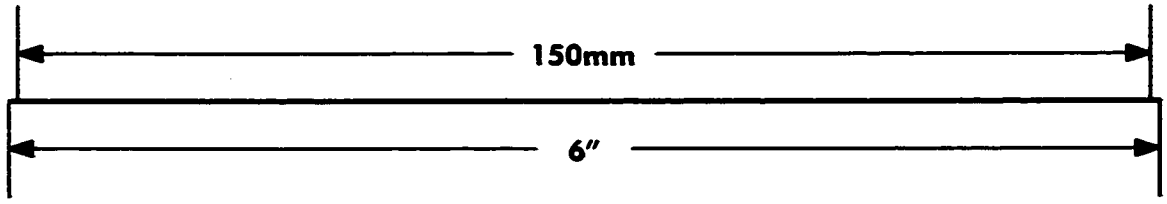

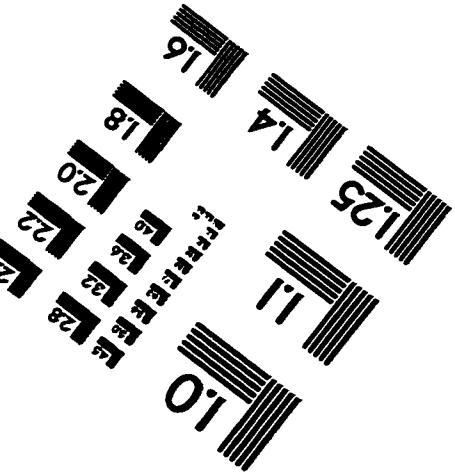

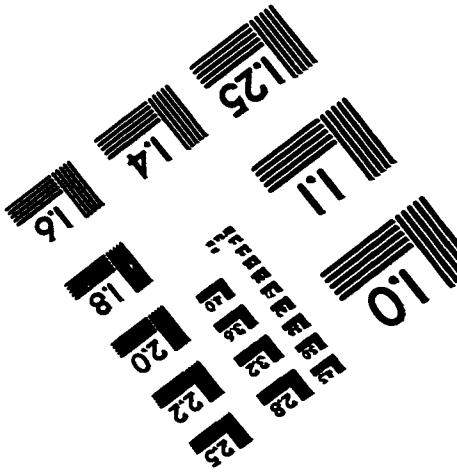

APPLIED IMAGE, Inc
1653 East Main Street
Rochester, NY 14609 USA
Phone: 716/482-0300
Fax: 716/288-5989